THE ROLE OF FUNCTIONAL SURFACES IN THE LOCOMOTION OF SNAKES

A Dissertation
Presented to
The Academic Faculty

by

Hamidreza Marvi

In Partial Fulfillment
of the Requirements for the Degree
Doctor of Philosophy in the
School of Mechanical Engineering

Georgia Institute of Technology
December 2013

THE ROLE OF FUNCTIONAL SURFACES IN THE LOCOMOTION OF SNAKES

Approved by:

Dr. David Hu, Advisor
School of Mechanical Engineering
Georgia Institute of Technology

Dr. Alexander Alexeev
School of Mechanical Engineering
Georgia Institute of Technology

Dr. Young-Hui Chang
School of Applied Physiology
Georgia Institute of Technology

Dr. Daniel Goldman
School of Physics
Georgia Institute of Technology

Dr. Jun Ueda
School of Mechanical Engineering
Georgia Institute of Technology

Date Approved: 23 July 2013

To my beloved wife, Sarah,

whose exceptional support and encouragements

made this journey possible,

and to my parents,

for their tremendous blessing and inspiration.

ACKNOWLEDGEMENTS

I would like to greatly thank my advisor, Dr. David Hu, for his exceptional help and supervision during my Ph.D. work. This research would not have been possible without his unreserved support and remarkable vision.

I greatly appreciate Dr. Daniel Goldman and his students at CRAB Lab (especially Nick Gravish, Feifei Qian, and Sarah Sharpe) for their tremendous help and support on sidewinding project. I also thank Dr. Howie Choset and Dr. Jeffrey Streator for their collaborations on sidewinding and snakeskin tribology projects, and Dr. Michael Shelley for his early contributions on the concertina locomotion project. Moreover, I sincerely thank my Ph.D. committee members for their insightful comments and discussions on this research.

I am very thankful to Dr. Joseph Mendelson and his wonderful team at Zoo Atlanta. I conducted most of my animal experiments at Zoo Atlanta and this has not been possible without their exceptional support. It has been a great pleasure working with such a professional and supportive team at Reptile section of Zoo Atlanta.

I would also like to thank Paul Cook, Jacob Bridges, Gregory Meyers, Geoffrey Russell, and many other undergraduate students for helping with experiments and data analysis, Tim Nowak and Candler Hobbs for photography, and the NSF (PHY- 0848894), NSF-PoLS, and the Elizabeth Smithgall Watts endowment for financial support.

Last but certainly not least, I would like to express my wholehearted gratitude to my wife, Sarah, for her unreserved love and support. This long journey would not have been possible without her patience, support, and persuasion. I am also very grateful to my parents for their wholehearted and sincere support and encouragements throughout my life. Hereby, I would like to dedicate this dissertation to my wife, and to my parents.

TABLE OF CONTENTS

LIST OF TABLES

LIST OF FIGURES

SUMMARY

Snakes are one of the world's most versatile organisms, at ease slithering through rubble or climbing vertical tree trunks. Their adaptations for conquering complex terrain thus serve naturally as inspirations for search and rescue robotics. In a combined experimental and theoretical investigation, we elucidate the propulsion mechanisms of snakes on both hard and granular substrates. The focus of this study is on physics of snake interactions with its environment. Snakes use one of several modes of locomotion, such as slithering on flat surfaces, sidewinding on sand, or accordion-like concertina and worm-like rectilinear motion to traverse crevices. We present a series of experiments and supporting mathematical models demonstrating how snakes optimize their speed and efficiency by adjusting their frictional properties as a function of position and time. Particular attention is paid to a novel paradigm in locomotion, a snake's active control of its scales, which enables it to modify its frictional interactions with the ground. We use this discovery to build bio-inspired limbless robots that have improved sensitivity to the current state of the art: Scalybot has individually controlled sets of belly scales enabling it to climb slopes of 55 degrees. These findings will result in developing new functional materials and control algorithms that will guide roboticists as they endeavor towards building more effective all-terrain search and rescue robots.

CHAPTER I

INTRODUCTION

1.1 Background

More than 450 million people were affected by 700 natural disasters worldwide over the past two years [9]. Robotic search and rescue is crucial for fast and effective rescue operations after such disasters [10, 11]. In addition to search and rescue, limbless and wheel-less propulsive devices can be designed for "robotic colonoscopy" to maneuver while minimizing pain and damage to the surrounding tissue [12, 13], or exploratory missions in deserts and on other planets [14]. In all these situations, terrain is complex, involving topography over a range of length scales and surface textures.

Snakes are one of the most versatile animals at ease traversing complex terrain, climbing steep inclinations, and advancing through narrow openings. They have been studied for over 200 years and have been source of inspiration for many great engineering discoveries. Snakes have four different modes of terrestrial locomotion: concertina locomotion, rectilinear, lateral undulation, and sidewinding. When a snake climbs inclined channels it usually uses an accordion-like motion called concertina [15]. In rectilinear motion, a snake propagates a longitudinal traveling wave along its body to move in limited spaces [16]. Lateral undulation is the fastest mode of snake locomotion and most snakes are capable of performing this gait on flat surfaces. During lateral undulation, snakes generate a 2-dimensional traveling wave propagating from head to tail [17]. When traversing a granular substrate such as sand, a snake usually uses the sidewinding gait, the second fastest and most energetically efficient gait of snake locomotion [18].

Understanding the kinematics and energetics of these gaits and mechanisms snakes use for making effective interactions with their environment is a major step forward for developing effective all-terrain search and rescue robots. In § 1.2, we briefly review these gaits and discuss about several robots inspired by snake locomotion. We then discuss scope, objectives, and outline of this thesis in § 1.3.

1.2 Previous studies

1.2.1 Concertina locomotion

Concertina locomotion is a series of folding and unfolding of body in an accordion-like manner. This movement is observed when the snake has to travel through straight or circular channels. This movement is sometimes observed on open, uniform surfaces [19]. Gray is among the first scientists who studies concertina locomotion of snakes [19]. He observes that some segments of the body move backwards which cause ventral scales to engage with the surface and create points of support [19].

The muscular activity of snakes during concertina locomotion is studied by Jayne [1]. In another study, Jayne and Davis discuss how kinematics and performance of concertina locomotion of black racer snakes are affected by tunnel width and tunnel treadmill speeds [20]. The climbing behavior of boa constrictors is also studied by Byrnes and Jayne [21]. They observe at large rope diameters, snakes use concertina locomotion for climbing [21].

Greene *et al.* [22] and Gans [23] note that concertina has inherently lower efficiency than lateral undulation because part of the snake is always stationary within each period of concertina motion resulting in periodic loss of momentum. Walton *et al.* [24] measured oxygen consumption of snakes on a treadmill to compare the energy consumption of different modes of locomotion. They find the net energetic cost of a snake performing lateral undulation is equivalent to the running of a limbed animal of the same mass, and seven times less energetically costly than concertina locomotion. The results of their study suggests that lower aerobic energetic cost is not a viable explanation of why species evolved into limblessness [24].

There are few models developed for studying concertina locomotion of snakes. Chernousko explains snake-like locomotion of multilink mechanisms by considering planar multi-body systems with two, three, and multiple links that are connected by actuated joints and moving on a horizontal plane [25]. In another study, Jing and Alben optimize motion of two- and three-link snake models and show that for a two-link snake concertina locomotion is the optimum mode of motion [26].

1.2.2 Rectilinear locomotion

Rectilinear motion is the slowest mode of snake locomotion. One of the first theories of rectilinear motion originates in 1812, where Everard Home attributes a snake's ribs as being responsible for the progressive motion of snakes [27]. Even though Home's rib walking theory was rejected by the mid 1900's, it was still believed that a snake's rectilinear movement was dependent upon the movement of its ribs. Bogert disagrees with this theory

and claims that rectilinear movement is possible due to the elasticity of the skin of the snake, the connection between the ribs to the integument through its muscle, ventral scutes and connective tissue [28].

Rectilinear locomotion is considered similar to snail [29] and caterpillar locomotion [30]. However, Lissman presents an extensive experimental study to show that rectilinear locomotion of snakes is most similar to earthworm motion [31]. He observes snakes propagate multiple traveling waves in their posterior direction similar to the peristaltic waves earthworms generate. He also uses x-ray imaging to prove ribs stay fixed during rectilinear locomotion of snakes [31].

1.2.3 Lateral undulation

Lateral undulation or slithering is a continuous motion in which snake propagates a two-dimensional sinusoidal traveling wave from head to tail. Gray reports this gait is observed when the snake is moving on substratum of irregular surface and is dependent on availability of ground projections against which the snake can engage [19]. In another study, Gray and Lissman conclude that propulsion of undulating grass snake is dependent on its ability to adopt a sinusoidal form and to push its body's lateral surface against external objects [32]. However, Hu *et al.* show that frictional anisotropy is the key for successful slithering rather than push points. They also present a mathematical model for this gait and show the importance of body lifting for reducing cost of slithering [17]. Mechanisms used by the muscular system to produce curvature, force exertion, and propulsion during terrestrial lateral undulation of gopher snakes are studied by Moon and Gans. Kinematic patterns and muscle activities of gopher snakes are recorded as they traverse over boards with a single peg and with an array of pegs [33].

1.2.4 Sidewinding

Mosauer is among the first people who qualitatively describes sidewinding of snakes. He uses a rolling helix of wire to compare the kinematics of snake sidewinding with a physical model. Using this model, he explains why snake tracks are parallel and the length of each track is the same as snake body length [34]. Sidewinding involves two body sections remaining at rest while the rest of the body is in motion [19].

Cowles explains the purpose of sidewinding and its origins. Sidewinding is compared to the other forms of locomotion available to snakes in the desert and it is noted that sidewinding is not necessary to successfully travel across loose surfaces such as sand. However, it is an effective means of quickly traveling across large areas of desert [35]. Sidewinding

is also the most energetically efficient mode of motion. Secor *et al.* examine the locomotor performance and energetic cost of sidewinding in the *crotalus cerastes*, by conducting burst speed and endurance testing. The authors note that sidewinding is very effective at conserving energy compared to slithering and concertina locomotion [36].

1.2.5 Snake robots

Snake-robots are categorized as having wheels, active treads, or flexible bodies that undulate using vertical waves or linear expansions [37]. The first category of snake robots discussed by Hopkins *et al.* are robots with passive wheels. Different designs are discussed, such as Hiroses ACM-R3 [38], where the robots segmented modules allow for increased maneuverability. The second category includes robots with active wheels to provide propulsion for the robot. One of the main advantages for using active wheels is the ability to simulate snake-like locomotion without a large number of segments for flexibility. This category; however, does add complexity to the robot. The third category involves robots with active treads, which use powered treads or crawlers to travel across rough terrain. The benefit of treads is that the robot will be able to travel in small and tight locations. The last category of robots discussed by Hopkins *et al.* are undulatory robots, which use vertical waves or linear expansion for locomotion. These robots can achieve rectilinear locomotion through linear expansion and contraction of the robots body.

The vast majority of snake-like robots sit atop free-rolling wheels, which provide a forward-transverse frictional anisotropy due to the relative ease of rolling compared to sliding; however these wheels preclude them from advancing uphill. Several snake robots do not have wheels [39], sliding their bellies on rough surfaces. Dowling [40] is among a few researchers who tried to fabricate artificial snake skin using a series of materials such as spandex, sequins, and polyethylene braids. However, a true artificial snake skin has yet to be invented for snake robots.

Tesch *et al.* study two specific forms of snake locomotion: parameterized and scripted gaits [41]. They explain most biologically inspired gaits like lateral undulation are classified as parameterized gaits. Stair climbing and other such gaits are called scripted gaits, which steps the snake robot through a series of predefined shapes. The paper discusses the energetics of both parameterized and scripted gaits. The goal of this paper is to continue improvements in reliability and robustness of hyper redundant machines.

There are several snake-like robots capable of performing concertina locomotion. As an illustration, Barazandeh *et al.* presents one of these snake-robots that can crawl up inclined channels via a mechanism called self-locking. Rigid beams of the robot are braced at

acute angles with respect to the channel walls, whereby the torque generated by their self-weight creates sufficient friction to resist sliding down the channel [42]. These methods are effective because the application of self-weight reduces the power expended by the motor to brace channel walls. In comparison, snakes must expend energy to brace channel walls.

Ghanbari *et al.* and Liu *et al.* are among researchers who work on developing rectilinear locomotion for robotic snakes [43, 44]. Ghanbari *et al.* study optimization of rectilinear locomotion for robot motion. They show that sequences of joint configurations allow the robot to move forward assuming there is enough friction such that at least one link is in static contact with the ground [43]. Liu *et al.* explore the use of Shape Memory Alloy actuators to mobilize an eight-segment robot similar to rectilinear locomotion of snakes [44].

Slithering is the fastest mode of snake locomotion and many roboticists have shown interest in studying this gait [45]. Khan *et al.* explain that lateral undulation is one of the most efficient forms of locomotion for snake-robots; however, specific conditions such as body curvature are required in order to meet the optimum point [46]. Sato *et al.* explore mathematical models for analysis and synthesis of slithering with a multilink robotic snake [47]. The focus of this article is on the planar slithering gait, which eliminates considerations of the more general three-dimensional motion found in the nature [17].

Several roboticists present models for snake sidewinding. Chirikjian and Burdick conduct a study of a 30 degree of freedom planar hyper-redundant robot that is of variable geometry truss construction [48]. Burdick *et al.* present an algorithm to produce sidewinding locomotion in this hyper-redundant robot [49]. This is accomplished by formulating a qualitative description of sidewinding and the necessary spatial kinematics using the backbone curve model. These papers are not studies of biological locomotion but of how to implement the various gaits of snakes with a hyper-redundant robot. Hatton and Choset discuss the effects of inclines on sidewinding motion. Sidewinding motion becomes unstable on slopes; however, increasing the portion of body in contact with the surface can reduce the instability. This can be accomplished in two ways, either by decreasing the height of the raised portions of the body, or increasing the curvature of the raised portion of the body [50].

1.3 Scope and objectives

Much of this thesis is drawn from recent papers and preprints [16, 51–55]. The main objective of this thesis is to study the underlying physics of snakes' interactions with their

deformable or granular environment. We develop novel experimental and theoretical techniques to discover some of the mechanisms snakes use to effectively move on a variety of complex terrain. Snakes have four different modes of motion or gaits. In this thesis, we study three of these gaits using the aforementioned approach.

We begin with a study of snakeskin tribology and the interaction of a snake scale with its deformable substrate in chapter 2. We present an experimental and computational methodology to understand how friction is generated during the interaction of two flexible beams: snake scale and a transparency film. We proceed with a study of concertina locomotion with a focus on the mechanisms snakes use to enhance frictional forces required for climbing in chapter 3. In chapter 4 we present two snake-like robots we developed inspired by concertina locomotion. In Scalybot 1 and 2, we control their ventral scales to adjust frictional forces as a function of position and time. We then develop a novel methodology for measuring total energetic cost of animal locomotion in chapter 5. We use Magnetic Resonance Spectroscopy (MRS) to measure cost of concertina locomotion on slopes of varying inclinations. We study kinematics, optimality, and energetics of rectilinear locomotion of snakes in chapter 6. In chapter 7 we discuss our study of sidewinding on granular media. We present a control strategy sidewinders use to effectively climb on sand at highest possible inclinations. Finally, in chapter 8 we summarize our findings and discuss future directions.

CHAPTER II

SNAKESKIN TRIBOLOGY: SNAKES CONTROL MECHANISMS FOR FRICTION ADJUSTMENT

2.1 Introduction

Frictional properties in the natural arena ranging from plants and flowers to fish and reptiles offer profound insight. Purposes ranging from locomotion to diaspores attachment, the list is inclusive to most species and most niche environmental applications. The equally significant corollary can be found in anti-adhesive and lubricating physiologies. These two facets combined make biological tribology an enlightening field that is in its frontier stages of engineering application [56–61].

The characteristics of snake scales are of particular frictional significance [57, 62]. Residing in most habitats across the globe they exhibit highly adaptable locomotive capacities. They can use finely orchestrated body movements to move within constraints of most substrate compositions and geometries. Each mode offers a level of effectiveness under different limiting circumstances, such as soft substrates, narrow passages, and aquatic environments to name a few. The point of contact between substrate and body is the more fundamental consideration to how these body movements translate into forward motion. The ventral scales usually act as points of contact.

A number of research groups around the globe have dedicated their expertise in characterizing snakeskin, whether in a frictional relation or otherwise [56, 57, 62–64]. Several researchers measure frictional properties of snakes sliding on different substrates and report on their frictional anisotropy [52, 65]. However, most of the studies on frictional properties of snakeskin are conducted at micro scale. Hazel *et al.* focus on mapping the microstructures on the surface of ventral scales [62]. They find that micro-structural characteristics of snake scales facilitate the friction anisotropy. They report tail to head (backward) friction coefficient of a single scale is three to four times higher than that of head to tail (forward) [62].

Gorb et al. use dorsal, lateral, and ventral scales of snakes to study the micro-ornamentations and frictional properties in each region [63]. They report ventral scales have frictional anisotropy of 26% compared to only about 4-5% for both lateral and dorsal. These characteristics prove a unique specialization of the ventral scales towards frictional utility in locomotion. In another study, Schmidt and Gorb conduct an extensive study of snakeskin

microstructures and physiology [66]. The importance of their work is the scope of species studied covering all habitats and evolutionary traits.

Frictional properties of snakeskin are also studied by Abdel-Aal et al. [67]. Studying the shed skin of a *python regius*, the research maps out coefficients of friction for scales on all parts of the body: lateral, dorsal, and ventral. They find location of scale on the snake body and scale color influence friction coefficients. They also find frictional anisotropy is more significant in the ventral scales than any other part of the body. It is observed that more fibril structures are on the ventral scales, particularly a higher density of fibrils at the middle of the trunk where the load bearing is highest [67].

In this study, we report on the role of torsional stiffness, bending stiffness, and angle of attack of a ventral scale in controlling the frictional properties of snakes. These are parameters snakes can actively control during locomotion. In § 2.2, we describe our experimental techniques for measuring snake friction coefficients. We present in § 2.3 a theoretical model for studying the interaction of a deformable scale with a transparent film. In § 2.4, we present our experimental results and compare them to predictions of our model. Finally, we summarize our findings and discuss our concluding remarks in § 2.5.

2.2 Experimental techniques

2.2.1 Animal care

We use two corn snakes *Elaphe guttatta* (**Fig.1**a) which are cared for in captivity for the duration of our experiments. The corn snakes had head-to-tail length of $L = 59.1 \pm 2.7$ cm and mass of $m = 40 \pm 4.2$ g when we conducted these experiments. The snake is fed weekly and housed in a terrarium with controlled temperature and humidity conditions.

2.2.2 Interaction of snakes' ventral scales with an array of transparencies

In order to understand the interaction of two deformable beams we conduct a series of experiments using an array of transparent films as shown in **Fig.1**b, c. We use 3M Dual Purpose CG5000 transparency film with a thickness of 0.12 mm for our experiments. An array of transparent films are placed into carved slits on a piece of wood as shown in Appendix **Fig.A.2**a,b. We carefully drag a snake over the film array with its ventral scales catching and displacing the films as the scales are rotating (**Fig.1**b, c). This experiment is conducted using both conscious and unconscious snakes. Loss of consciousness is achieved using the anesthetic Isoflurane, according to procedures given by Hu et al. [17]. All of these experiments are filmed using a high definition digital video camera (Sony HDRXR200). The main data extracted from videos are transparent film tip deflection as a function of snake

displacement. The details of measuring scale geometry and material properties, calibration process, and friction measurements are explained in Appendix A.1.

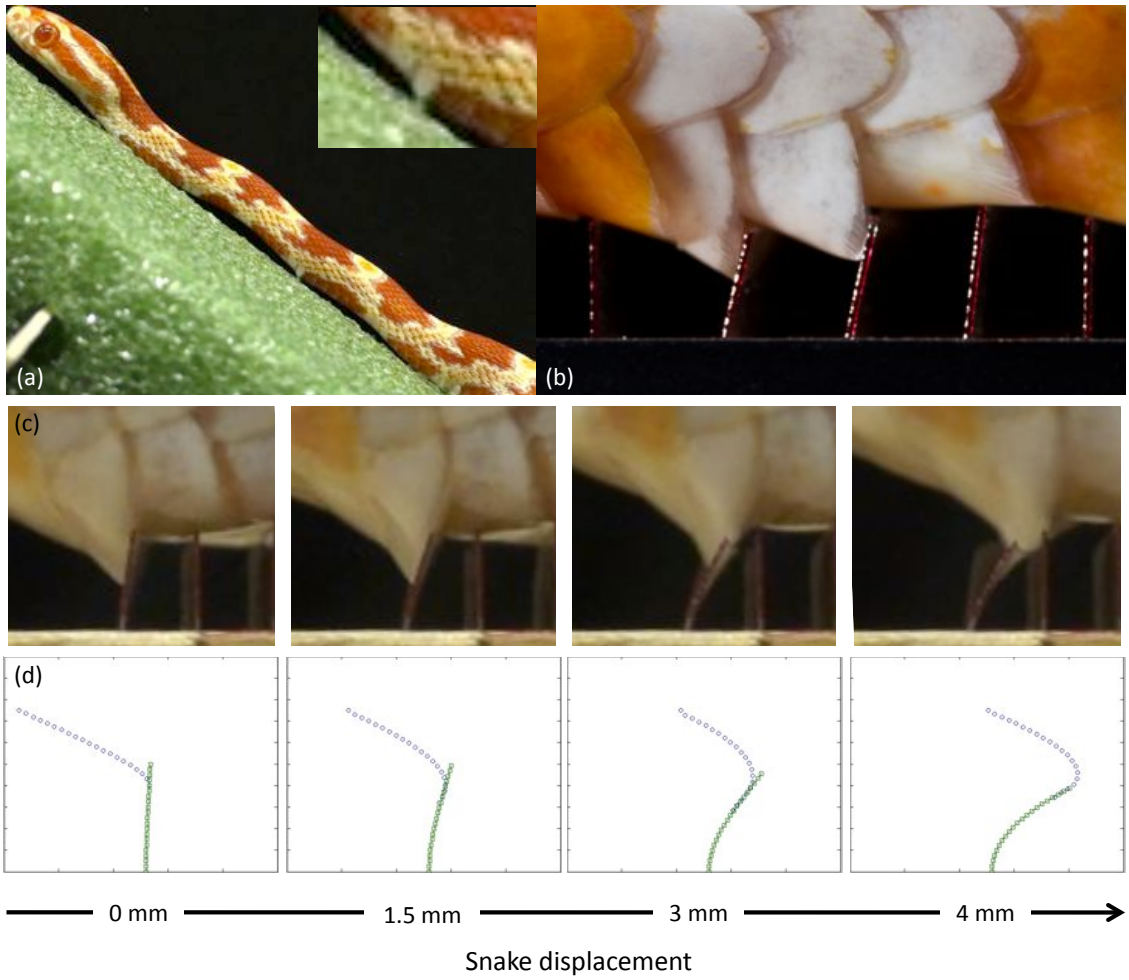

Figure 1: (a) A corn snake climbing Styrofoam at inclination of 45 degrees, (b) snake scale interacting with a transparency. Video sequence of a snake scale interacting with a transparent film: (c) experiment vs. (d) model.

2.3 Model

In order to investigate the role of scales bending stiffness, torsional stiffness, and angle of attack on frictional properties of snakes we develop a numerical model to study interaction of two elastic cantilever beams. Eq. (1) is the fundamental governing equation of each beam (elastica) [68–70]; the local curvature $d\theta(s)/ds$ is determined by the local moment $M(s)$:

$$\frac{d\theta(s)}{ds} = \frac{M(s)}{EI(s)}, \tag{1}$$

where s is arc-length, measured from base of beam toward its free end, E is the modulus of elasticity, and $I(s)$ is moment of inertia for cross-sectional area.

Integrating Eq. (1) we can find slope at any point along the beam:

$$\theta(s) - \theta_0 = \frac{F}{E}\int_0^s \frac{y(s_c) - y(s')}{I(s')}\,ds' - \frac{W}{E}\int_0^s \frac{x(s_c) - x(s')}{I(s')}\,ds'. \tag{2}$$

where $x(s)$ and $y(s)$ are local horizontal and vertical positions relative to the base of beam, and s_c is contact arc-length distance. Contact horizontal and vertical forces are also denoted as F and W.

For a given function $\theta(s)$ along with slope angle of beam at its base θ_0, evaluation of integrals in Eq. (3) provides functions $x(s)$ and $y(s)$. Eq. (3) should be solved iteratively with Eq. (2).

$$\begin{cases} x(s) = \int_0^s \cos(\theta(s'))\,ds', \\ y(s) = \int_0^s \sin(\theta(s'))\,ds'. \end{cases} \tag{3}$$

Knowing the rotational spring constant, k_t at scale base, its base angle could be found as following:

$$\theta_0 - \theta_{0i} = \frac{M(0)}{k_t} = \frac{1}{k_t}(Fy(s_c) - Wx(s_c)), \tag{4}$$

where θ_{0i} is the initial base slope angle of scale which is the same as the unloaded base angle. Solving Eq. (2)-Eq. (4) together in an iterative manner would give us the local slope as well as local horizontal and vertical positions with respect to base of the beam. In Appendix A.1.3 and Appendix **Fig.A.3** we present the verification of this model with our experimental data. The input values to the model are listed in Appendix A.2 and are shown in Appendix **Fig.A.2**b. The detail outline of computational algorithm is also explained in Appendix A.3.

2.4 Results

The difference in forward and backward friction coefficients of unconscious snakes has been reported by several scientists [52, 53, 65]. Marvi et al. report that the friction coefficients of conscious corn snakes are almost twice as those of unconscious snakes implying the importance of active mechanisms [52]. Scales bending stiffness, torsional stiffness, and angle of attack are among the parameters snakes can actively control during locomotion. They can use the muscles attached to each of their ventral scales to adjust its torsional stiffness. They can also warp a ventral scale to change its bending stiffness. Moreover, as shown in **Fig.1**a, we observe a snake can lift parts of its body to change the relative angles between its ventral scales and the substrate. To investigate the role of such active

mechanisms in controlling frictional forces of snakes we conduct a set of experiments and develop a numerical model as discussed in § 2.2, § 2.3, and Appendix A.1.

We model a ventral scale as a deformable material that has a rotational spring attached to its base. Thus, we need to measure the torsional stiffness of the spring as well as the stiffness of the scale itself. We drag a snake over a transparency film array with snake ventral scales interacting with the array (**Fig.1**b, c). We can calculate the torsional stiffness k_t at the base of a ventral scale as following: $k_t = (Fd_1 - Wd_2)/\theta$, where θ is the scale base rotation. The horizontal and vertical components of the contact load are denoted as F and W. d_1 and d_2 are also horizontal and vertical distances between the scale base and where it touches the transparent film. According to our experiments, the torsional stiffness of a conscious snake is $k_t = 10.14 \pm 0.91$ N.mm/rad. We can then use our model to find the stiffness of snake scale being the only unknown parameter in this experiment. We find stiffness of corn snake ventral scale to be approximately 400 MPa. Benz et al. use microindentation to measure Young's modulus for ventral scales of a California King Snake. They report a stiffness of 413 MPa for ventral scales of this snake [64].

Knowing the scale geometry, torsional stiffness of the base spring, and stiffness of scale we can use our model to study the interaction of a snake scale with its substrate. **Fig.2**a presents the experimental data compared to simulation results for a snake ventral scale interacting with a transparent film. The discrepancy between these two plots is due to some complexities in the biological scale that we have not considered in our model. As an illustration, we ignore the effect of adjacent scale overlapping with the individual scale interacting with transparency.

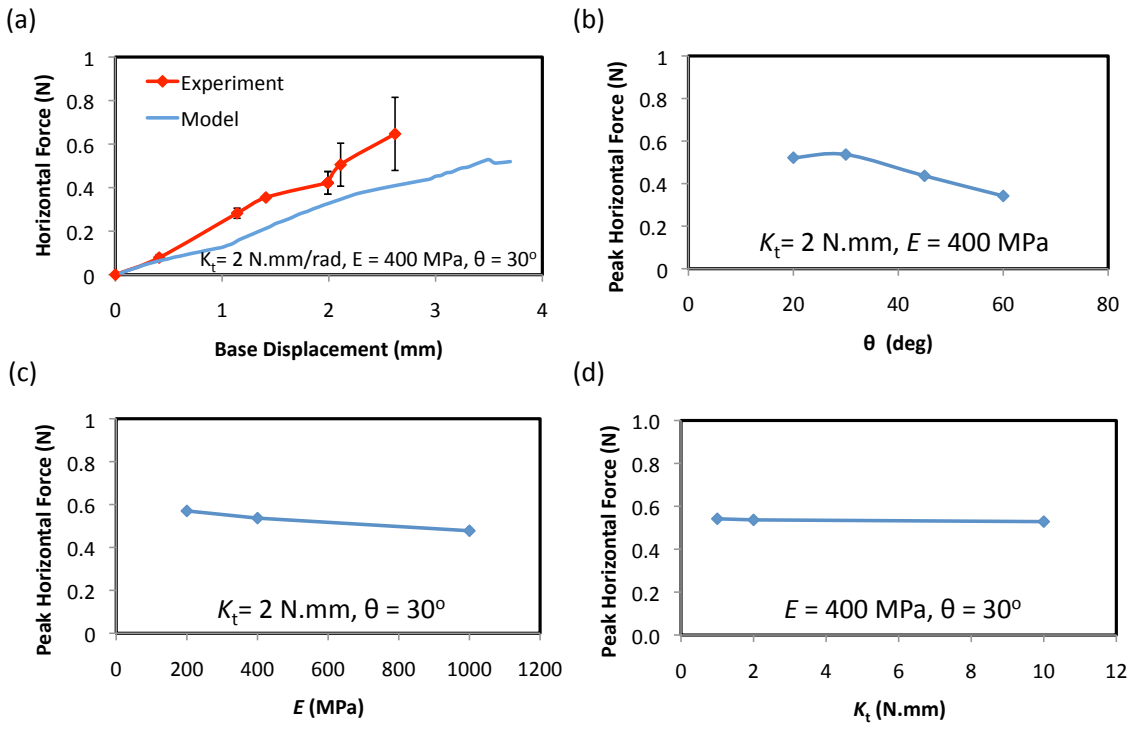

Figure 2: Experimental data and simulation results for a ventral scale of a conscious corn snake interacting with a transparent film. (a) Experimental data compared to simulation results for horizontal force vs. snake displacement. Simulations results for peak horizontal force vs. (b) initial angle of attack, (c) elastic modulus, and (d) torsional stiffness of snake scale.

Fig.2b-d show our model predictions for peak horizontal force as a function of angle of attack, elastic modulus, and torsional stiffness of snake scales. We find elastic modulus and torsional stiffness change the peak horizontal force insignificantly. Increasing elastic modulus from 200 to 1000 MPa decreases peak horizontal force by 16%. One order of magnitude increase in k_t would also decrease peak horizontal force by only 5%. However, initial angle of attack has a major role in adjusting horizontal force. A very low initial angle of attack would cause a snake scale to slide upwards on the transparent film resulting in low peak horizontal force. If the initial angle of attack is larger than this threshold, snake scale slides downwards on the transparent film. As shown in **Fig.2**b, increasing the angle of attack would also cause a decrease in the peak horizontal force. In this case scale slides less towards the transparency base and as a result it can create less horizontal force. Specifically, increasing the initial angle of attack from 30 to 60 degrees would decrease the peak horizontal force by 37%. Thus, adjusting scale angle of attack allows snakes to control

their frictional forces. Based on our experimental observations, a snake can lift parts of its body to set the relative angle between ventral scales and the substrate. We measure this angle for two corn snakes climbing on styrofoam at four different inclinations in the range of 7 to 30 degrees. It turns out snakes lift their bellies such that their initial relative angles of attack are $\theta_{0i} = 22^\circ \pm 2^\circ$. This is an effective strategy to increase the frictional force in the backwards direction and avoid sliding down the hill.

2.5 Summary and future directions

Snakes are one of the most successful species in traversing a wide range of complex terrain. They have four different modes of motion and take advantage of several mechanisms to effectively interact with their environment. They can use their ventral scales to adjust their frictional properties and reduce the cost of their locomotion. In this experimental and computational study, we investigate the generation of frictional forces due to the interaction of snake scales and deformable substrates. We study the effect of three parameters snakes can actively control during their locomotion: angle of attack, elastic modulus, and torsional stiffness of snake ventral scales. We find out change of a scale initial angle of attack plays a significant role in adjusting frictional forces. In fact, a snake can increase its backward frictional force and climb higher inclinations by lifting parts of its body. The idea of controlling frictional properties as a function of position and time could result in developing new functional surfaces for making effective interactions with complex environment and reducing cost of locomotion.

CHAPTER III

FRICTION ENHANCEMENT IN CONCERTINA LOCOMOTION OF SNAKES

3.1 Introduction

In order to climb a channel, human rock-climbers use a "chimneying" process in which the legs and back provide stationary anchorage by pushing against channel walls. The arms are stretched forward to create a new anchorage point, after which the remainder of the body is pulled forward. An analogous method of anchorage and propulsion is common to limbless soft-bodied and burrowing organisms, such as worms, mollusks and snakes. Their propulsion in this manner is referred to as accordion, concertina or horizontal inchworming. The goal of this study is to investigate concertina locomotion of snakes in order to help roboticists build more efficient limbless robots.

Several biologists have investigated concertina locomotion through channels, beginning in 1932 with Wiedermann [29]. Gray [71] observed concertina locomotion in both straight and curved channels and described qualitatively the muscular activity required to bend the body into a kinked shape. Wall friction forces were estimated by Gray and Lissman [65], who report sliding friction coefficients of dead grass snakes on various materials. Frictional anisotropy, the ratio of backward to forward friction coefficients, was 1 for a snake on dry metal and up to 4.8 on rough sand paper. We extend these results in § 3.5.1 by showing how a snake's active control of its scales can increase frictional anisotropy.

Jayne & Davis [72] conducted experiments using an annular channel atop a circular treadmill. They measured the effect of wall spacing and treadmill speed on parameters such as frequency, period, and distance traveled per cycle. Jayne [1] also characterized the muscle activation during concertina and sidewinding motion using synchronized electromyography and cinematography. He finds transverse pushing generates the principal muscular activity during concertina locomotion.

In parallel with biological work, interest has arisen in mathematical modeling of concertina-like locomotion. Keller *et al.* report a continuous model for worm locomotion [73] which predicts speeds and periods close to that of worms [74]. Body speed is shown to be bounded by the maximum rate of change of internal pressure. Zimmermann *et al.* present a discrete model for worm locomotion by considering nonlinear non-symmetric frictional forces [75]. Chernousko presents a two-link, three-link and multi-link model for snake locomotion and

discusses associated torque control algorithms [25]. He presents the optimal values for mechanical and geometrical parameters corresponding to maximum speed.

In this study, we report on the propulsion of a snake through a channel. In § 3.2, we describe our experimental techniques for measuring snake friction coefficients and transverse forces applied by the snake to the channel walls. We present in § 3.3 a theoretical model for propulsion based on the combined roles of snake scales and the snake's transverse pushing of the channel. An experimental justification of the parameters in this model is presented in § 3.4. In § 3.5, we present our experimental results and compare them to predictions of our model. In § 3.6, we discuss the implications of our work followed by concluding remarks in § 3.7.

3.2 Experimental Techniques

In this section, we present the experimental methods used in our study. First, we give details on caring for the corn snakes used in our experiments. Next, using our work in Hu *et al.* (2009) [17] as a basis, we provide new experimental techniques for measuring the frictional properties of the snakes, an important component of our model. We proceed by describing the smart channel apparatus used to measure transverse forces.

3.2.1 Animal care

Three six-month-old corn snakes (N=3), *Elaphe guttatta* were purchased from Florida Herps and cared for in captivity for one month, the duration of our experiments. The corn snakes had head-to-tail lengths of $L = 61 \pm 4$ cm and masses of $m = 42 \pm 5$ g. Snakes were fed weekly and housed in separate terrariums with controlled temperature and humidity conditions.

3.2.2 Friction measurements

The bottoms of our channels were lined with open-cell rigid styrofoam of roughness 240 μm. This material was employed because its roughness was greater than the corn snake scale thickness of 45 μm. In this regime, friction coefficients μ_{st} are significantly affected by scale angle of attack, as shown in [53]. Static friction coefficients of the snake's ventral surface were measured using the inclined plane method on a 90 x 30 cm styrofoam plank [17]. Measurements were taken using both conscious and unconscious snakes. Loss of consciousness was rendered using the anesthetic Isoflurane, according to procedures given in Hu *et al.* [17].

Dynamic friction coefficients μ were measured by filming snakes sliding down an incline of angle ϕ and measuring their displacement x and duration of sliding t. The dynamic friction coefficient was estimated using the implicit relation $x = \frac{1}{2}g(\sin\phi - \mu\cos\phi)t^2$. Frictional anisotropy was measured by placing the snake in one of two orientations on the plane (head up or head down).

3.2.3 Smart-Channel construction

We constructed a rectangular Smart-Channel, 90 cm in length and 4 cm in height, capable of measuring forces applied by the snake. The channel bottom consisted of styrofoam to enable gripping by the snake. Polished wood was used as sidewalls for the channel, as shown in **Fig.3**. The channel top was left open to facilitate filming. Snakes entering the channel from one end readily pressed the sidewalls of the channel in order to climb. Inclination of the channel was adjusted by supporting one end of the channel at variable height. Width of the channel was adjusted by moving the sidewalls and bracing them with an additional wood block held in place by self-weight.

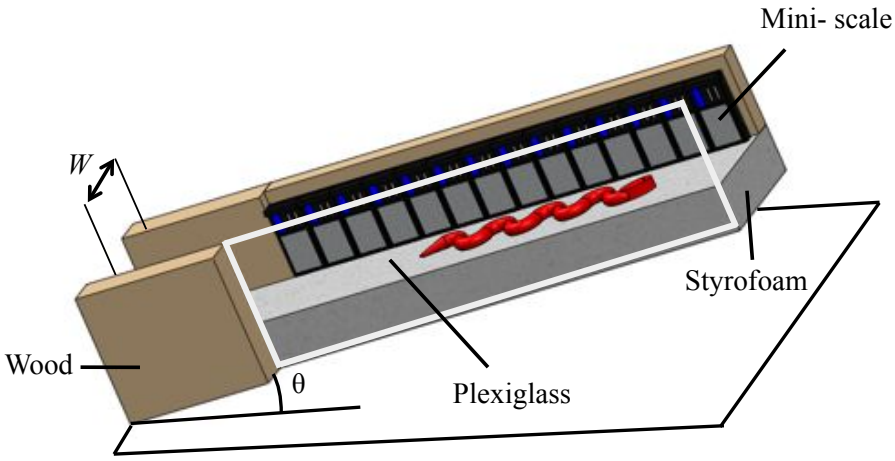

Figure 3: Schematic of the apparatus used to study concertina locomotion. Here θ is the inclination angle with respect to the horizontal and W is the channel width. The front wall is composed of plexiglass. All of the experiments are conducted on Styrofoam.

An electronic "measuring wall" was used to measure the transverse forces applied by the snake to one of the two channel walls. The measuring wall consisted of a linear series of fourteen force sensors with a precision of 0.1 g and a size of 3 x 4 cm (Matchbox digital

mini-scales from American Weigh). During force measurements, the opposite wall of the channel was replaced with transparent plastic to facilitate reading of the force sensors. Thus, during locomotion in the channel, the snake's flanks pressed against three types of materials: the force sensors, wooden sidewalls and transparent plastic. To ensure that the variation in materials did not affect the friction force generated, we measured the static and dynamic friction coefficients on all materials. We observed that flank friction coefficients (both static and dynamic coefficients) on these materials are direction independent. We also found that dynamic friction coefficients on all three materials were comparable (0.19 - 0.31).

3.2.4 Filming

Plan and side views of the channel were filmed using two high definition digital video cameras (Sony HDRXR200). The position and speed of the snake's center of mass were found using MATLAB image processing. Reported body speeds are averages from films of 3 periods of motion.

3.2.5 Statistical Analyses

A two-way ANOVA was used to determine the significance of changing channel width and inclination on the kinematics and performance of corn snakes (N=3) [76]. $P < 0.05$ was used as the criterion for significance. All statistics were performed using the Statistics Toolbox in MATLAB, and the results are summarized in Table 1.

Table 1: Effects of width and slope on kinematics and performance. Tabulated values are given in the form of F(p) where F is the F-statistic and p is the p-value. Bold type indicates statistically significant values.

Variable \ Effect	Width (d.f.=2,6)	Slope (d.f.=2,6)	Width × Slope (d.f.=4,18)
τ	1.65 (0.2204)	**6.41 (0.0079)**	0.29 (0.8779)
ΔL	1.04 (0.3743)	**12.96 (0.0003)**	**3.15 (0.0398)**
$L_{\min}$	**20.48 (0.0000)**	0.56 (0.5806)	0.52 (0.7229)
$L_{\max}$	**13.09 (0.0003)**	**6.31 (0.0084)**	0.90 (0.4852)
$C_{\min}$	**5.36 (0.0149)**	3.03 (0.0735)	0.78 (0.5540)
$C_{\max}$	**94.11 (0.0000)**	2.19 (0.1403)	2.44 (0.0840)
$C_{\min}/C_{\max}$	**12.29 (0.0004)**	**8.99 (0.0020)**	2.52 (0.0775)
V	1.04 (0.3743)	**12.96 (0.0003)**	**3.15 (0.0398)**
$T_{\min}$	3.15 (0.0919)	**20.01 (0.0005)**	0.56 (0.6992)
$T_{\max}$	0.94 (0.4247)	**18.54 (0.0006)**	1.04 (0.4381)

3.3 One-dimensional concertina model

We modeled a snake as a one-dimensional n-linked crawler by discretizing snakes of mass m into n nodes of equal mass m/n. The repercussions of this simplification will be discussed in § 3.4. Nodes are connected in series by $n-1$ inter-nodal lengths $l_i(t)$, whose kinematics will be recorded from our experiments. A schematic is shown in top and side views in **Fig.4**.

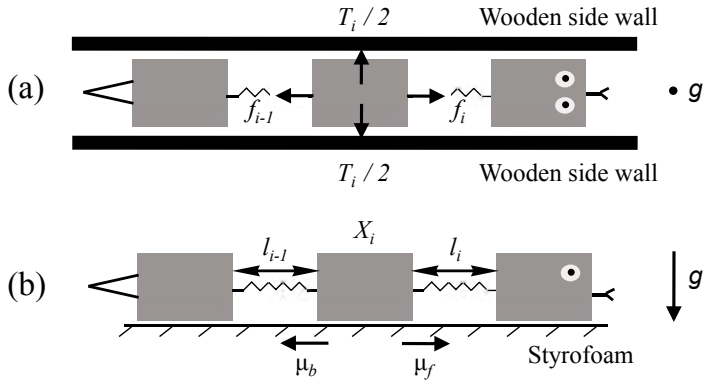

Figure 4: (a) Plan view, and (b) side view of the 3-mass model.

The inputs to our model are the observed extensional kinematics $l_i(t)$, and our output will be the snake's center of mass position $\bar{x}$, defined by

$$l_i = x_i - x_{i-1} \tag{5}$$

$$\bar{x} = \frac{1}{n}\sum_{i=1}^{n} x_i \tag{6}$$

where x_i is the position of the ith node. The kinematics of a node x_i may be written using the relations

$$x_i = \begin{cases} \bar{x} - \frac{1}{n}\sum_{j=1}^{n-1}(n-j)l_{n-j} & \text{if } i = 1 \\ x_{i-1} + l_{i-1} & \text{if } i > 1, \end{cases} \tag{7}$$

which arise from definitions in Eq. (6). To move forward, the snake adjusts the distance between its nodes by applying internal extensile or contractile forces, causing the body to fold or unfold between nodes, which in turn slides the belly along the axis of the channel. We will focus on propulsion based on a single traveling wave of extension, starting from the head and moving towards the tail.

A node's body inertia is balanced by gravitational forces mg/n, frictional forces F_i, and internal forces f_i and f_{i-1} generated by the snake's muscles on either side of node i. Newton's second law applied along the axis of the channel yields

$$(m/n)\ddot{x}_i = F_i + f_i - f_{i-1} - (mg/n)\sin\theta, \tag{8}$$

where $\ddot{x}_i$ is the acceleration of a node along the snake's body and θ is the inclination of the channel.

3.3.1 Friction force

In general, the friction force F_i consists of components associated with the belly and flanks which are the only surfaces in contact with the open-topped channel. Moreover, this friction force has two regimes, static or sliding, depending on magnitude of the internal force applied.

The static friction force is defined according to Coulomb's law. This law states that, at zero velocity, the friction force F_i is equal and opposite to $f_i - f_{i-1} - (mg/n)\sin\theta$ up until the friction is maximized. This yield point is given by the static friction $\mu_{st}(mg/n)\cos\theta + \mu_{st,w}T_i$ where T_i is the force applied to the wall, $mg/n\cos\theta$ is the normal force against the bottom of the channel and μ_{st} and $\mu_{st,w}$ are the static friction coefficients of the belly and flanks, respectively. Static friction between the flanks and the wall, $\mu_{st,w}$, is direction independent, as we confirm in our experiments. However, the static friction coefficient

between the belly and the Styrofoam, μ_{st}, depends on the direction: $\mu_{st,f}$ is the belly static friction in the forward direction and $\mu_{st,b}$ is that of backward direction. Once the snake begins sliding, the friction force decreases, transitioning to sliding friction. For each surface of the snake in contact with the channel, we use a sliding friction law in which the friction force is $F_i = -\mu N \text{sgn}(\dot{x}_i)$ where μ is the sliding friction coefficient corresponding to the two surfaces in contact and N is the normal force applied by the snake to the channel. The sliding friction of the snake's flanks is isotropic and characterized by a single friction coefficient $\mu = \mu_s$. On the belly, sliding friction coefficients in the forward and backward directions are μ_f and μ_b, respectively. Each node applies a normal force T_i on the sidewalls and $mg/n\cos\theta$ on the bottom of the channel. Together, the friction on the snake may be written

$$F_i = \begin{cases} -(f_i - f_{i-1} - (mg/n)\sin\theta), & \text{if } f_i - f_{i-1} - (mg/n)\sin\theta > 0 \\ & \text{and } |f_i - f_{i-1} - (mg/n)\sin\theta| \leq \mu_{st,f}(mg/n)\cos\theta + \mu_{st,w}T_i \\ -\mu_f(mg/n)\cos\theta + \mu_s T_i, & \text{if } f_i - f_{i-1} - (mg/n)\sin\theta > 0 \\ & \text{and } |f_i - f_{i-1} - (mg/n)\sin\theta| > \mu_{st,f}(mg/n)\cos\theta + \mu_{st,w}T_i \\ -(f_i - f_{i-1} - (mg/n)\sin\theta), & \text{if } f_i - f_{i-1} - (mg/n)\sin\theta < 0 \\ & \text{and } |f_i - f_{i-1} - (mg/n)\sin\theta| \leq \mu_{st,b}(mg/n)\cos\theta + \mu_{st,w}T_i \\ \mu_b(mg/n)\cos\theta + \mu_s T_i, & \text{if } f_i - f_{i-1} - (mg/n)\sin\theta < 0 \\ & \text{and } |f_i - f_{i-1} - (mg/n)\sin\theta| > \mu_{st,b}(mg/n)\cos\theta + \mu_{st,w}T_i. \end{cases} \tag{9}$$

The friction force on node i for non-zero velocities may be written

$$F_i = \begin{cases} -\mu_f(mg/n)\cos\theta + \mu_s T_i & \text{if } \dot{x}_i > 0 \\ \mu_b(mg/n)\cos\theta + \mu_s T_i & \text{if } \dot{x}_i < 0. \end{cases} \tag{10}$$

We simplify Eq. (10) by using the Heaviside step function $H(x) = \frac{1}{2}(1 + \text{sgn}x)$ to distinguish the components in the forward and backward directions. Using this notation, the sliding friction force from Eq. (10) may be written

$$F_i = (mg/n)\cos\theta[-\mu_f H(\dot{x}_i) + \mu_b H(-\dot{x}_i)] + \mu_s T_i. \tag{11}$$

For the sake of simplicity (as shown by the relative simplicity of Eq. (11) compared to Eq. (9)), we neglect static friction effects. We will instead use only our sliding friction law given in Eq. (11).

3.3.2 Transverse Force

To capture the snake's behavior of pushing the sidewalls to resist sliding backwards, we make assumptions regarding the magnitude and spatial distribution of the forces applied. First, we assume snakes apply a total transverse force $2T_{\text{wall}}$ sufficient to prevent sliding backwards. Sliding backwards is defined as having an average negative velocity for center of mass over three periods of motion.

Second, we assume only certain parts of the snake apply force. Namely, parts of the snake apply force only if they are sliding backwards. Consequently, the parts moving forward apply zero transverse force.

Third, among the parts of the snake applying force, we assume the force per unit length is constant. We accomplish this uniform transverse force by discretizing the total transverse force into $n-1$ equal portions applied along their points of contact. This assumption is justified because the positions of the force will not affect the speed of the center of mass. Although it may affect the snake's balancing torques, two-dimensional effects are beyond the scope of our model. We will examine the validity of these assumptions in § 3.4.

All our assumptions together yield the following definition for the net transverse force T_i applied by the ith node:

$$T_i = \frac{2T_{\text{wall}}}{n-1} H(-\dot{x}_i), \tag{12}$$

where T_{wall} is the sum of the transverse force applied to a single wall and $\dot{x}_i$ is the velocity of the ith mass.

3.3.3 Governing equation

Using our definitions of kinematics, friction and transverse force, we may proceed with determining the governing equations for our system, specifically, for the position of the snake's center of mass. Substituting (11) into (8) yields

$$\ddot{x}_i = g\cos\theta[-\mu_f H(\dot{x}_i) + \mu_b H(-\dot{x}_i)] + \frac{n\mu_s T_i}{m} - g\sin\theta + \frac{n}{m}(f_i - f_{i-1}). \tag{13}$$

Elimination of the internal forces f_i is accomplished using the definition of center of mass in Eq. (6). Applying the definition of transverse force T_i in Eq. (12) yields

$$\ddot{\bar{x}} = \frac{g\cos\theta}{n}\left[-\mu_f \sum_{i=1}^{n} H(\dot{x}_i) + \mu_b \sum_{i=1}^{n} H(-\dot{x}_i)\right] + \frac{\mu_s 2T_{\text{wall}}}{m(n-1)}[\sum_{i=1}^{n} H(-\dot{x}_i)] - g\sin\theta. \tag{14}$$

Non-dimensionalization of Eq. (14) using the snake's length L and period τ yields

$$Fr\ddot{\bar{x}} = \frac{\cos\theta}{n}\left[-\mu_f \sum_{i=1}^{n} H(\dot{x}_i) + \mu_b \sum_{i=1}^{n} H(-\dot{x}_i)\right] + \frac{\mu_s T}{n-1}\left[\sum_{i=1}^{n} H(-\dot{x}_i)\right] - \sin\theta \tag{15}$$

where Fr and T are the dimensionless groups

$$\begin{aligned} Fr &= \frac{\text{inertia}}{\text{gravity}} = \frac{L}{\tau^2 g} \\ T &= \frac{\text{applied force}}{\text{gravity}} = \frac{2T_{\text{wall}}}{mg}, \end{aligned} \tag{16}$$

whose values will be determined in our experiments. The combination of equations (15) and (7), along with the prescribed kinematics $l_i(t)$, provide a closed system which can be iterated to determine the snake' steady-state speed.

3.3.4 Numerical simulation

Using the state-space form of Eq. (15), the acceleration, velocity and position of the center of mass are calculated in MATLAB. We apply the Dormand-Prince pair method, a member of the Runge-Kutta family of ordinary differential equation solvers, to find the solution of Eq. (15) numerically. The Dormand-Prince pair method uses six function evaluations to calculate fourth and fifth-order accurate solutions [77]. Using a time step $\Delta t = 10^{-4}$, we solve Eq. (15) iteratively to determine the position of the snake's center of mass $\bar{x}(t)$. We assume the snake applies a constant transverse force during its period, and use our numerical solution to calculate the magnitude of the force T_{wall}. This magnitude is the minimum value of T_{wall} for which snake velocity is positive, and is found by starting with a guess of $T_{\text{wall}} = 0$ and increasing T_{wall} in steps of 0.1 snake weights.

3.3.5 Energetics

Using the energetics of our one-dimensional model, we now examine how channel width and inclination can affect snake kinematics. During a period τ, the average power P of a snake performing concertina motion is given by the time rate of change of its kinetic energy P_{kinetic}, gravitational potential energy P_{gravity}, and frictional dissipation D_{fric}. This summation may be written

$$P = P_{\text{kinetic}} + P_{\text{gravity}} + D_{\text{fric}}. \tag{17}$$

We estimate these rates of working in Eq. (17) by first estimating the corresponding instantaneous energy states. The kinetic energy of the ith segment of the snake is $(1/2)m_i V_i^2$ where m_i and V_i are its mass and velocity. The gravitational energy of a segment is $m_i g z_i$ where z_i is the vertical displacement. The frictional energy dissipation of a segment is $m_i g \cos\theta (\mu_t s_t + \mu_f s_f)_i$ where μ_t and μ_f are friction coefficients in the transverse and forward directions and s_t and s_f are the corresponding displacements in these directions.

Backwards friction is not used to dissipate energy because we assume the snake is moving forwards.

All together, the rate of change of these energies for n segments over period τ is given by

$$P \approx \frac{1}{2\tau}\sum_{i=1}^{n}(m_i V_i^2) + \frac{g}{\tau}\sum_{i=1}^{n} m_i z_i + \frac{g\cos\theta}{\tau}\sum_{i=1}^{n}\left[m_i(\mu_t s_t + \mu_f s_f)_i\right]. \quad (18)$$

The power associated with kinetic energy P_{kinetic} will vanish because each point on the body is periodically at rest. Since $\sum_{i=1}^{n} m_i z_i = m z_c$ where $z_c = \sin\theta\Delta L$ is the vertical displacement of center of mass, the rate of change of gravitational energy may be simplified to $mg\sin\theta\Delta L/\tau$. To provide an upper bound for power, we note that the maximum axial displacement during a period is ΔL and the maximum transverse displacement is equal to the channel width w. Eq. (18) may be approximated as

$$P \leq \frac{mg\sin\theta\Delta L}{\tau} + \frac{mg\cos\theta(\mu_f\Delta L + \mu_t w)}{\tau}. \quad (19)$$

At high inclinations, the most significant term in Eq. (19) is the one involving gravity. The friction dissipation is of secondary importance because its multiplication by friction coefficients of order 0.2-0.4. Moreover, as illustrated in Appendix B.4, snakes regularly lift parts of their body during concertina locomotion, presumably to reduce the friction dissipation and the associated skin wear. According to Eq. (19), in order to maintain constant power during climbing of steeper slopes (larger θ), the snake should increase its period τ and decrease its body extension ΔL, a prediction we will test in § 3.5.2.

3.4 Justification of assumptions in our model

We use our experimental observations to justify the assumptions in our model. Specifically, we provide evidence that (1) an adequate number of nodes n is three and (2) the motion of the center of mass can be approximated as one-dimensional.

3.4.1 Node number depends on incline angle

Fig.5a shows a series of body shapes of a corn snake moving through a channel of width 2 cm. Segments of the snake's body have two possible configurations, extended, where the body is mostly straight, or contracted, where the body folds into a series of bends whose apices contact the channel walls. These contact points are the source of anchorage forces for the snake and so are dynamically important in our model. The number of contacts with the walls (**Fig.6**b) varies from a minimum value, $C_{\min} = 5-7$ when the snake is in a contracted configuration, to a maximum value, $C_{\max} = 7-15$ when the snake is extended.

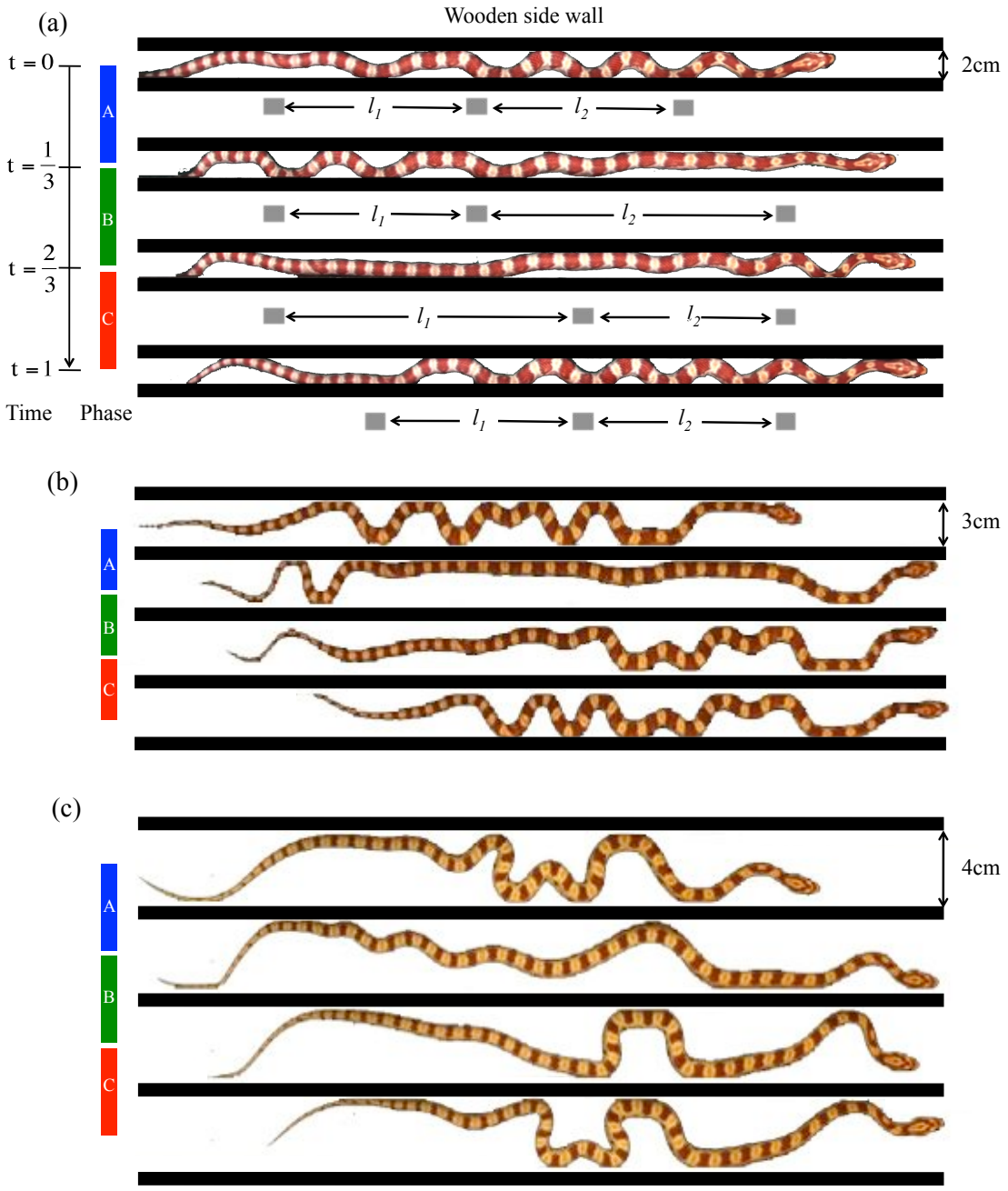

Figure 5: (a-c) Video sequences of corn snakes performing concertina locomotion in channels of 2 cm, 3 cm and 4 cm width. Three phases of concertina locomotion are highlighted in each video sequence.

Fig.6d shows the ratio of the minimum to the maximum number of contact points with the sidewalls, $C_{\min}/C_{\max}$. This ratio may also be approximated by $\frac{n-1}{n}$, where n is the number of nodes in our model. Notably, on horizontal surfaces for all three channel spacings, this ratio is constant ($\frac{n-1}{n} = 0.62 \pm 0.16$). Consequently, a good approximation for n is 3

and we model the snake as 3-link crawler.

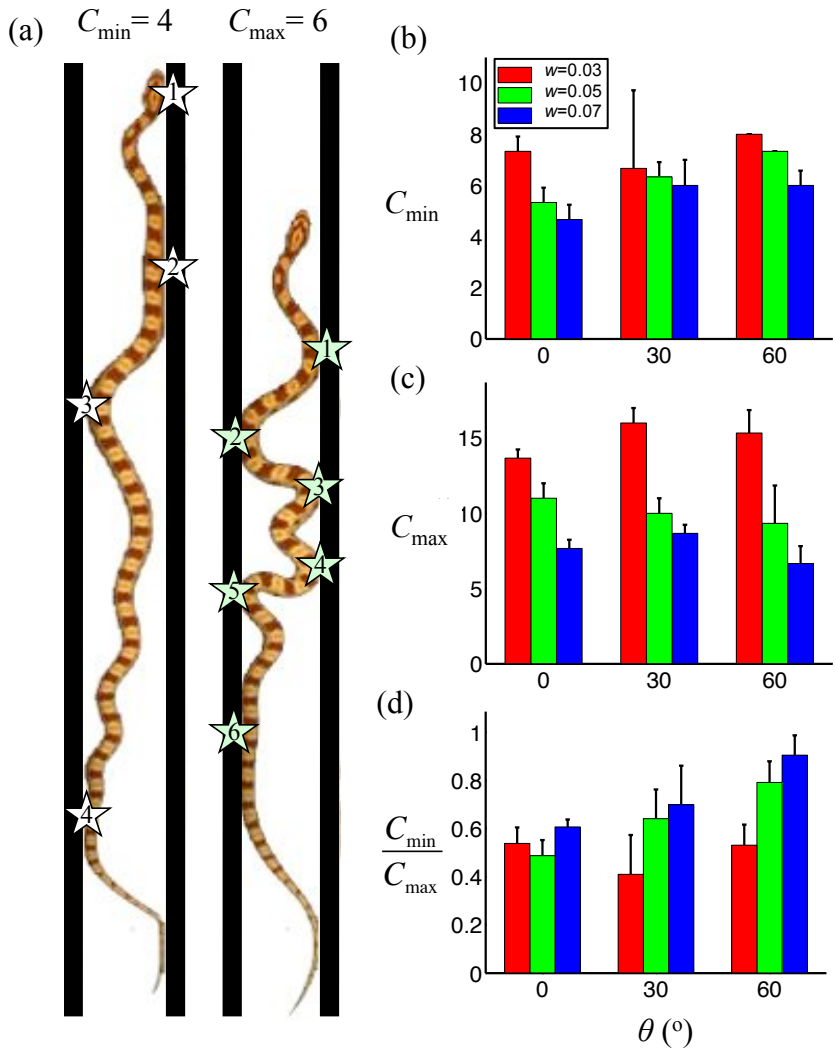

Figure 6: Total number of contact points of the snake with the channel walls. (a) Minimum and maximum number of contacts for a corn snake performing concertina locomotion in a horizontal channel of width 4 cm. (b-c) Minimum and maximum number of contact points and (d) their ratio, as a function of channel width and inclination. As shown in (a), a corn snake moving in a horizontal channel of 4 cm width makes minimum of 4 and maximum of 6 contacts with the sidewalls.

We note that the number of nodes is strongly affected by inclination. For higher inclinations, C_{min}/C_{max} varies between 0.4 - 0.9, suggesting that a 4 or 8-mass model may be a better model for higher inclinations. Physically, this behavior makes sense as the snake is using more transverse force on steeper slopes to avoid slipping. By increasing the number

of contacts during locomotion, the snake can have more points of support and so less transverse force per contact. Nevertheless, for simplicity, we fix the number of masses as n=3 throughout this discussion.

3.4.2 Center-of-mass moves one-dimensionally

Fig.7a-b indicate the axial ($\bar{x}$) and transverse ($\bar{y}$) position of the snake's center of mass in a channel of 2 cm over 10 periods. The snake moves at constant velocity in the x-direction. Notably, displacement of the center-of-mass in the y-direction is less than 10% the width of the channel. These features are consistent with extension and contraction of the body in one-dimension.

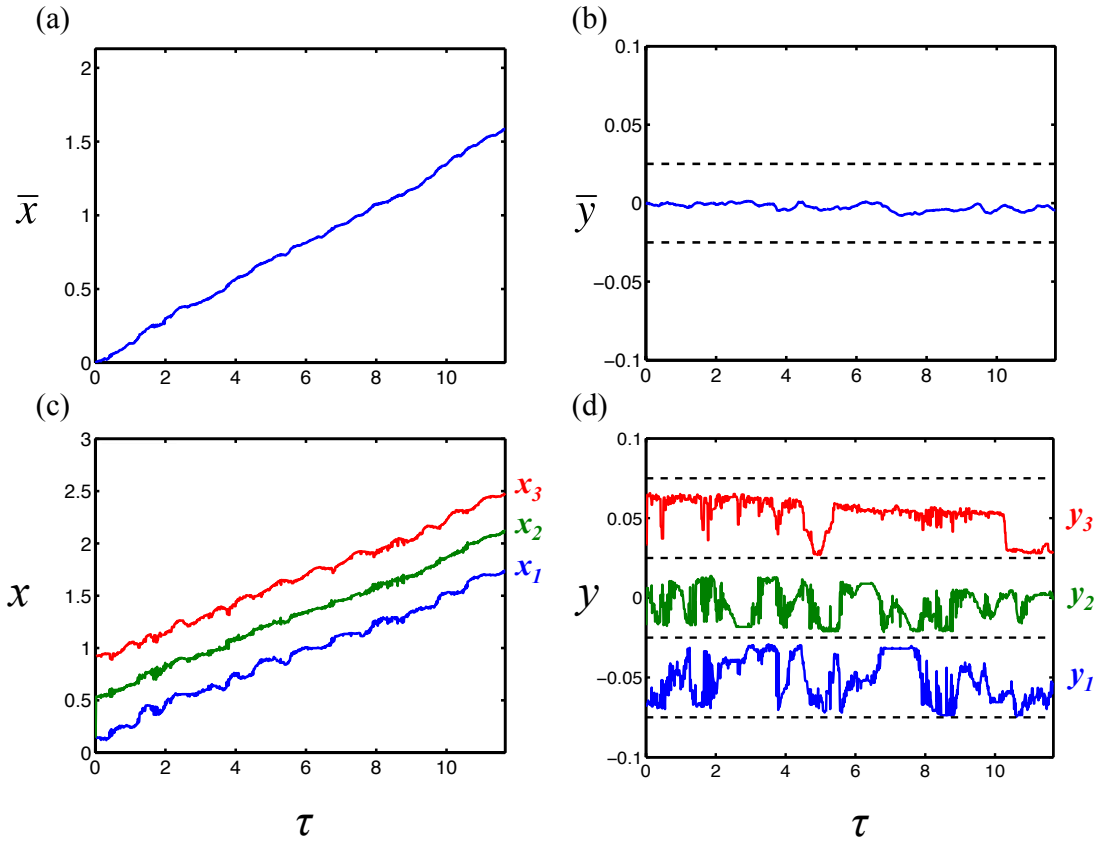

Figure 7: Dynamics of center of mass motion in a horizontal channel of width 2 cm. (a) Axial and (b) lateral positions of the snake center of mass. (c) Axial and (d) lateral positions of three points on the snake (1: posterior section, 2: mid section, and 3: anterior section of the snake body) as a function of time in dimensionless units. The channel sides are shown in (b,d) using dashed lines. The curves y_1 and y_3 in (d) are offset vertically by -0.05 and 0.05, respectively.

Although the motion of the center of mass is one-dimensional, this is not the case for the individual parts of the snake. **Fig.5**a shows the center of mass of each third of a snake in a 2 cm channel. Transverse motion is clearly necessary in order for the snake to make contact with the channel sidewalls, as shown by the transverse undulations of each third of the snake. Further observation indicates that concertina, like other snake gaits, is strongly three-dimensional, a feature of the locomotion which has received little attention in the literature. Appendix B.4 shows side and top views of a corn snake performing concertina in which it lifts portions of its body while extending them forward. This behavior is favorable if the energy required for lifting, $m_i g z_i$, is less than the energy dissipated due to sliding forward, $\mu_f m_i g \cos\theta s_f$. Nevertheless, for simplicity we neglect two or three-dimensional motions in our model.

3.5 Results

We present experimental and computational results of our study in § 3.5.1 - 3.5.5. We first discuss our measurements of corn snake frictional properties, body kinematics, force applied to channel sidewalls and snake speed. In the data reported in **Fig.9**-**Fig.14**, we non-dimensionalize length according to the snake length L, time by the snake period τ, and transverse force by the snake weight mg. The dimensionless position and time are defined as $x = x^*/L$ and $t = t^*/\tau$, respectively where x^* is dimensional position and t^* is dimensional time.

3.5.1 Snakes double their friction coefficients

We observed that snakes can actively orient their scales to prevent sliding down an incline. **Fig.8**a-c shows a corn snake digging its scales into the bark of a tree, enabling it to remain vertically perched for long periods of time. **Fig.8**d-e shows a conscious snake atop styrofoam angling its scales to resist being pulled by its tail. Appendix B.1, and video frames given in **Fig.8**f-g, show a snake performing concertina locomotion up a styrofoam plane inclined at 35°. On slopes of this inclination, uphill locomotion is precarious and the snake often loses its grip and begins to slide. To resist sliding, the snake freezes its body in an S-shaped "emergency braking" configuration causing the snake's ventral contact with the ground to be limited to a few discrete points. It is noteworthy that none of the mechanisms in **Fig.8**a-g are observable on unconscious snakes, suggesting that these responses are consciously rather than passively activated.

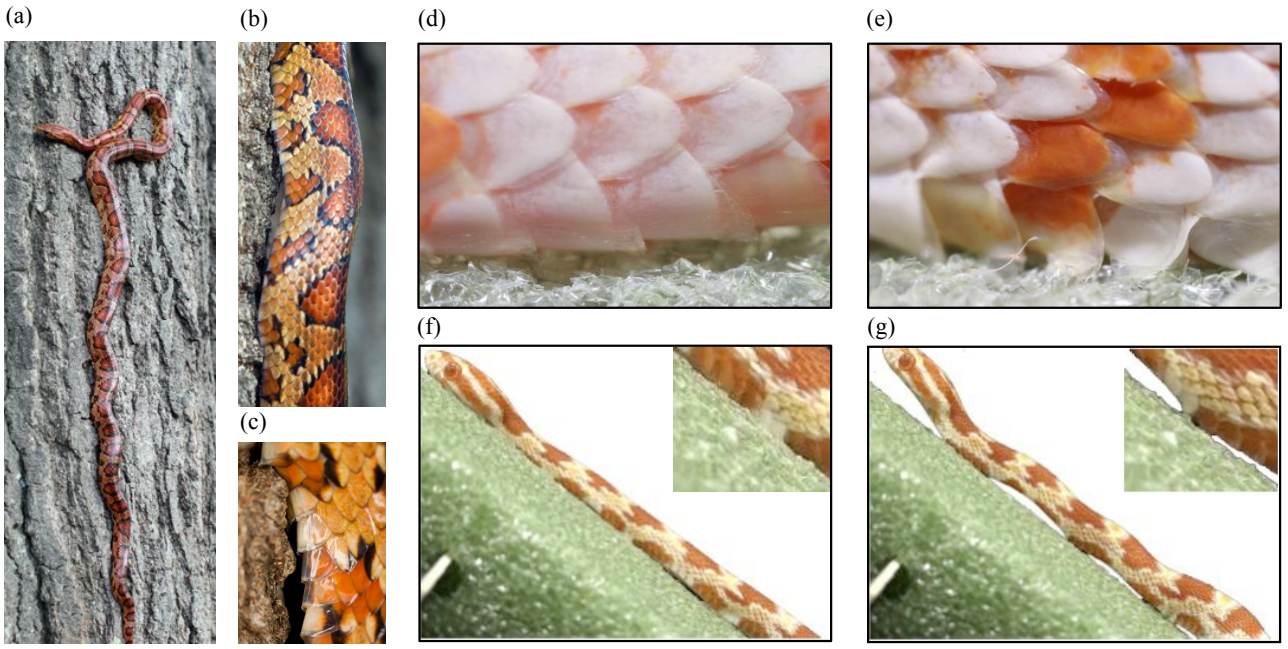

Figure 8: (a) A corn snake ascending a tree. (b-c) Scales are used to grip tree bark asperities. Snake scales at their (d) minimum and (e) maximum angles of attack (flat). (f-g) A snake climbing an inclined surface. Sliding is prevented by emergency braking associated with lifting of the body.

Previous methods to measure friction have relied upon unconscious snakes [17, 65], which cannot capture the control of scales we have observed. Consequently, we measured the dynamic friction coefficients of both unconscious and conscious snakes. Table 2 lists the dynamic and static friction coefficients for both conscious and unconscious snakes. The coefficients for unconscious snakes depict a snake's resistance to sliding if it were unable to activate its scales. We calculated the p-value for friction coefficients of conscious and unconscious snakes in forward (p=0.02) and backward directions (p=0.0004). The P-value indicates that it is with over 98% probability that the friction coefficients of unconscious snakes are greater than or equal to those of conscious snakes [76].

We found static friction coefficients for conscious snakes were double the corresponding coefficients of unconscious snake (Table 2). Physically, this meant that conscious snakes could maintain their positions on 41° inclines, compared to 19° for their unconscious counterparts. Differences in sliding friction coefficients were not as high: conscious snakes had coefficients nearly 30% higher than their unconscious counterparts. On rougher surfaces, it may be possible for snakes to further increase their friction coefficients.

Table 2: Static and dynamic friction coefficients of (a) conscious and (b) unconscious corn snakes on a styrofoam substrate.

(a)

Friction type / Direction	Static	Dynamic
Forward	0.51 ± 0.08	0.49 ± 0.09
Backward	0.88 ± 0.04	0.79 ± 0.04

(b)

Friction type / Direction	Static	Dynamic
Forward	0.3 ± 0.08	0.21 ± 0.03
Backward	0.35 ± 0.03	0.35 ± 0.06

3.5.2 Kinematics of concertina motion

Image processing was used to partition the snake into equal thirds which we refer to as the head, middle and tail. As an example, we use the motion of a snake moving through a 2-cm channel in **Fig.5**a. The center of mass position of each third is shown by the gray blocks. The kinematics of the snake is given by the inter-nodal distances, l_1 and l_2, which the snake adjusts by folding and unfolding. We divide the snake's period into three phases (A, B, and C), as shown in **Fig.9**. The cycle begins with the snake extending its head in phase A, which is accomplished by bracing the middle and rear parts of its body firmly against channel walls. In phases B and C, the snake's middle and rear, respectively, are drawn forward to meet its head.

The time course of l_1 and l_2 is shown by the circles and diamonds in **Fig.9**. We roughly approximate ($R^2 = 0.45$) the waveforms using two triangle waves of period τ, and a phase difference $\tau/2$. These waves have amplitudes bounded between $L_{\min}/n$ and $L_{\min}/n + \Delta L$, corresponding to the snake's contracted and extended body configurations. Using image analysis, we measured the periods and amplitudes of the corresponding triangle waves for all snakes filmed for snakes over range of inclines (0, 30, and 60°) and channel widths (2,3 and 4 cm).

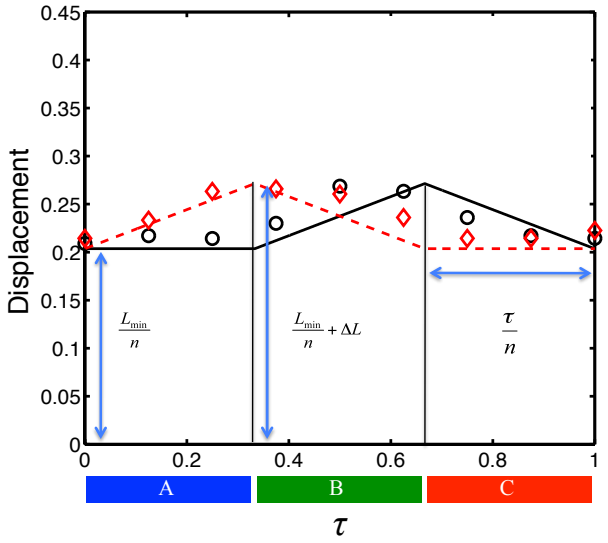

Figure 9: Inter-nodal distances l_1 and l_2 given in terms of the kinematic parameters. Circles and diamonds are the experimental data for l_1 and l_2, respectively. Solid and dashed lines are the corresponding approximate waveforms used in the model.

Fig.10a shows the changes in period τ over a range of inclinations and channel widths. We observed τ increases significantly with increasing inclination. Specifically, snakes moved slower on increasing inclinations: periods increased from 3 to 6 seconds as inclination increased from 0 to 60° at a channel of width 4 cm. This slower climbing is qualitatively consistent with the greater energy needed to climb higher inclinations. By climbing more slowly at higher inclines, snakes can keep their power use constant, as previously predicted in § 3.3.5.

Fig.10c shows that extensional length ΔL is significantly reduced by increasing channel inclination (p=0.0003). **Fig.10**c,d shows that contracted lengths L_{min} and extended lengths L_{max} are highly dependent on channel width. For the thinnest channels, snakes exhibited L_{min} values of 0.8 snake lengths, which decreased to 0.68 for the widest channels. This decrease in contracted length with wide channels is due to a snake's finite length: as channels widen, a snake cannot reach as far along the channel while simultaneously maintaining its contact points with the sidewalls. For instance, in horizontal channels of 5 cm width, snakes make fewer than seven contact points with the walls, which is fewer than the observed maximum of 15 contacts in 2 cm wide channels. Snakes in 5-mm or wider channels often abandon concertina motion and resort to slithering motion as shown in Appendix B.3.

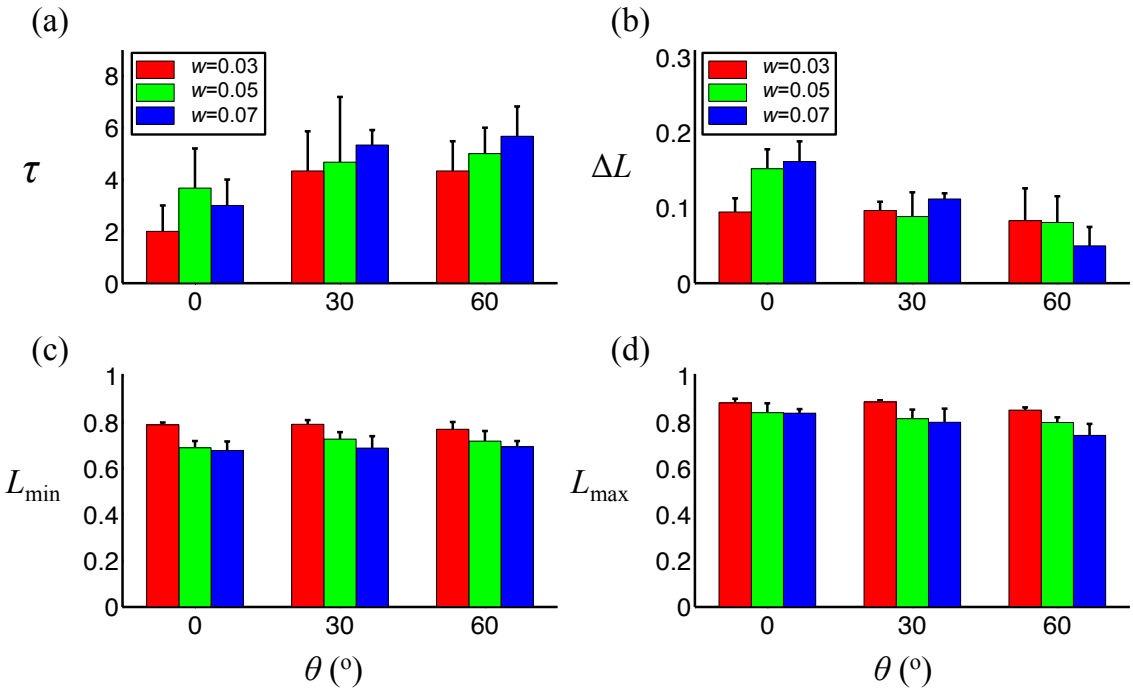

Figure 10: (a) Period, (b) normalized ΔL, (c) normalized minimum length, and (d) normalized maximum length of corn snakes as a function of slope and non-dimensionalized channel width.

3.5.3 Body speed

Fig.11a shows measurements of body speed $\bar{V}$. Clearly, snake speed is significantly affected by channel slope (p = 0.0003). Speed $\bar{V}$ decreases from 0.17 to 0.05 as channel inclination increases from horizontal to 60°. For comparison we also include snake speeds measured by Jayne [1] on horizontal surfaces of various channel widths, as shown by the open circles. The correspondence between our experimental results and others is good, despite the different snake sizes and species used by Jayne (*Nerodia fasciata* and *Elaphe obsoleta* of lengths 100 cm and 159 cm, respectively). This correspondence suggests that snakes of a variety of sizes and species may use similar kinematics to move through channels.

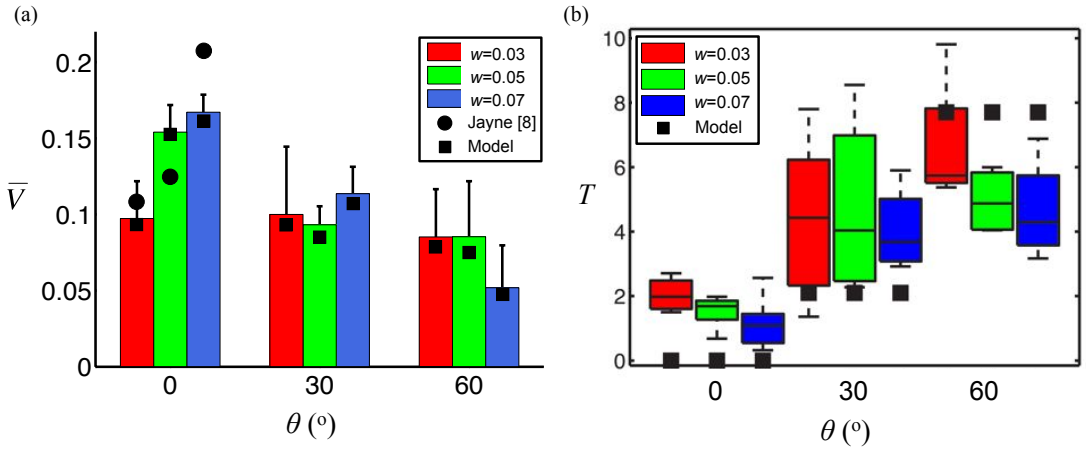

Figure 11: (a) Speed and (b) applied transverse force as a function of slope and channel width. Model predictions are given by black squares; velocities measured by Jayne [1] are given by black circles for comparisons.

To check consistency of our model, we also plot in **Fig.11**a speed predictions from our theoretical model. Speed is calculated using Eq. (15) using the methods described in §3.3.4. The speed predicted is based on the assumption the snake applies sufficient transverse force to prevent backwards sliding. As a result the predicted speed corresponds roughly to the ratio of the extension ΔL to the period τ:

$$\bar{V} = \frac{\Delta L}{\tau}. \tag{20}$$

Differences between the predicted speed and Eq. (20) result from the snake sliding backwards due to our modeling of sliding rather than static friction. Comparisons between our model and experiments are favorable suggesting that our model is consistent with the locomotion observed.

Our model can also predict the variation of snake speed with frictional anisotropy. This trend would be more difficult to study experimentally as it would require experiments with new substrates such as styrofoam of varying roughness. We examine in **Fig.12**a the predicted speed of a 3-mass snake model in a horizontal 3-cm channel. In our experimental data on styrofoam, the backward sliding friction is 1.6 times greater than forward friction. In fact, this is the optimum anisotropy for a snake. Below this anisotropy, the snake slides backwards and must modulate body kinematics to maintain its position. Above this anisotropy there is a negligible 3% gain in speed.

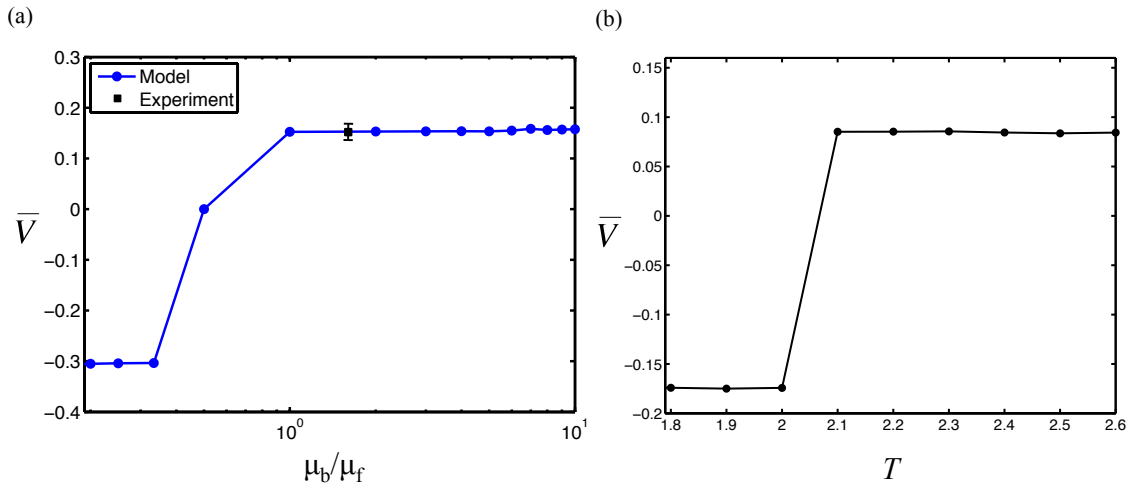

Figure 12: (a) The velocity of center of mass as a function of dynamic friction anisotropy $\frac{\mu_b}{\mu_f}$ in a horizontal channel of 3 cm width. (b) The velocity of center of mass as a function of transverse force T for a channel of width 3 cm and inclination of 30°. Note: the negative velocities are not steady-state velocities, but represent average values over three periods of motion.

3.5.4 Measured transverse force

We measured the transverse force applied by the snake over a range of channel widths and inclinations. **Fig.13** shows the forces applied to one wall of a channel (of width 3 cm, inclination 30°). The snake's instantaneous body configurations are shown in the insets of **Fig.13**, and show clearly that peaks in force are associated with kinks in the snake. Individual wall contacts have an associated force magnitude ranging from 0.5 - 1.5 snake weights. The tips of the snake's head and tail applied a transverse force less than the resolution of our sensors (1 mN).

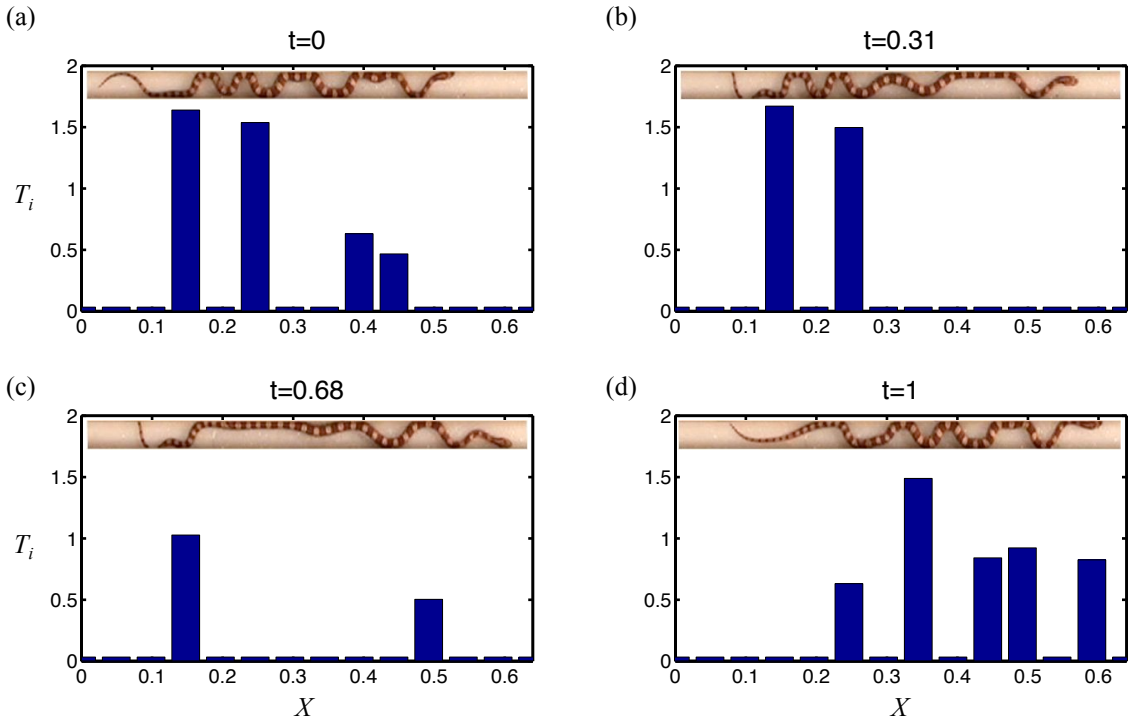

Figure 13: The transverse force applied by a corn snake, as a function of time and position along the body. The channel has a width of 3 cm and inclination of 30°. Plots (a)-(d) show instantaneous force profiles during one period of motion. Insets show the corresponding body shape of the corn snake.

We observed the segments of the snake remained stationary when applying force to the sidewall. We can thus apply Newton's 3rd law to infer that the force applied to the opposite wall was equal in magnitude to that measured. This observation justifies the use of Eq. (12) in our modeling section.

The solid line in **Fig.14** shows the time course of the total applied force T associated with the snake in **Fig.13**. The applied force T is double that measured on one wall of the channel and is non-dimensionalized by the snake weight. The dotted line shows the minimum applied force (two times body weight) required to prevent sliding. Clearly, the snake is pushing with greatest force (8 times body weight) in phases A and C, when moving either its head or tail. It pushes with least force (2 times body weight) in phase B, when moving its middle.

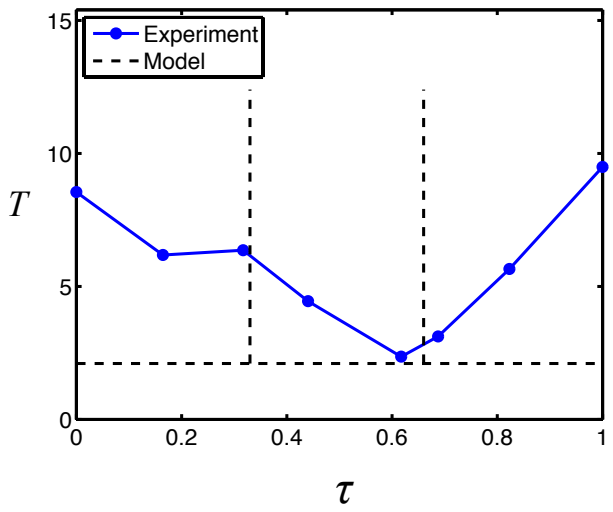

Figure 14: Time course of the transverse force applied by a corn snake (solid lines). Dashed lines show the model predictions for the minimum required transverse force to prevent sliding. The channel has a width of 3 cm and inclination of 30°.

We measured the minimum and maximum force applied by the snakes across a range of channel widths and inclines. The box and whiskers plot in **Fig.11**b shows the range of forces measured. Transverse forces increase significantly with increasing inclination angle. At 60° and a channel width of 4 cm, transverse pushing forces increase to 400% of the value measured on a horizontal surface (from $T = 0.9$ to 3.6).

3.5.5 Predicted transverse force

The dashed lines in **Fig.14** shows the time course of our predicted transverse force, which is the minimum force to prevent sliding backwards. The force is calculated by integrating Eq. (15) using the snake's measured kinematics and friction coefficients for a channel of 3 cm width and 30° inclination. The minimum required force averaged over the period is $T = 2.1$ snake weights. This magnitude is constant within each phase (A-C) of locomotion, as the snake is moving at a steady-state speed. However, additional force must be applied at the transition between phases, when the snake accelerates one part of its body and decelerates another. This additional force is manifested as delta functions because our kinematic input is characterized by triangle waves which contain discontinuities in slope.

Fig.12b shows the sensitivity of steady-state velocity to the magnitude of the normal force. For applied forces less than 2.1 times snake weight, the snake will slide backwards. Thus, it is of utmost importance that the snake's applied force exceeds this threshold. As we shall see snakes appear to apply a factor of safety in order to avoid being below this

threshold.

Square points in **Fig.11**b represent force predictions from our model for various inclines. Our model performs well in predicting the transverse force at inclinations of 30 and 60°. On horizontal surfaces, snakes appear to be pushing with more force than necessary. We surmise that the additional transverse force applied by the snake act as a factor of safety.

3.6 Discussion

3.6.1 Active control of friction

An important and surprising finding of our study was that snakes can double their friction coefficients on styrofoam by active control of their scales. This ability may extend to materials in the snake's habitat, as shown by our qualitative experiments with tree bark. Future investigators of snake locomotion should choose their test surfaces carefully as snakes have tremendous control of their friction over certain surfaces.

Previous literature on snake locomotion neglects discussion of active control of friction, possibly for several reasons which we speculate on here. Traditionally, measurement of friction coefficient was performed on unconscious snakes. Furthermore, these measurements were done using man-made materials such as glass, sand paper, and wood [65]. Such surfaces are not sufficiently rough and compliant as the rough nappy materials found in nature, which in our observations generate high anisotropy. Previous studies in which friction coefficients were measured on smooth surface have importance in their own right, as they demonstrate the range of snake adaptability. As we saw in our model, a snake climbing a channel uses both belly friction and flank friction from transverse pushing. If the former is insufficient, the snake will compensate with increased pushing, and vice versa.

3.6.2 Safety factors in concertina motion

Over six decade ago, Gray [71] and Jayne [72] reported that pushing channel sides was a necessary part of concertina motion. A key result of our study is our measurement of the transverse force applied. While force platforms are quite typical in studies of legged locomotion [78], they are quite rare in limbless locomotion, with the exception of the measurement of caterpillar [79] and earthworm forces [8].

We observed that snakes can push sidewalls with up to 9 times their own weight and with a safety factor of 400% relative to the minimum force to prevent sliding. Such a large safety factor has been observed by previous workers for studies of gripping. Johansson *et al.* studied the grip force applied by human hand to rough as well as slippery objects [80]. They found a human hand applies grip force with a safety margin of around 175% (for

lifting an object weighing 400 g). They emphasize that the lower the friction coefficient of the object, the higher the factor of safety.

What are the limits of concertina locomotion? The steepest incline climbable depends on the limits of the snake's transverse force. In studies of earthworms, Quillin reports a maximum radial force of 10 times body weight for a 6 g earthworm in a horizontal burrow of 0.6 worm diameters [8]. This value is comparable to the snake's pushing ability (9 times body weight), suggesting the possibility of a universal law across scales. In a much narrower burrow of 0.97 worm body diameters, the radial force drops to only 1.5 times the earthworm weight [8]. In comparison, we find snakes are more effective in narrow channels: they have no problem applying forces 9 times their weight. The snake's bending of the body into folds thus appears to be a robust method for generating transverse force across channel widths.

During concertina on steep inclines, snakes appear to be approaching their limits of transverse force. We observed a corn snake performing concertina while dragging a load. In a channel of width 3 cm and slope 30°, a corn snake pushed transversely with 11 times its weight while dragging axial loads of 2.5 times its weight. This transverse force is only 30% more than the corresponding maximum of transverse force (2-8 times its weight) without a load.

3.6.3 The need for higher dimensional models

The main contribution of our simple model is the ability to compare quantitatively the contributions of ventral friction to transverse pushing. Such comparisons would be more difficult to do experimentally. Since there is no closed-form analytical solution for Eq. (15), we presented numerical integration methods to determine these trends, which may be of use to other investigators studying climbing.

Our model could be improved in several ways to decrease its error and to provide further insight into the mechanisms underlying concertina motion. First, our model does not consider the effect of body lifting and lateral motion which clearly have effects on energy consumption, as discussed in § 3.3.5. A 3-D model involving friction has not been attempted, although 3-D models assuming infinite friction have been developed for sidewinding [81]. Perhaps similar methods may be applied to concertina motion.

Stochasticity or behavioral matters will need to be taken into account if a higher dimensional model is implemented. In our experiments we observed body segments often move transversely in an irregular manner (see **Fig.7**d). The source of this irregularity is unclear. We speculate that small changes in channel width or roughness may cause the snake to

choose one side of the channel over another. The head or tail of the snake often clings preferentially to one side of the channel for several periods at a time. For example, the head is slid along the left side of the channel for most of the 10 periods shown in **Fig.7**d. One mechanical advantage of this behavior is the channel walls provide stability during forward motion. Biologically, the preference for one side of the channel is consistent with the view that snakes have a "handedness" [82, 83].

Finally, because our model neglects static friction, it cannot capture the stick-slip phenomena that we observed in our experiments. We have implemented static friction in a model for Scalybot, a 2-segment snake robot [53]. We are currently working on a generalized static friction model for nodes of higher order using Eq. (9). We are also currently studying the mechanics of a single scale's stick-slip phenomena.

3.7 Summary and future directions

We performed a series of experiments to measure frictional properties of snakes and their kinematics when climbing in a channel. A theoretical model was used to predict the snake's transverse force. Using this prediction, we were able to measure the snake's factor of safety in generating these transverse forces.

In summary, like most kinds of snake locomotion, propulsion through channels relies heavily on frictional effects. A snake propels itself in a channel using a series of extensions and contractions, in which a portion of its body extends forward while the remainder anchors. We found anchorage relies on two mechanisms to augment friction: (1) transverse pushing against channel walls and (2) the control of belly scales to grip the bottom of the channel. The former is an active mechanism requiring energy. The latter is a passive structural means of achieving anchorage, whereby force is mediated by the snake's weight. These dual anchorage methods are necessary to overcome the challenges of climbing uphill. On slopes of increasing inclination, anchorage via belly friction becomes less effective due to the decreasing normal force between the belly and the channel bottom. Consequently, snakes tend rely upon belly friction when traveling on horizontal surfaces and transverse pushing when on steep slopes.

CHAPTER IV

SCALYBOT: A SNAKE-INSPIRED ROBOT WITH TEMPORAL AND SPATIAL CONTROL OF FRICTION

4.1 Introduction

Designing an all-terrain robot is a challenging task that has drawn the attention of roboticists, biologists and applied mathematicians. Such a robot has a variety of applications, from interplanetary exploration, exploration within the human body as in "robotic colonoscopy" [12], and search-and-rescue missions beneath the rubble of collapsed buildings [10]. One challenge for such robots is overcoming slopes of varying inclination. Steeper slopes are more difficult to climb because of the reduction in friction force with the underlying surface and the consequences of losing one's grip and sliding down the slope.

Previously built bio-inspired climbing robots rely upon successful functionalities observed in their biological counterparts. For climbing smooth surfaces like glass, Geckobot [84] relies upon suction cups and Stickybot [85] upon directional dry adhesives such as found in gecko feet. For climbing rougher surfaces like brick, Spinybot [86, 87] uses spines to dig into asperities. The range of such legged robots is limited by their inability to cross large obstacles in their path, move through crevices smaller than their body width and transition from horizontal to vertical surfaces. Overcoming these limitations will require a climbing robot that marries anchoring abilities with snake-like flexibility. This ability is clearly observed in certain snakes, which are known to climb up trees as shown in **Fig.15**a.

The versatility of snakes across a range of topography, inclination and surface textures has drawn much interest over the years towards building snake-like robots. Reviews of snake-like robots are presented by Hirose and Hopkins [88, 89], which categorize snake-like robots into those with free-rolling or motorized wheels, those with motorized tank treads, or extensible bodies relying upon vertical waves or linear expansions [89]. Wheels provide the snake-like robots with a forward-transverse frictional anisotropy associated with the wheel's relative ease of rolling forward compared to sliding sideways. However, a reliance on wheels prevents most robots from climbing slopes (with an exception provided by Choset [39], whose robot can climb both poles and vertical channels).

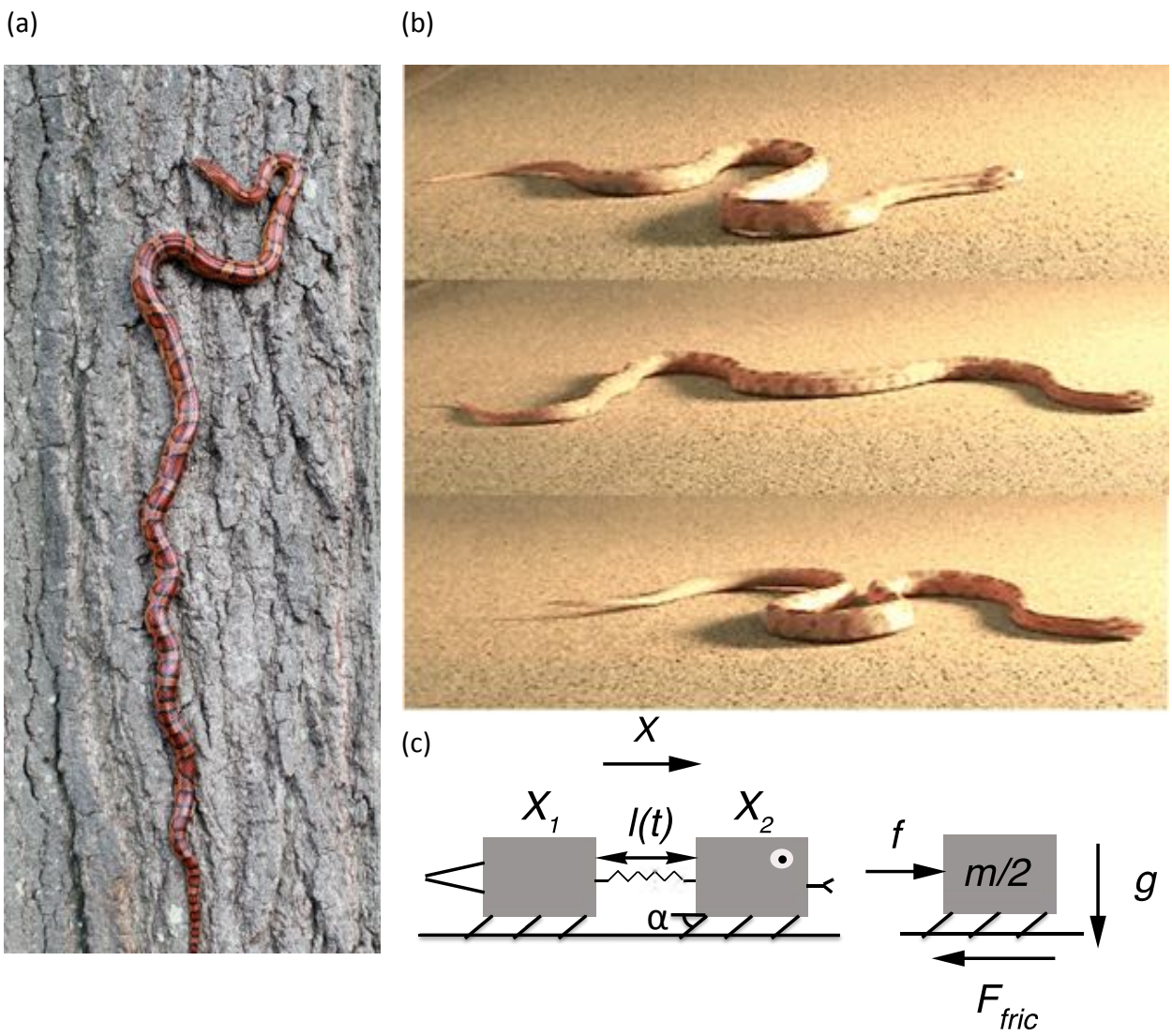

Figure 15: (a) A corn snake climbing a tree. (b) The image sequence of the concertina locomotion of a corn snake. (c) The corresponding 2-mass model describing Scalybot's dynamics.

Few attempts have been made to design artificial snake scales to aid the locomotion of snake-like robots uphill. Dowling [40] used plain spandex, sequins, and polyethylene braids for providing purchase in his snake-like robot. Recent work indicates that such an approach may be potentially valuable to robotics: In experiments of live snakes over flat surfaces, Hu *et al.* [17] found the scales of snakes provide a frictional anisotropy that aids slithering locomotion over flat surfaces.

The goal of the current study is to determine if this paradigm of locomotion-via-scales

has potential for improving the climbing ability of snake-like robots. We begin by reporting our methods for robot construction, friction measurement and testing. We proceed with a theoretical model for the robot's locomotion. Numerical results of this model are then presented along with our experimental measurements of the robot's motion. We close with a discussion of the limitations of our model, an evaluation of the robot's performance and suggestions for its improvement and incorporation of its design into other snake-like robots.

4.2 Methods

4.2.1 Building Scalybot

We have designed our robot to mimic a "concertina" mode of locomotion in which the body is sequentially extended and contracted, as shown by a corn snake in **Fig.15**b. The simple kinematics of concertina motion is similar to that of inchworms or earthworms, which can be crudely considered as having one degree of freedom, the length of their bodies. Propulsion consists of two phases. In the first, tail is anchored while the head is pushed forward (**Fig.15**b). In the second, the head is anchored while the tail is pulled forward. This "ratcheting" is fundamentally a slow process because of the loss of body inertia due to decelerating and anchoring each part of the body. However, the simplicity of the associated kinematics will allow us to highlight the importance of the belly scales during propulsion.

We based our robot's scales on those of a corn snake. A snake's belly scales resemble the overlapping shingles of a house. This geometry provides the snake with a preferred direction of sliding: the scales slide easily over surfaces when the snake slithers forward (**Fig.16**a), but dig in when the snake is gently pulled by its tail (**Fig.16**b). The friction anisotropy of dead snakes was first reported by Gray and Lissman [65]. They measured dynamic friction coefficients of grass snakes on several materials. Based on their experiments the friction anisotropy (ratio of backward to forward friction coefficients) on dry metal is 1 and on rough sand paper is 4.8. Although not obviously critical on horizontal surfaces, we shall see in our experiments that this level of anisotropy is useful for climbing.

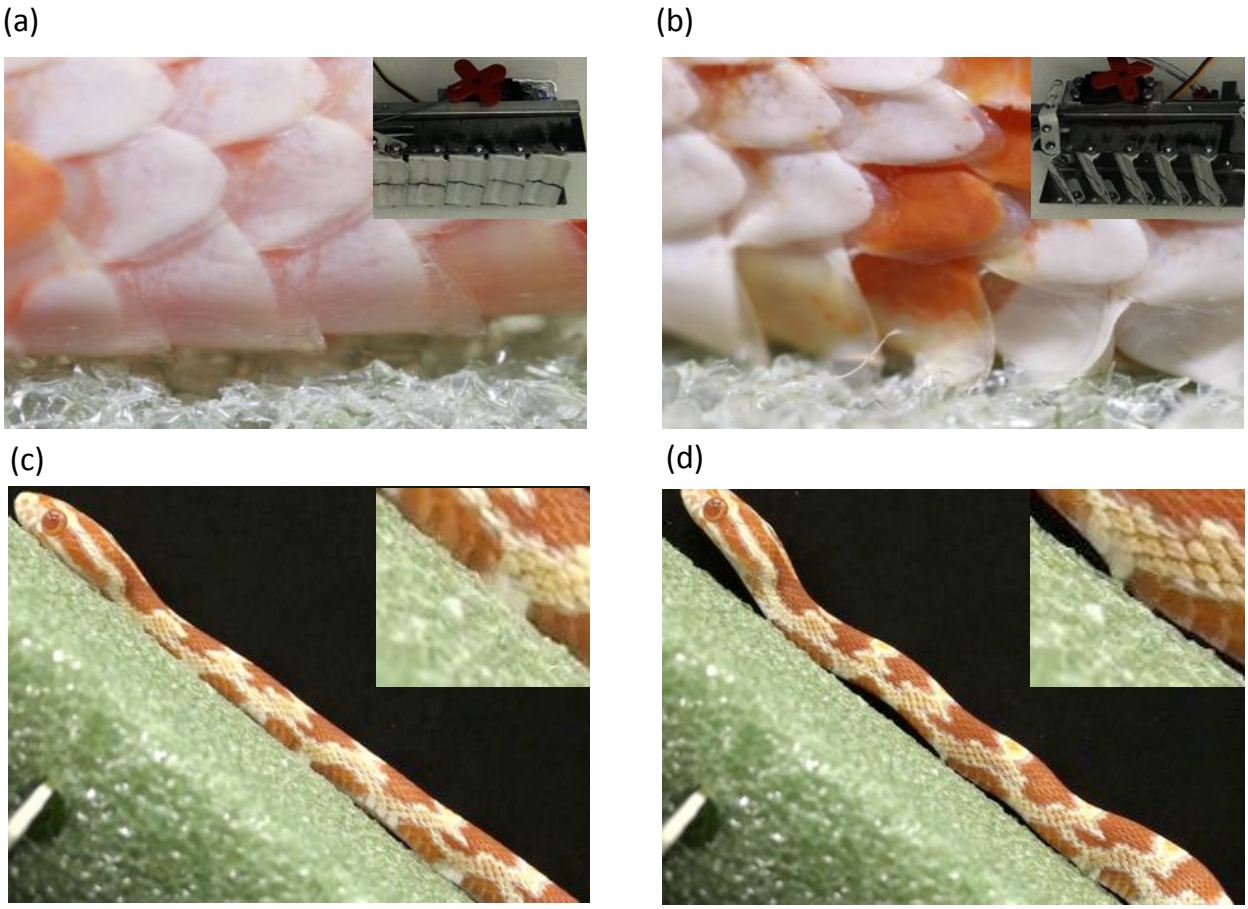

Figure 16: (a,c) Corn snake and Scalybot scales at their minimum angles of attack (flat), and (b,d) at maximum angles of attack. Snakes can modify their scales' angles of attack to increase their friction anisotropies. Scalybot uses the same concept to climb steep slopes, as shown by the insets.

Based on corn snake concertina locomotion kinematics and snake scale design, we have built Scalybot, a simple extensional robot that can control the angle of attack of its scales to modify its resistance to sliding in different directions. The robot is made of 2 similar segments (**Fig.17**). The segments are each housed in a steel casing and connected to each other by an SMC pneumatic actuator. Two 24vDC solenoid valves control the pneumatic cylinder position. Two manual flow control valves and an inline miniature air regulator are used to control air flow rate and pressure, respectively. A household ventilation register was modified to manufacture the scales. Each body segment contains 5 steel scales arranged as louvers whose pitch is varied by a linkage system connected to a servo motor (HS-311 Hitec). Both solenoid valves and servos are controlled using an Arduino UNO microcontroller board which is programmed using Arduino software. The total weight of

the robot is 1.16 kg, which does not include the sources of pneumatic pressure or electric energy.

4.2.2 Friction Measurements

Friction coefficients were measured by placing the robot in two orientations on the plane (facing up the slope corresponding to use of the backward friction coefficient). Static friction coefficients μ^s were given by $\tan\theta$ where θ is the minimum incline angle at which the robot begins to slide. Dynamic friction coefficients μ were measured by filming the robot sliding down an incline of angle ϕ and measuring its displacement x and duration of sliding t. The dynamic friction coefficient can then be estimated using the implicit relation $x = \frac{1}{2}g(\sin\phi - \mu\ \cos\phi)t^2$ [52].

Friction measurements of our robot and three corn snakes were taken on open-cell rigid styrofoam. This material was chosen because its roughness of 1.2 mm was greater than both the robot and corn snake scale thickness (0.8 mm and 45 μm, respectively). In this regime, friction coefficients are significantly affected by scale angles of attack, in comparison to on smoother surfaces such as a tabletop with a roughness of 20 μm.

(a)

PARTS LIST	
ITEM	DESCRIPTION
1	Scale Platform
2	Linear Guide Assembly
3	Pneumatic Cylinder
4	Scales
5	Servo
6	Servo Horn
7	Linkage Bar

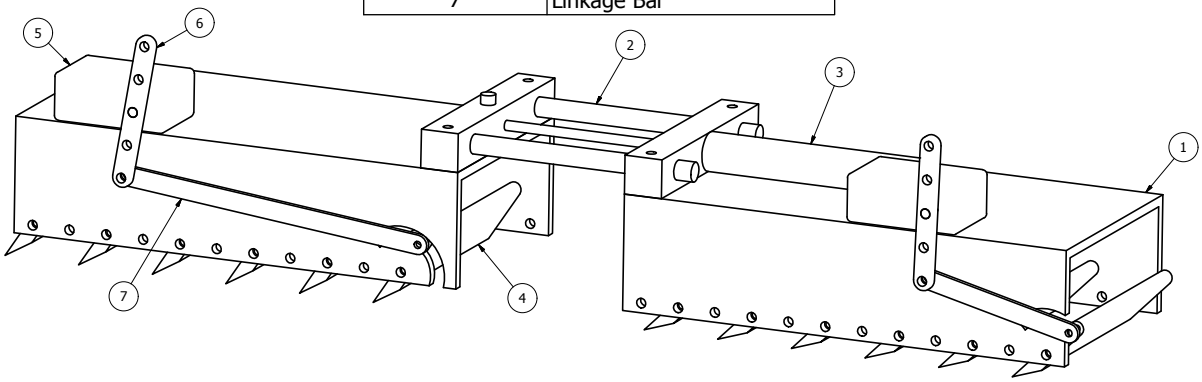

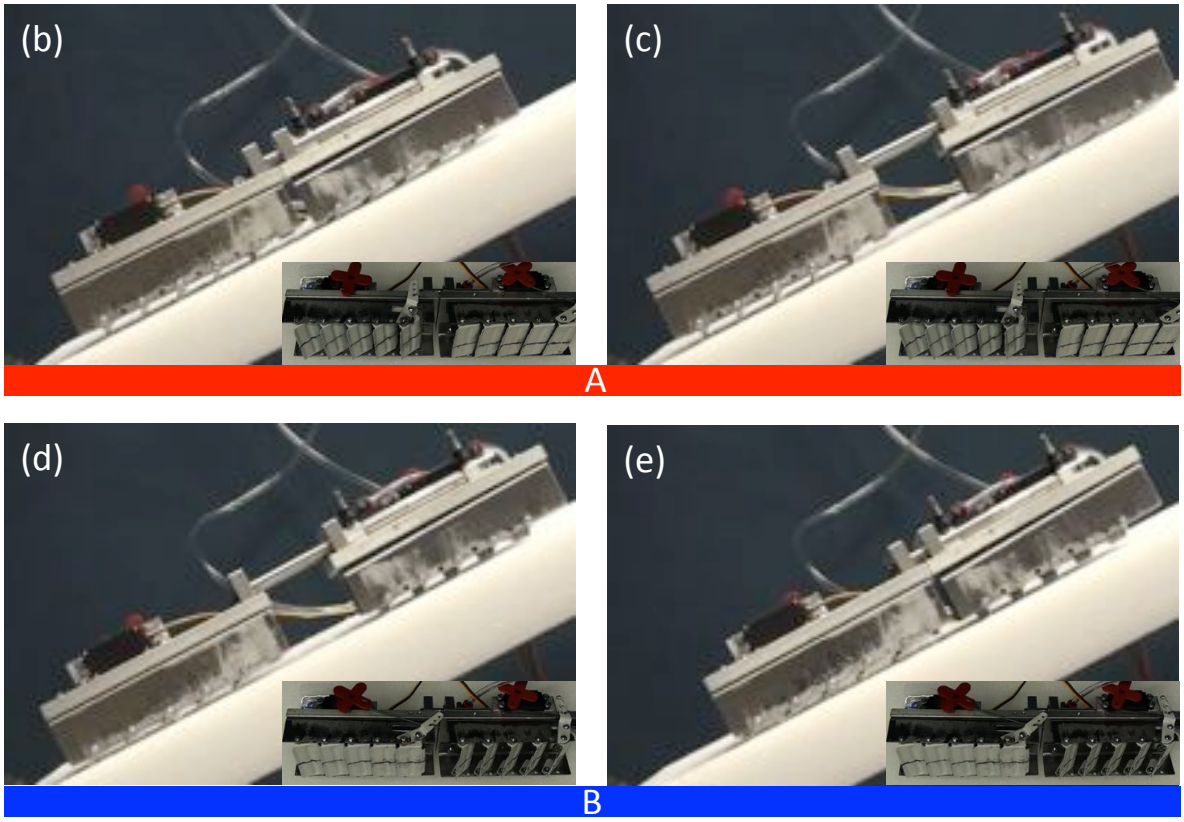

Figure 17: (a) CAD drawing of Scalybot and list of item descriptions. (b-e) The image sequence for one period of motion of Scalybot. Insets show oblique views of the belly scales for the stationary and moving segments. Phases A and B denote kinematic phases defined in **Fig.18**.

4.3 Model

The speed, $\bar{V}$, of our robot was predicted using the following simple model of its dynamics, whose schematic is shown in **Fig.15**c. We partition the device into 2 nodes representing point-masses of mass $m/2$, where m is the total mass of Scalybot. These nodes, labelled i = 1 or 2, are separated by an inter-nodal distance $l(t)$. The robot can adjust the relative position of its nodes by applying internal forces f using its pneumatic piston. Resisting motion of the masses are inertia and dynamic frictional forces along the ground. The dynamic friction coefficients of the belly sliding in the forward and backward directions are μ_f and μ_b, respectively. Newton's second law applied to each of the nodes yields:

$$\begin{aligned} \ddot{x}_1 &= g\cos\theta[-\mu_f H(\dot{x}_1) + \mu_b H(-\dot{x}_1)] - g\sin\theta + \frac{2}{m}f \\ \ddot{x}_2 &= g\cos\theta[-\mu_f H(\dot{x}_2) + \mu_b H(-\dot{x}_2)] - g\sin\theta - \frac{2}{m}f, \end{aligned} \tag{21}$$

where θ is the substrate inclination angle, x_i is the position of the ith mass and $H(x) = \frac{1}{2}(1+sgn(x))$ is the Heaviside step function. Sum of the equations in (21) yields the center-of-mass acceleration, $\ddot{\bar{x}}$:

$$\ddot{\bar{x}} = \frac{g\cos\theta}{2}[-\mu_f \sum_{i=1}^{2} H(\dot{x}_i) + \mu_b \sum_{i=1}^{2} H(-\dot{x}_i)] - g\sin\theta. \tag{22}$$

Non-dimensionalizing Eq. (22) using the Scalybot length L and its period of motion τ, we obtain

$$Fr\ddot{\bar{x}} = \frac{\cos\theta}{2}\left[-\mu_f \sum_{i=1}^{2} H(\dot{x}_i) + \mu_b \sum_{i=1}^{2} H(-\dot{x}_i)\right] - \sin\theta \tag{23}$$

In our experiments, the Froude number is $Fr \sim 0.39 - 1.77$ over the range of $\dot{l}$ prescribed. A small Froude number indicates the inertial is small compared to gravitational forces.

Numerical integration of Eq. (23) allows us to determine steady state behavior given prescribed kinematics. The robot's kinematics is given by the inter-nodal distance, l. This function is characterized by three parameters, L_{min}, ΔL, and τ, as shown in **Fig.18**. An explicit Runge-Kutta (4,5) formula, the Dormand-Prince pair, is used to solve Eq. (23) numerically in MATLAB [77]. Using the state-space form of Eq. (23), acceleration, velocity and position of center of mass are calculated. We characterize the effectiveness of the robot's motion by two parameters, its center of mass steady speed, $\bar{V}$, and the steepest incline it can climb of our prescribed test surface. Speed is non-dimensionalized according to the robot's length L and period τ.

By solving Eq. (23) numerically we can check for static friction upon each iteration. This is accomplished by using velocity data from previous iterations to predict each node's acceleration $\ddot{x}_i$, and in turn the internal force f. If a node reaches a velocity that is sufficiently close to zero, a force balance is computed on that node using the values obtained for f and $\ddot{x}_i$. If the static friction coefficient is large enough to hold the node still, then it is locked in place allowing the other node to move at a speed of $\dot{l}$. This condition is then rechecked upon each iteration to ensure static friction continues to act; if it does not the model resorts back to sliding friction. The only difficulty this method presents is in checking for whether or not static friction is happening initially, as there are no historic points available from past iterations. To address this case, it is assumed that both nodes are starting from rest, and then constant acceleration occurs for the first 10% of the period. The acceleration obtained from a quadratic regression (R^2=0.987) on the inter-nodal distance l shown in **Fig.18** is used to determine internal forces and check if static friction is initially holding.

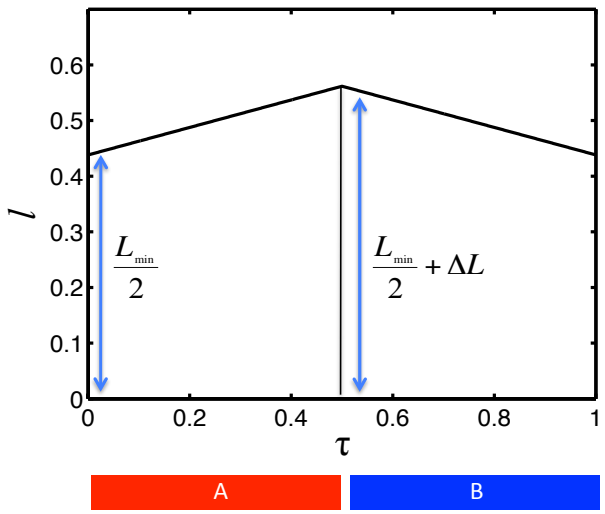

Figure 18: The time course of inter-nodal spacing. There are two phases in this function: In phase A (extension), the head is pushed forward; in phase B (contraction) the tail is pulled forward. The stationary segment uses active friction changes to provide anchorage.

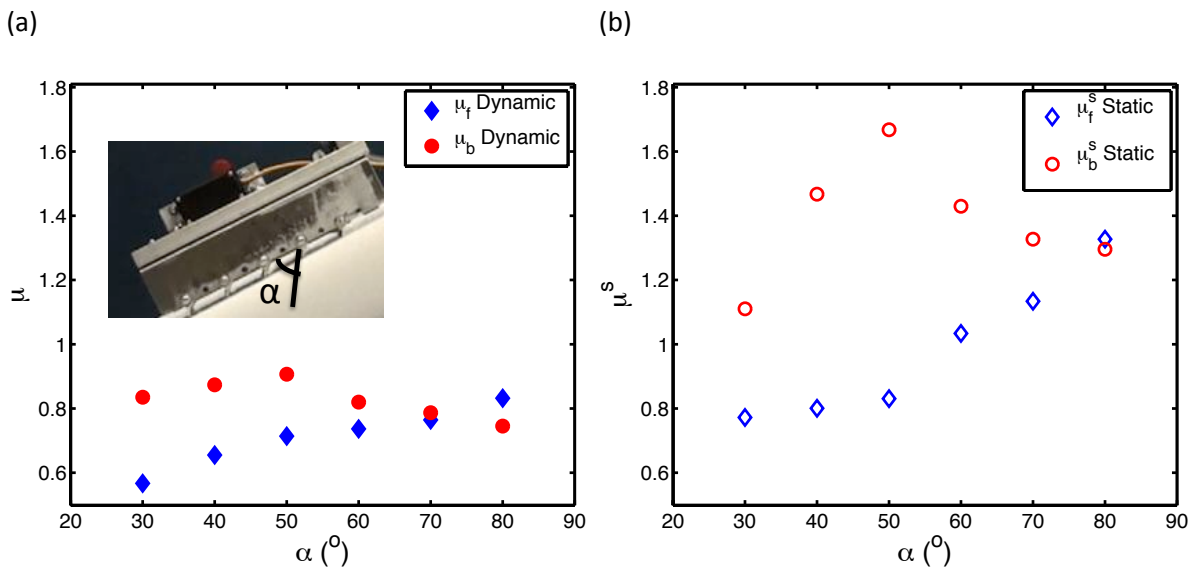

Figure 19: Effect of Scalybot scales' angles of attack, α, on (a) dynamic friction coefficients, and (b) static friction coefficients on Styrofoam. Both forward and backward directions are measured. For obtaining maximum available friction anisotropy, Scalybot sets the scales of its stationary segment at 50° and those of its moving segment at 30°. The friction anisotropy μ_b/μ_f is 1.6 for dynamic friction coefficients and 2.16 for static ones.

4.4 Results

We report upon the frictional properties and performance of Scalybot and corn snake.

4.4.1 Friction Measurements

We observed snakes performing a combination of rectilinear and concertina gaits to ascend inclined planes. In rectilinear motion, snakes used a slow creeping of their bellies and lifting of their scales. Snakes exhibited clear adaptations to prevent falling down the incline. On surfaces inclined greater than 20°, snakes used a form of "emergency braking" to prevent from sliding backwards. **Fig.16**c-d shows a snake performing concertina up a 35° incline. When it begins to lose its grip, the snake freezes its body in an S-shaped configuration. This limits the snake's ventral contact with the ground to a few discrete points where scales appear to be catching as shown in insets of **Fig.16**c-d. After the snake has circumvented sliding and regained its grip, it resumes moving up the incline.

The braking mechanism we observed suggests that behavior is important in modifying the snake's friction. This hypothesis is consistent with our measurements of corn snake friction coefficients, which show conscious snakes have greater dynamic friction anisotropies

(μ_b/μ_f =1.65±0.25, N=3) than unconscious snakes (1.55±0.15, N=3).

To obtain insight into the mechanism of friction modification, we conducted experiments using snake-scale mimics constructed of 0.8-mm thick steel sheets. These sheets were later used as the scales of our robot. We characterize the anchoring ability of a scale according to its angle of attack α with respect to the body (**Fig.15**c). During locomotion, the angle of attack with respect to the underlying substrate may slightly exceed α as a result of small inclinations (3°) of the robot relative to the substrate due to the combined effects of scale lifting and piston flexibility.

As shown in **Fig.19**, the backwards friction is highly dependent on a scale's angle of attack α. Specifically, there exists an optimal angle (α = 50°) that best resists sliding backwards. This optimal angle is comparable to the scale angle of attack (20-30°) observed for live snakes as they are gently pulled by their tails (**Fig.16**a-b). When snakes wish to progress forward, they flatten their scales to 0° to reduce frictional sliding. Corn snake have a minimum scale angle of zero degrees because their scales and body are flexible. However, since we manufactured the robot's scales to be both rigid and overlapping, the minimum angle for Scalybot's scales is 30°, which will be referred henceforth as the scales' default "flat" orientation.

To maximize friction anisotropy, Scalybot sets the scales of its stationary segment to 50° and those of its sliding section to 30°. At this setting dynamic friction anisotropy μ_b/μ_f is 1.6 and static friction anisotropy is 2.16. This is substantially greater than the friction anisotropies for scales kept flat at 30° (1.47 and 1.44, respectively). The activation of the scales thus clearly improves friction anisotropy. Moreover, by activating its scales, Scalybot has similar dynamic and static friction anisotropies to conscious corn snakes on Styrofoam ($\mu_b/\mu_f = 1.6$ for dynamic and $\mu_b^s/\mu_f^s = 1.76$ for static), further suggesting we have done well in optimizing the frictional properties of our robot.

4.4.2 Kinematics

In analogy to a snake's concertina motion (**Fig.15**b), we prescribed the kinematics of the robot using the function $l(t)$, shown by the triangular waveform in **Fig.18**. The robot has two phases of motion (A-B) during its period τ: these consist of expansion and contraction phases at constant inter-nodal velocities $\dot{l}$ and $-\dot{l}$, respectively. The minimum and maximum lengths of the robot are L_{min} and $L_{max} = L_{min} + \Delta L$, respectively. During testing, we varied the speed of expansion and contraction by keeping ΔL constant and adjusting the period τ.

The kinematics of the scales during concertina was chosen to best prevent backwards sliding of the anchoring mass. In phase A, the tail is stationary while the head moves

forward; in phase B, the segments reverse roles. During these phases, moving segment has scale angles of 30° to minimize friction and moving segment has scale angles of 50° to provide anchorage.

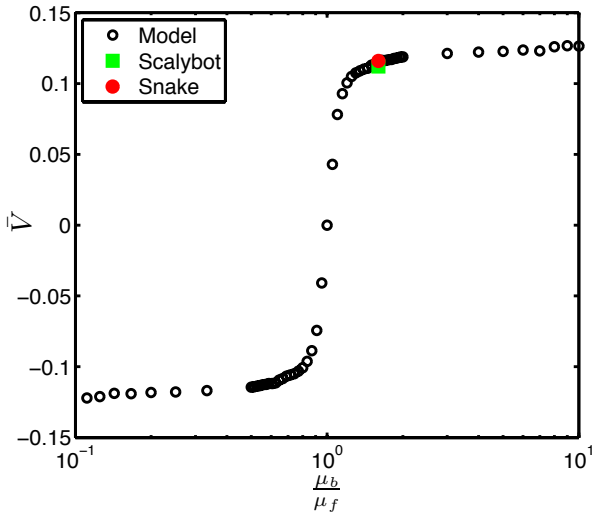

Figure 20: Numerical predictions of the velocity of center of mass, $\bar{V}$, as a function of friction anisotropy μ_b/μ_f, predicted by Eq. (23); Scalybot and corn snake velocities are included for comparison. Scalybot uses active anisotropy by changing its scales' angles of attack so that $\mu_b/\mu_f = 1.6$.

4.4.3 Performance

In terms of maximum climbing angle, our robot showed a similar performance to that of a corn snake. Using active scales, we observed that our robot was capable of climbing up 45° slopes and remaining at rest on slopes of 60°. This is comparable to the climbing performance of a corn snake, which on the same material can climb at 35° and remain at rest at 43°.

Fig.20 shows the predicted steady velocity as a function of dynamic friction anisotropy on a horizontal surface. With activated scales and a contraction speed of $\dot{l} = 24$, Scalybot can move forward at a speed of 0.112, well-predicted by our model. This speed is similar to that of a corn snake (0.116) on the same material in a channel of width 2cm although a corn snake obtains further anchorage by pushing transversely against walls. Moreover, the predicted speeds are near the maximum speeds for such motion, as shown by the asymptotic behavior of $\bar{V}$ at higher anisotropies (**Fig.20**). This correspondence suggests we have reached an ideal frictional anisotropy in our robot. **Fig.21** shows the speed of the robot over a range of contraction speeds ($24 < \dot{l} < 61$). Again, our model does an excellent job

of predicting the forward motion on a horizontal surface.

The limits of our model are illustrated by its difficulty predicting snake speed in a few important cases. First, our model is unable to predict horizontal speeds if the robot scales are kept at rest. Under the contraction speeds tested ($24 < \dot{l} < 61$), the robot with its scales kept flat ($\alpha = 30^\circ$, μ_b/μ_f is 1.4) would not move forward. In contrast, our model predicts a speed of 0.1. The poor performance of the robot with scales at rest demonstrates active control of scales are necessary for locomotion in the regime of speeds tested.

In contrast, our model predicts motion up an incline reasonably well, albeit still not perfectly. **Fig.21** shows the robot's speeds on inclinations of 15 and 30°. Our model can predict forward motion for inclines up to 30°, however, it predicts a negative velocity for slopes of higher than 30° while Scalybot is capable of climbing up to 45°. Our under estimate of maximum climbing angle is likely due to the measurements of the friction coefficients. Since the scales of the robot are at an angle and the surface material it moves upon is malleable, then under acceleration the scales will either bite in deeper or lift out of the material depending on the direction of travel. This process will change the friction coefficients based on the force of the pneumatic cylinder and it is not accounted for in the model.

A picture of Scalybot emerges as one sensitive to kinematics, particularly on inclines. According to our model, to move faster, the robot should increase its rate of contraction $\dot{l}$ which in turn decreases τ and increases its center-of-mass dimensional speed, $\bar{V}L/\tau$. This can be done by increasing airflow to the pneumatic cylinder. However, speed gains are lost, particularly on inclines, when the piston moves sufficiently quickly that the stationary part of the Scalybot can no longer maintain static friction. Thus, undesirable sliding of both segments occurs at an applied force $f > \frac{1}{2}mg(\mu_b^s \cos\theta - \sin\theta)$ where μ_b^s is the backwards static friction. In our tests, such sliding was observed at contraction speeds of $\dot{l} > 40$. At such high contraction speeds, the robot no longer maintains static friction with its stationary part, and as a result, slides down the incline. In general for both snakes and snake robots, maintenance of static friction becomes increasingly important at higher angles of inclination.

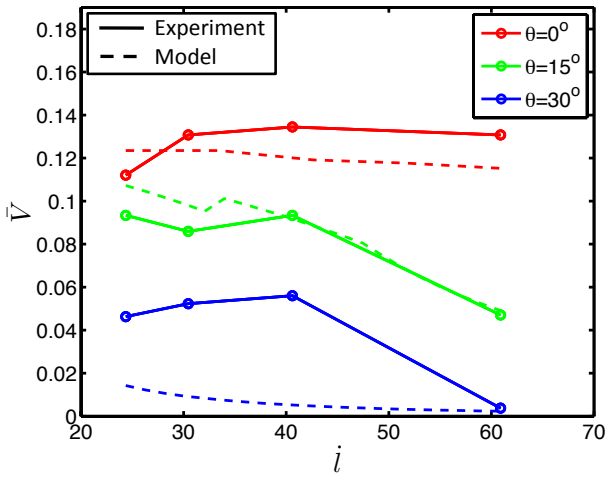

Figure 21: The velocity of center of mass, $\bar{V}$, as a function of $\dot{l}$ and inclination angle, θ. On horizontal surfaces (black lines), increasing $\dot{l}$ increases $\bar{V}$ for low contraction speeds ($\dot{l} \leq 40$). However, at sufficiently high contraction speeds ($\dot{l} > 40$) and angles of inclination (green and blue lines; $\theta \geq 15$), the velocity of Scalybot decreases due to loss of static friction anchorage.

4.5 Discussion

We have modeled, designed, and constructed a simple robot that slides forward by actively modulating its belly friction. Our work was inspired by the behavior of snakes crawling up inclined surfaces, whereby they prevent backwards sliding by actively re-orienting their scales. Our two-link robot uses a simple time-dependent behavior for its scales to climb slopes of 45°. This is a vast improvement in mobility: if its scales are not active, it cannot move forward even on horizontal surfaces.

Tests of Scalybot yielded insight into the subtleties of climbing. Specifically, we found on inclines of increasing steepness, static friction became increasingly important to prevent sliding backwards. Moreover, we observed the robot contraction speed has an optimum. It must be as large as possible to maximize center-of-mass speed, yet not so high as to generate forces that would break static contact of the anchored part of the robot.

To enhance its performance, we suggest the following improvements to Scalybot. More links as well as compliant joints would make Scalybot more flexible and capable of handling obstacles in its path. Snakes use transverse pushing to increase their friction force while moving through channels; adding this functionality to the robot would enable it to increase its speed and maximum inclination of climbing. Increasing the scale's range of rotation to 180° would enable Scalybot to crawl both uphill and downhill. Moreover, adding

an accelerometer to provide feedback would enable the robot to detect backward sliding and respond by digging its scales like the snakes in our experiments. Finally, by sharpening its scales, or making them compliant like that of a snake, the robot may obtain greater traction on a greater range of topographies. The scales of a corn snake are highly tapered, with a variation in thickness from 450 μm at the base to only 45 μm at the tip.

Our reported robot weight was only 1.16 kg, which did not account for a power supply or supply of pressurized air. A self-contained Scalybot housing these items would be considerably heavier. The motors powering the belly scales would then have to be chosen so that they could still lift a heavier robot. A detailed study into the forces required by snakes to activate their belly scales and lift their bodies would be of use in this regard.

We are currently working on the second version of this robot, Scalybot 2 (**Fig.22**). There is an accelerometer installed on Scalybot 2 to provide sensory information for the closed loop control system of the scales. The control system will allow the robot to adjust its scales angles of attack according to the frictional properties and inclination of the substrate in order to avoid sliding down the hill. The propulsion system of the robot is composed of four servo motors connected to four chain and sprocket transmission systems. Two DC motors are used for front and rear steering of Scalybot 2, and two servo motors control the scales angles of attack. Scalybot 2 can be controlled using a VEX wireless joystick and one of its potential applications is moving on ice. It turns out if we put heater elements at the tip of its aluminum made scales, they can quickly melt ice and provide an enhanced grip for moving on surfaces covered by snow or ice.

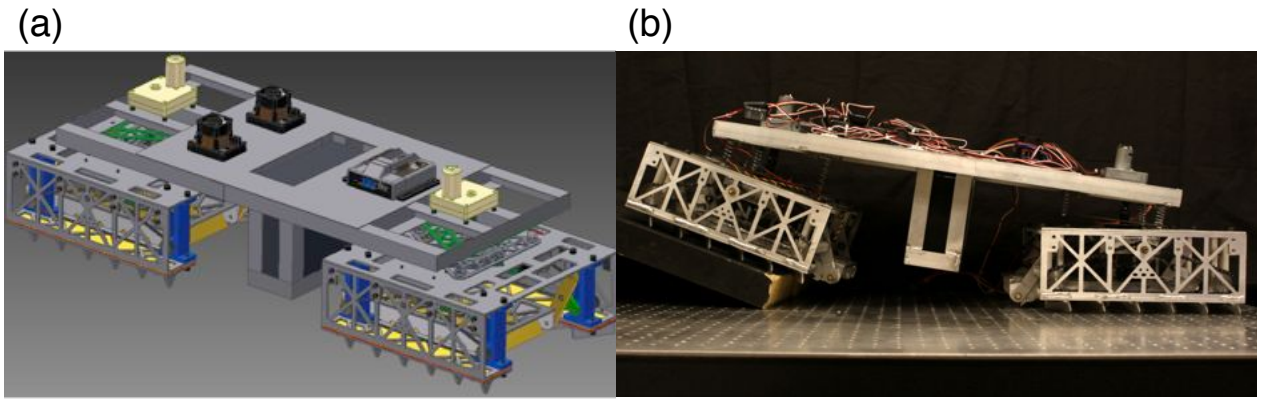

Figure 22: (a,b) Scalybot 2.

There are many other attributes and behaviors of snakes that would improve the climbing ability of snake-like robots. Snakes succeed at climbing because of their high redundancy of climbing mechanisms. They have 120-350 vertebrae [90], which can both bend

and twist. This allows them to lift their bodies to decrease frictional drag when sliding forward. To prevent sliding backwards they can fold their bodies and press their flanks transversely against the sides of crevices. Finally, each of their ventral scales are activated by individual muscles, which allows them even greater potential to increase their contact area over rough topographies. In our study, we have focused on their use of scales to climb, although all the above mechanisms will be important to build a successful climbing robot.

What new path planning behaviors could be incorporated into Scalybot? To climb uphill, animals are known to take diagonal paths to reduce their rate of power consumption: squirrels run in helical paths up trees and antelopes travel diagonally up slopes [78]. Previous investigators have not yet observed snakes climbing diagonally or helically. On pillars much thinner than a snake length, Jayne showed that snakes perform concertina motion by coiling; however, the motion of their center of mass is purely linear [91]. A modular snake-like robot by Choset forms a helix around a column, climbing by rolling its parts while maintaining its helical configuration [92]. On pillars fatter than a snake length, we observe snakes simply climb linearly, sometimes deviating from straight paths to follow crevices that provide greater anchorage, as shown in **Fig.15**. One reason snakes do not climb diagonally is their avoidance of transverse gravitational forces which may cause transverse slipping. Thus, their preference for vertical climbing may stem from the large coefficients of dynamic backwards friction (0.79 ± 0.03) relative to transverse friction (0.38 ± 0.07), according to our measurements of corn snakes on styrofoam. Although our robot cannot perform efficient path-planning strategies like moving diagonally, such topics would be of interest to future designers of climbing snake robots.

In the long run, snake-inspired robotics may benefit from consideration of a recent study by Vincent *et al.* , which presents an elegant comparison between biological and engineering systems [93]. They show technology-based problem solving relies upon the use of energy, and in contrast, biology upon information and structure. Snakes use their perceptions (eyesight, smell, vibration sensitivity, and infrared sensitivity) to gather information from their surroundings which clearly makes them more efficient and effective at moving on complex terrain. In this study, we also find snakes take advantage of their flexible, anisotropic, and multi-functional surface structure. We hope future development of snake-like robots will take into account structural factors such as the effects of scales.

CHAPTER V

EVALUATION OF ENERGETIC COST OF CONCERTINA LOCOMOTION VIA *IN VIVO* ^{31}P NMR SPECTROSCOPY

5.1 Introduction

Both legged and limbless animals employ a series of locomotory modes known as gaits. Managing energetic cost of locomotion is one of the main reasons behind any change of gait [78, 94]. Many researchers have been working to develop methodologies for measuring this energetic cost, which is a combination of aerobic and anaerobic metabolism [78, 95, 96]. However, a reliable and repeatable approach for measuring both types of metabolism has yet to be introduced.

The energetic cost of snake locomotion is traditionally characterized by respirometry techniques which measure the production of carbon dioxide by animals while they run treadmills [24, 78]. Energetic costs of concertina locomotion, lateral undulation [16, 24, 78] and sidewinding [18] of snakes have been measured primarily using respirometry. Energetic costs are typically reported in terms of Net Cost of Transport (NCT), defined as energy required for locomotion per unit mass per unit distance travelled. Secor *et al.* and Walton *et al.* find that sidewinding is the most energetically efficient gait employed by snakes (NCT = 8 J/kg·m); lateral undulation (NCT = 23 J/kg·m) and concertina (NCT = 170 J/kg·m) are found to be less efficient [16, 78].

One drawback to the respirometry technique is that it neglects anaerobic metabolism. Anaerobic costs accrue when snakes apply large normal forces to walls, climb high inclinations, or sprint at burst speeds. In anaerobic metabolism, energy is released through conversion of glucose to lactic acid. This process provides much less energy from a given mass of food compared to aerobic metabolism. Power supply during aerobic metabolism is limited by the rate oxygen is provided to the muscles and the rate mitochondria can use it. Anaerobic metabolism is not limited in this way; however, an organism's body cannot withstand excessive accumulation of lactic acid, limiting the, energy provided during anaerobic metabolism [78].

Gratz and Hutchison study *Natrix rhombifera* snakes and suggest that anaerobiosis accounts for over 66-86% of the total energy expended during 5-10 min of maximum activity induced by electrical stimulation [97]. In another similar study, Ruben studies aerobic and

anaerobic metabolism of four snake species: *Coluber constrictor*, *Crotalus viridis*, *Lichanura roseofusea*, and *Masticophis flagellum* after about 5 min of maximal activity induced by mechanical stimulation. He reports anaerobic metabolism provides more than 50% of total energy production for all of these species [98]. In both of these studies blood and tissue samples are taken from snakes and the concentrations of important metabolites are measured and are compared to respirometry data [97, 98]. However, no one has measured total aerobic and anaerobic cost of transport for snakes performing locomotion.

Commonly used methods of measuring NCT in living organisms are respirometry, indirect calorimetry, and direct calorimetry [78, 94]. Neglecting anaerobic metabolism eliminates both respirometry [24, 99] and indirect (gas exchange) calorimetry [96] as viable choices for snake research. Direct calorimetry eschews this issue by measuring the heat dissipated by a snake; however, data acquisition times for direct calorimetry range from several hours to several days for statistically significant results [100, 101]. The high energetic cost of concertina gait limits the endurance of snakes using this mode to an approximate maximum average of 34 minutes [24], effectively eliminating direct calorimetry as a potential experimental technique for determining the energetic cost of locomotion.

Phosphorous-31 magnetic resonance spectroscopy (^{31}P MRS) is a technique used to measure the energy use of cells, mammals, and other reptiles except for snakes [102–105]. In such studies, changes in phosphate metabolite concentrations are indicative of combined energy use by both aerobic and anaerobic metabolism. Jackson *et al.* monitor the Adenosine-diphosphate (ADP) levels in a turtle's heart using ^{31}P MRS to investigate how turtles are able to slow their hearts and energy consumption and go into survival mode for months with limited oxygen [106]. Wemmer *et al.* observe the energy consumption of a diving turtle in a hypoxic state through measuring the recovery times of phosphocreatine (PCr) and inorganic phosphate (P_i) metabolite concentrations of the diving turtle [107]. Metabolite recovery rates in ectotherms are found to be on the order of several hours [107, 108].

In this study, we develop a technique for characterizing the energetic cost of transport of organisms for which conventional methods such as direct calorimetry are not feasible. We apply this technique to measure energetic cost of concertina locomotion of snakes. We discuss our experimental procedures and data analysis in § 5.2. In § 5.3 we explain our calculations of both mechanical and metabolic power. We then present and discuss our results in § 5.4 and § 5.5. Finally, in § 5.6 we summarize our findings and discuss possible future directions.

5.2 *Methods*

5.2.1 Exercise and Spectroscopy

In this section, we present methods for caring for snakes, characterizing their pre-exercise state, exercising them in a controlled manner, and measuring their metabolic rate. Throughout our experiments, we use a sample of two corn snakes, *Elaphe guttatta* ($N = 2$, $m = 0.80 \pm 0.06$ kg). Snakes were fed weekly and housed in separate terrariums with controlled temperature and humidity conditions. Experiments in this study took place over a period of 12 sessions over 12 weeks. All of the experiments are conducted at 23°C.

For each trial, we begin with a baseline check of the snake's energetic levels. For this measurement as well as measurements at the end of the trial, we use a Bruker PharmaScan 7.0 T Magnetic Resonance system (**Fig.23**b). A $^{1}H/^{31}P$ dual tune coil with an inner diameter of 60 mm manufactured by M2M imaging allowed the interleaved recording of ^{31}P NMR spectra and MR images without the need of major hardware changes. Associated TopSpin and ParaVision software packages are employed to analyze the system's data.

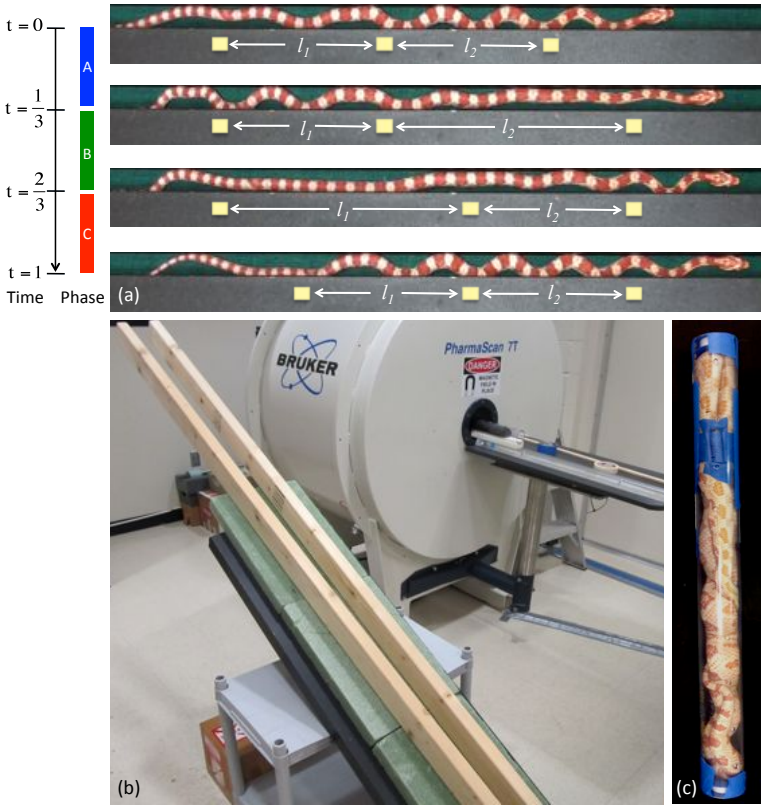

Figure 23: (a) Three phases of concertina locomotion, (b) Bruker PharmaScan 7.0 T MR system, and (c) plastic tube used for putting the snake in the MRI machine.

We place a snake into an aerated acrylic tube (outer diameter 59 mm, inner diameter 55 mm) shown in **Fig.23**c. As an internal standard, a glass vial containing an aqueous solution of diisopropyl methylphosphonate (DIMP, 95% w/w, 270 mg, 1.42 mmol) is placed in the tube. The tube is then guided into the MR system. We first acquire a 3-dimensional image of snake to calculate its interrogated volume in the MR system. This step is necessary because the MR system's chamber generally only holds half the snake. We then record ^{31}P pre-exercise reference spectra according to the following parameters: 2000 ms repetition delay, 4 spectra, and 32 repetitions, resulting in a data acquisition time of 4.26 minutes. The length of the exciting RF-pulse is 100 μs leading to a shorter than $\pi/2$ pulse length with the maximum achievable RF-power of the instrument (300W). Experiments varying the length of the repetition delay are conducted to ensure a complete T1-relaxation between scans to allow an unambiguous quantitative analysis of the spectra.

Once we record the reference ^{31}P spectra, we remove the snake from the MR system and place it on our custom-built raceway. As illustrated in **Fig.23**b, the raceway is composed of two 5 cm x 10 cm x 185 cm wood planks arranged parallel to each other on a styrofoam substrate, which is placed on a wooden board. The active length of the raceway, defined as the length of the raceway less the length of the snake, is 1 m. Since channel width does not have a statistically significant effect on kinematics of concertina locomotion [52], we fix the channel width at 5 cm and only change the inclination angle in our experiments.

We observe the snake performing concertina motion in the channel and cycle it back to the beginning once it is finished. This procedure is repeated for 5-10 minutes while a video records the snake's motion. We use open source Tracker, a Video Analysis Modeling Tool (`www.cabrillo.edu/~dbrown/tracker/`), to extract kinematic information from the recorded video in order to calculate the mechanical energy expenditure of the snake during concertina locomotion. The kinematic parameters we measure include period of motion, distance travelled per period, total time, total displacement, and average speed as tabulated in Table 3.

Table 3: Kinematics parameters of concertina locomotion. Number of trials n, period τ, displacement of body per period ΔL, total time T, total displacement D, and velocity V of two corn snakes moving at inclinations of 0, 10, and 30 degrees.

θ (°)	Snake	n	τ (s)	ΔL (m)	T (s)	D (m)	V (m/s)
0	1	2	2.5 ± 0.1	0.12 ± 0.04	484.5 ± 78.5	9.00 ± 2.55	0.04 ± 0.03
	2	2	3.2 ± 0.1	0.16 ± 0.03	373.0 ± 62.5	8.00 ± 0.00	0.07 ± 0.01
10	1	1	1.3	0.02	555.0	4.00	0.01
	2	2	3.5 ± 2.6	0.12 ± 0.09	330.5 ± 41.7	5.60 ± 3.39	0.01 ± 0.00
30	1	1	3.7	0.06	550.0	4.80	0.02
	2	3	2.4 ± 1.4	0.12 ± 0.10	342.7 ± 133.7	3.73 ± 0.46	0.01 ± 0.01

Immediately following exercise, we insert the snake into the tube and guide it into the MR system. We then record ^{31}P spectra according to the following parameters: 2000 ms repetition delay, 64 spectra, and 16 repetitions, resulting in a data acquisition time of 34.13 minutes. Finally, we acquire the 3-dimensional image of snake in the machine to find the fraction of snake body that is in the spectrometer. We repeat this procedure for each snake at raceway incline angles of 0°, 10°, and 30°. Resting reference measurements and post-exercise recovery measurements are in two trials per snake per angle. We check that the snake speed is constant across trials, and we drop trials for which speed changes occur. We limit our experiments to one experiment per snake each day to enable the snakes to recover between experiments.

5.2.2 Data Analysis

The free induction decays (FIDs) recorded with the MRS technique are processed using standard techniques including line broadening (filtering of noise by multiplication of the time data with an exponential function), Fourier-transformation, phase correction, and baseline correction. We integrate PCr, P_i, and DIMP peaks and calculate the ratios of PCr to P_i peak integrations (PPR) at each time step. For obtaining a 3-dimensional image of snake in the MR system, we perform a volumetric reconstruction procedure on the acquired sequence of cross sectional images for each snake (inset of **Fig.24**a).

5.3 Energetics

In this section, we present mathematical relations for rate of mechanical and metabolic energy expenditure. To calculate mechanical energy, we consider the kinematics of concertina

locomotion, a gait typically performed within a tunnel. During this gait, a snake wedges its body against walls of the passage by folding its body into a series of bends, creating points of static contact from which the snake propels itself forward [20, 52] (**Fig.23**a). As illustrated in **Fig.23**a, propulsion in concertina locomotion is accomplished by extending the anterior elements of the body in the direction of motion (phase A), establishing new anchor points and moving mid-section of body forward (phase B), and propagating the movement posteriorly through the body (phase C). Consider a snake of mass m traveling through a channel of width w and inclination θ.

Work is expended gravity and friction forces, as was reported by Marvi *et al.* [52]. The total rate of mechanical energy expenditure is:

$$P_{\text{mech}} \leq \frac{mg\sin\theta\Delta L}{\tau} + \frac{mg\cos\theta\left(\mu_f\Delta L + \mu_t w\right)}{\tau} \tag{24}$$

where m is snake mass, g is gravitational acceleration, θ is the inclination angle, and w is channel width. μ_f and μ_t are the conscious snake forward and transverse friction coefficients ($\mu_f = 0.49$ and $\mu_t = 0.40$ on Styrofoam). τ is period of motion, and ΔL is the distance traveled by the snake in one period which are measured from video analysis (Table 3).

We now define the metabolic power of the snake as measured by the MR system. In ^{31}P NMR, the CK conversion of PCr during a period of increased activity is measurable by tracking the temporal integrated peak intensity of PCr. Integrated peak intensity is proportional to the molar concentration of a compound:

$$\frac{n_{\text{PCr}}}{n_{\text{DIMP}}} = \frac{I_{\text{PCr}}}{I_{\text{DIMP}}}. \tag{25}$$

where n_{PCr} and n_{DIMP} are number of moles of PCr and DIMP and I_{PCr} and I_{DIMP} are integrated intensity of signal corresponding to PCr and DIMP, respectively.

The change in integrated peak intensity of PCr is converted to the amount of energy released by ATP during exercise. Considering that transient concentrations of ATP are approximately constant due to buffering action by PCr, changes in PCr are indicative of the quantity of ATP consumed during exercise. The energy released, E due to conversion of PCr is as following [109, 110]:

$$E = n_{\text{PCr}}(\Delta G_{\text{ATP}} + \Delta G_{\text{PCr}\rightarrow\text{ATP}}), \tag{26}$$

where ΔG_{ATP} is energy released in hydrolysis of ATP; ATP + $H_2O \rightleftharpoons$ ADP + P_i, ΔG^o = -30.5 kJ/mol. $\Delta G_{\text{PCr}\rightarrow\text{ATP}}$ is also energy released in converting PCr to ATP; ADP + PCr $\rightleftharpoons$ ATP + Cr, ΔG^o = -12.5 kJ/mol. Substituting n_{PCr} from Eq. (25) and considering field inhomogeneity we find:

$$E = I_{\text{true}}\,\frac{I_{\text{PCr}} n_{\text{DIMP}}}{I_{\text{DIMP}}}(\Delta G_{\text{ATP}} + \Delta G_{\text{PCr}\rightarrow\text{ATP}}) \tag{27}$$

where I_{true} is a field inhomogeneity correction factor used to correct for any spatial inhomogeneities in the magnetic field of the MR system. The value we calculate for I_{true} is 1.458 in all of our experiments.

Metabolic power P_{met} is defined as expended energy over duration of snake exercise: $P_{\text{met}} = (E_2 - E_1)/T$, where E_1 and E_2 are reference and post-exercise energies and T is total time of exercise. Substituting E from Eq. (27) and considering the fact that entire snake body does not fit in our MRI machine the total metabolic power expended is calculated as follows:

$$P_{\text{met}} = \frac{I_{\text{true}}\, n_{\text{DIMP}}\, (\Delta G_{\text{ATP}} + \Delta G_{\text{PCr}\rightarrow\text{ATP}})}{T} \left[\alpha_1 \frac{I_{\text{PCr,1}}}{I_{\text{DIMP,1}}} - \alpha_2 \frac{I_{\text{PCr,2}}}{I_{\text{DIMP,2}}} \right] \tag{28}$$

where $\alpha = V_{\text{snake}}/V_{\text{interrogated}}$ is total volume of snake over its volume interrogated by MR system. Subscripts 1 and 2 denote reference and post-exercise measurement, respectively. The energetic efficiency η is then the ratio of mechanical power of concertina locomotion from Eq. (24) to the metabolic power from Eq. (28):

$$\eta = \frac{P_{\text{mech}}}{P_{\text{met}}} \tag{29}$$

Minettei *et al.* define efficiency as vertical work rate, work due to climbing over time, divided by the rate of aerobic energy expenditure [111]. However, we include work of friction in mechanical work, P_{mech} and thus we can calculate efficiency at zero degrees inclination. We also include anaerobic metabolism in P_{met} to account for the total energy expenditure.

5.4 Results

The pre-exercise ^{31}P spectrum of a corn snake is shown in **Fig.24**a. Peaks are exhibited for P_i, PCr, and γ-, α-, and β-ATP. Depending on the chemical structure experienced by a particular ^{31}P nucleus, the emitted radio frequency will be slightly different from the excitation frequency leading to an NMR spectrum with peaks corresponding to individual chemical moieties [112, 113]. The reference spectrum for a diving turtle exhibits the same peaks as that for a corn snake, confirming the validity of our experimental technique [107].

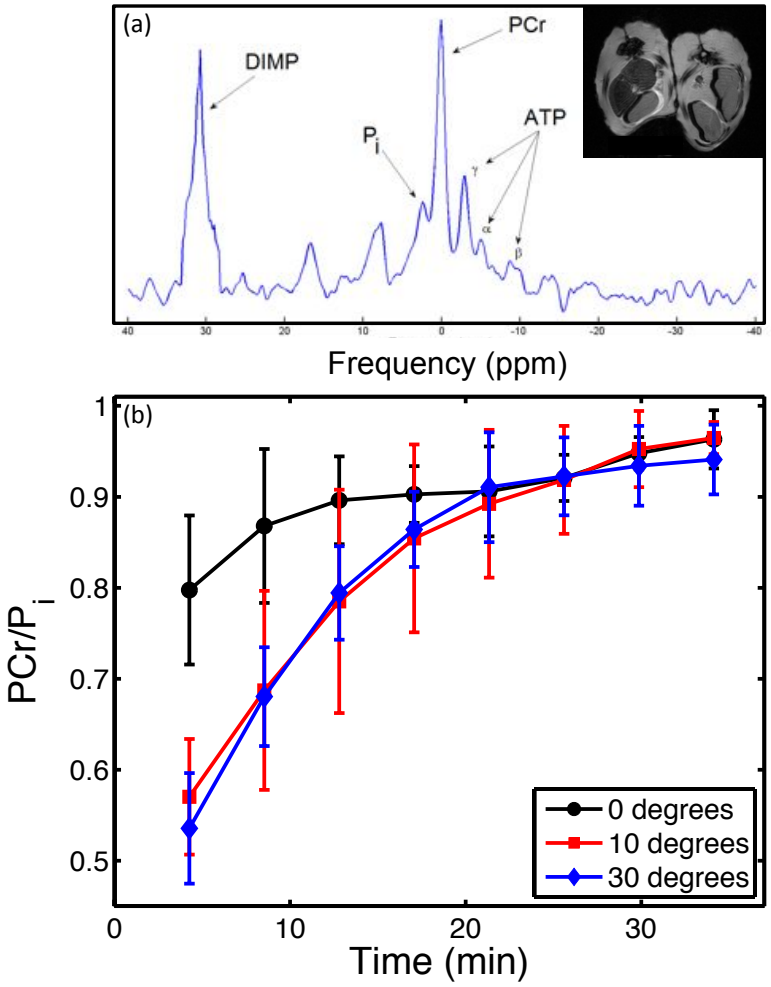

Figure 24: (a) Pre-exercise ^{31}P time-averaged reference spectrum for a corn snake. Data acquisition time for capturing this spectrum is 1.07 minutes. Inset shows cross section of snake body in the MR system. (b) Phosphocreatine to inorganic phosphate ratio recovery rate.

Fig.24b shows the time evolution of PPR. Full recovery is defined as a return of the PPR from a post-exercise minimum value to approximately the value of the PPR for the pre-exercise measurement. As shown in **Fig.24**b, the measured PPR recovery time varies between 13 to 25 minutes for different inclinations (**Fig.24**b). Phosphorous metabolite recovery rates in snakes are similar to those observed in turtles [107]. Moreover, the immediate post-exercise intensities of PCr are smaller for larger inclinations corresponding to a higher metabolic energy consumptions at higher incline angles.

The kinematics of concertina locomotion are tabulated in Table 3. We record concertina locomotion of two corn snakes at inclinations of 0, 10, and 30 degrees. We mechanically

stimulate snakes, by stroking their tail gently, to make sure they move at a constant speed. We stop each experiment once the snake is exhausted and does not move any more. This usually takes about 5-10 minutes corresponding to 4-9 meters of total displacement depending on the inclination angle. We use τ and ΔL to calculate mechanical power, P_{mech} using Eq. (24). Total time T, is used to calculate P_{met} using Eq. (28).

The mechanical power, P_{mech} metabolic power, P_{met}, and energetic efficiency, η of corn snakes are tabulated in Table 4. P_{mech} is calculated using Eq. (24) for a snake performing concertina locomotion in a 5 cm wide channel as discussed in § 5.3. P_{met} is also obtained using Eq. (28) and thus, η is calculated according to Eq. (29). As discussed in § 5.2, we conduct 3-4 experiments at each inclination (Table 3). The reported parameters in Table 4 are the means and standard deviations of these four experiments at each inclination. Alexander [78] reports efficiency of 10% for legged reptiles, mammals, and birds of mass 1 kg which is similar to our measurements in this study.

Table 4: Metabolic power, P_{met}, mechanical power, P_{mech}, and efficiency, $\eta = P_{\text{mech}}/P_{\text{met}}$ for two corn snakes moving on inclinations of 0, 10, and 30 degrees. The channel width for all of the experiments is set to 5 cm.

θ (°)	P_{met} (Watts)	P_{mech} (Watts)	η
0	2.20 ± 0.23	0.24 ± 0.05	0.11 ± 0.02
10	3.35 ± 0.14	0.27 ± 0.05	0.08 ± 0.01
30	3.98 ± 0.68	0.34 ± 0.16	0.09 ± 0.05

We used JMP software to conduct two-way ANOVA and determine the effect of animal and slope on P_{mech}, P_{met}, and η. Using a significance level of $\alpha = 0.01$ we find that animal does not have a statistical significant effect on any of the aforementioned parameters. Moreover, slope has a significant effect only on P_{met} (P-value < 0.001). Thus, mechanical power P_{mech} (which includes work of friction) and efficiency η are not statistically different across the range of inclinations we study.

5.5 Discussion

Taylor *et al.* report respirometric cost of transport for a variety of legged animals including mammals, birds, reptiles, amphibians, and insects over a wide range of body mass; 0.1 mg to 100 kg. Surprisingly, the cost of transport for all of them fall on the same line: $T_{met} = 10.7m^{-0.32} + \frac{6m^{-0.3}}{V}$, where T_{met} is metabolic cost of transport (J/kg·m), m is mass in kg, and V is speed (m/s) [78, 114]. We measure total metabolic cost of a *Elaphe guttatta*

snake of mass $m = 0.82 \pm 0.04$ kg performing concertina at 0 degrees to be 196.4 ± 26.9 J/kg·m. Walton *et al.* measure NCT of *Coluber constrictor* snake performing concertina locomotion at an angle of inclination of 0° using respirometry technique (only aerobic metabolism) [24]. For a *Coluber constrictor* snake of mass $m = 0.12$ kg, NCT is 170 J/kg·m [24, 78]. Using Taylor's equation for snake of the same mass yields an NCT of 170.6 J/kg·m, which is similar to Walton's measurement, as expected.

Our metabolic measurements capture both aerobic and anaerobic metabolism, thereby improving in accuracy over previous techniques. Our measurement of mean NCT is 16% more than that predicted by respirometry, indicating the importance of anaerobic metabolism. Our study focused only on a single gait, and other snake gaits may have even larger contributions from anaerobic metabolism. When snakes are performing energetically costly activities such as striking or sprinting at burst speed, they can become physically exhausted: in these cases, anaerobic metabolism can exceed 50% of the total energetic cost [97, 98].

The efficiency of snake locomotion as a function of inclination angle had not been previously measured. Minettei *et al.* measure the efficiency of human walking on slopes of 5 to 25 degrees and they show that efficiency remains constant at 18-23% across this range of inclinations [111]. This is consistent with the efficiencies we calculate for concertina locomotion of corn snakes on slopes of 0 to 30 degrees. We find efficiency of snake concertina locomotion remains constant at 8-11% over this range of inclinations. Marvi *et al.* show that in concertina locomotion of snakes the effect of slope on velocity, period, body extension, and transverse pushing is statistically significant [52]. We hypothesize that with increasing inclination angle, snakes adjust their kinematics such that metabolic power increases consistently with mechanical power and thus efficiency remains constant.

Our measurements show concertina locomotion has a low efficiency which does not change significantly in the range of 0 to 30 degrees inclination. We hypothesize this low efficiency is one of the main reasons snakes avoid this gait unless they encounter a terrain in which other gaits are not feasible. Faced with high inclinations, narrow channels, or low friction substrates lateral undulation, sidewinding, or rectilinear locomotion are not effective. In such circumstances, snakes need to use concertina locomotion to provide additional friction force and traverse those terrain successfully.

The size of the MRI machine was a limit to our study, specifically by preventing us from snake's entire snake body in the MRS. To compensate, we measure the interrogated volume in the machine, and modified our calculations accordingly. This calculation adjustment is based on the assumption that muscles are uniformly distributed in snake body. To resolve this problem, future workers might consider using a smaller snake or an MRS with a larger spectrometer. Noise in measurement is caused by movement of the snake during the 30

minute MR spectroscopy. We minimized such noise by using a specially chosen snake container that minimizes the available space for snake to move while recording data. Lastly, the MRI technique is best for providing average measurements over some time because of the inability to record data while conducting experiments. Not being able to start measuring the spectrum at time $t = 0$ immediately after the snake exercise would also cause some error in measuring energetic cost of locomotion. Although, the time it takes to put a snake in the container and start recording ^{31}P spectrum is negligible compared to the recovery time.

5.6 Summary and future directions

We present an experimental technique for measuring both anaerobic and aerobic energy use, improving in comprehensiveness compared to previous methods. We apply our method on corn snakes to determine the energetic cost and efficiency of their concertina locomotion. First of all, our measurement of total metabolic cost for corn snakes of mass m = 0.82 ± 0.04 kg performing concertina at 0 degrees is 16% higher than that measured using respirometric techniques [24]. This indicates the importance of anaerobic metabolism in concertina locomotion. Moreover, we discover the efficiency of concertina locomotion on a horizontal surface is 11%, similar to the value of 10% for legged locomotion of reptiles, mammals, and birds with similar mass [78]. Finally, we find snakes manage to maintain the same efficiency across different inclinations. This is consistent with Minettei's measurements of human walking efficiency on slopes of 5 to 25 degrees [111]. The methodology proposed in this study may be applied for measuring cost of locomotion for snakes and other animals.

CHAPTER VI

SNAKES MIMIC EARTHWORMS: PROPULSION USING RECTILINEAR TRAVELING WAVES

6.1 Introduction

Snakes have long flexible bodies that enable them to easily traverse complex terrain such as sand, foliage, narrow crevices or tree trunks. In narrowly confined terrain, snakes employ a gait called "rectilinear locomotion" to propel themselves in a straight line, similar to earthworms. Understanding how snakes propel themselves unidirectionally provides a more complete picture of why snakes are so versatile in environments where both legs and wheels are known to fail. In terms of practical applications, rectilinear locomotion may provide added versatility to limbless snake-like robots, designed for use in search-and-rescue processes during natural disasters [10, 39]. Rectilinear locomotion may also be implemented in the control of medical snake-robots used to reach parts of the human body that physicians have difficulty accessing [115]. Such applications involve locomotion through tight crevices and so require the application of rectilinear locomotion.

Rectilinear locomotion is one of four "gaits," or modes of snake locomotion, each specialized for a particular type of terrain. Slithering is applied on flat surfaces or through structured environments such as between rocks, used as push-points [17]. Sidewinding is used on granular surfaces such as sand [116]. An accordion-like concertina motion is used within intermediate-sized crevices which are much wider than the snake's diameter [52]. Within more tightly confined crevices, snakes cannot use these gaits because of the lack of space and so instead employ rectilinear locomotion. For example, rectilinear locomotion is used to travel vertically upward along the interstices of tree bark, across narrow tree boughs, and alongside walls. We have observed snakes using rectilinear locomotion to crawl out of their own skin during shedding, a periodic event that removes parasites and permits growth. The body trajectory for rectilinear locomotion is linear, which minimizes the path length traveled by parts of the body and, in turn, the sounds produced. Thus, rectilinear locomotion is naturally applied to stealthy activities such as stalking prey.

Rectilinear locomotion is the least studied of the snake gaits. Home published the first study of rectilinear locomotion nearly two centuries ago, describing rectilinear locomotion as "rib-walking" [117]. He observes that the ribs of *Coluber constrictor* move forward in sequence, like the feet of a caterpillar. Since then, several studies have overturned the

rib-walking hypothesis [28, 30, 31]. The most extensive experimental study on rectilinear locomotion is conducted by Lissman [31], who studies two specimens of *Boa occidentalis*. He uses x-ray imaging to show a snake's ribs maintain their fixed spacing during propulsion. He reports ventral kinematics, proposing propulsion is achieved using traveling waves of muscular contraction and expansion on the ventral surface. This finding draws attention because it shows the snake's skeletal structure performs no lever action, a rare occurrence among locomotion of vertebrates. In rectilinear locomotion, a snake is propelled by virtue of its soft body alone, as an earthworm [31].

The energetic expenditure of rectilinear motion is unknown, but promises to be low given the low inertia and lateral movement involved. The traditional measure of the rate of working is the Net Cost of Transport NCT of snakes, found by measuring the oxygen consumption of snakes on treadmills. The most efficient gait is sidewinding (NCT = 8 J/kg m), followed by slithering (23 J/kg m) and lastly concertina motion (170 J/ kg m) [24, 116]. The NCT of rectilinear locomotion has yet to be measured. To improve this situation, we perform a calculation of the physical rate of work in rectilinear motion in § 6.5.4.

Unidirectional limbless locomotion has also drawn the attention of theoreticians. One of the simplest models proposed is the two-anchor model, consisting of a two-segment extensible worm that uses frictional anisotropy to propel itself [78]. Keller *et al.* present a continuous model for a series of these segments connected together [73]. They find trends for period and average speed as a function of body mass that are qualitatively similar to Gray's observations of worms [74]. Moreover, they derive the relationship between the time-rate of change of the worm's internal pressure and body speed. Zimmermann *et al.* also present a discrete model for worm locomotion considering nonlinear asymmetric friction [118].

In this combined experimental and theoretical study, we report on the rectilinear locomotion of three species of snakes on a horizontal substrate. In § 6.2, we describe our methods. We proceed in § 6.3 with our theoretical model for rectilinear locomotion. In § 6.4 and § 6.5 we present our experimental results and our numerical predictions. We discuss the unique wave frequency scaling in § 6.6. Lastly, in § 6.7, we summarize the implications of our work and suggest directions for future research.

6.2 Methods

6.2.1 Animal care

To identify snakes that reliably perform rectilinear locomotion, we initially observe 21 species of snakes, listed in Appendix D.1. Among these species, the vast majority do

not perform rectilinear locomotion reliably on our Styrofoam trackway. We here report upon three species that perform well. Among them, we filmed six individuals, including three juvenile red-tailed boa constrictors (*Boa constrictors*, **Fig.25**a-b), two Dumeril's boa constrictors (*Boa dumerili*, **Fig.25**c), and one Gaboon viper (*Bitis gabonica*, **Fig.25**d).

Figure 25: Snake species used in our experiments. (a-b), Boa constrictor, (c) Dumeril's boa, and (d) Gaboon viper. Snakes (b)-(d) perform rectilinear motion against a wall.

Red-tailed boas are purchased from Florida Herps. They are fed weekly and housed in separate terrariums with controlled temperature and humidity conditions at Georgia Tech. Dumeril's boas and the Gaboon viper are housed at Zoo Atlanta, also in separate cages with controlled conditions. All animal care and experimental procedures are approved by IACUC.

The lengths and masses of the snakes studied are given in Table 5. As reported in this table, snake mass scales linearly with body length (m(kg)=0.027L(cm), $R^2 = 0.73$). Hereon we report allometric results in terms of body length.

Table 5: Animal subjects. The number of snakes (N) used in our experiments, their lengths (L), masses (m), forward and backward sliding friction coefficients (μ_f and μ_b), and number of naturally-occurring spots (n). The data for each individual snake is provided in Appendix D.11.

Species	N	L (cm)	m (kg)	μ_f	μ_b	n
Boa constrictor	3	53.3 ± 1.5	0.06 ± 0.01	0.3 ± 0.06	0.42 ± 0.05	23 ± 2
Dumeril's boa	2	175.5 ± 10.6	5.7 ± 1.1	0.017 ± 0.002	0.06 ± 0.01	25 ± 1
Gaboon viper	1	120	2.26	0.12	0.32	20

6.2.2 Friction measurements

We line the bottom of our trackway with open-cell rigid Styrofoam. In our previous work [52], this surface was effective at engaging a snake's ventral scales with surface asperities. We measure friction coefficients of conscious snakes using the inclined-plane method, developed in our previous work [17, 52].

6.2.3 Trackway construction, filming, and image processing

We construct a 5 m $\times$ 60 cm rectangular trackway to provide a controlled environment for studying rectilinear locomotion. A single wooden sidewall guides the snake along the trackway, as shown in **Fig.26**. However, this sidewall does not provide snake with any significant thrust force as discussed in Appendix D.2. The trackway's substrate consists of a series of 5 blocks of Styrofoam. Underneath the Styrofoam, reinforcement is provided using 2 wooden planks of thickness 5 cm to reduce bending due to the combined animal and trackway weight. The trackway length measures 10 snake body lengths for the boa constrictor, 3 body lengths for the Dumeril's boas and 4 body lengths for the Gaboon viper. This length ensured a large number of periods are obtained from each trial.

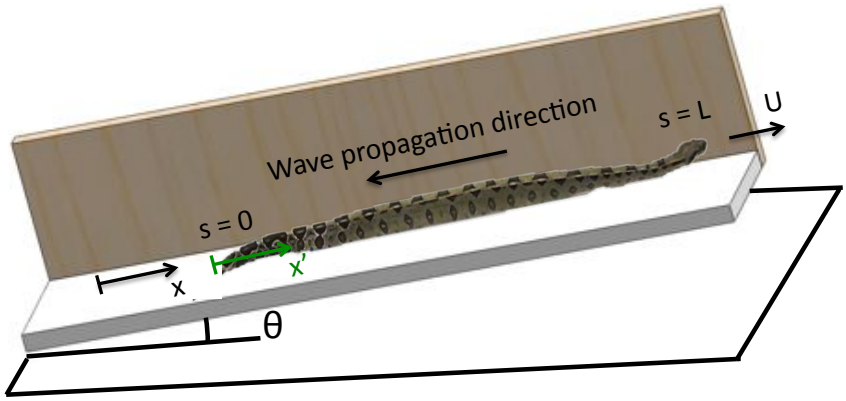

Figure 26: Schematic of the apparatus used to study rectilinear locomotion. Here θ is the inclination angle with respect to the horizontal. The front wall (not shown) is composed of plexiglass. The ground coordinate frame (x) and moving coordinate frame (x') are indicated by the arrows. The direction of wave propagation in rectilinear locomotion is opposite to the direction of motion.

Experiments are conducted outdoors. We film snakes from the side using a high definition digital video camera (Sony HDRXR200). Open source Tracker, a Video Analysis Modeling Tool (`www.cabrillo.edu/~dbrown/tracker/`), is used to measure the time course of the positions of approximately 20 naturally-occurring spots on the snake. Average body speeds are measured over 7 - 15 periods. The wave processing algorithms and peak detection method are discussed in Appendices D.3 and D.4.

6.2.4 Definition of reference frames

To describe body kinematics, we begin with a formal definition of two reference frames illustrated in **Fig.26**. Most previous work on snakes uses two or three-dimensional coordinate frames. However, for rectilinear locomotion, we require kinematics and dynamics along a single dimension. Kinematics is described by unidirectional contractions and extensions. Body lifting is prescribed using a direction-dependent friction coefficient in § 6.4.1.

Two reference frames are of interest: the first is the ground coordinate system x which is fixed to the trackway. The second is a moving coordinate frame x' fixed to the snake's tail, and travels with the snake's steady body speed V. Appendices D.5 and D.6 show snakes rectilinear motion in these two coordinate systems. Initially, the origins of both coordinate frames coincide at the tip of snake's tail. For each time t, the relation between the two coordinate frames is:

$$x' = x - Vt, \tag{30}$$

where distances are given in cm and time in seconds. The use of the snake coordinate frame (x') permits prescription of kinematics without reference to center of mass. In this frame, positions of points on the body are purely oscillatory due to the passage of a traveling wave, as shown in Appendix D.6. The snake spans a distance from its tail ($s = 0$) to its head ($s = L$), where L is the snake length. We characterize traveling wave kinematics using time t and distance s along the snake, measured from the tail. Traveling waves propagate towards the tail, in the negative x' direction.

6.3 Model

We model snakes as one-dimensional n-linked crawlers (**Fig.27**). For this purpose, we adapt a model we developed previously for concertina locomotion [52]. Snakes are discretized into n nodes connected in series by $n-1$ inter-nodal elements, or extensible "muscles", whose length dynamics characterize the traveling wave. The inputs to our model are the snake's traveling wave kinematics and friction coefficients, both measured in our experiments. The output to the model is the snake's center of mass position $\bar{x}$. For each node in contact with the substrate, we use a sliding friction law in which the friction force is

$$F_i = -\mu_i F_N \mathrm{sgn}(\dot{x}_i) \tag{31}$$

where F_N is the normal force due to the node's weight, and $\dot{x}_i$ the node's speed. The sliding friction coefficients μ_i of the ventral surface are μ_f and μ_b, respectively, for the forward and backward directions. We apply Newton's second law to each of the n nodes, considering both friction and inter-nodal forces. Details are given in Marvi *et al.* [52]. The non-dimensionalized governing equation for the center of mass is:

$$Fr\ddot{\bar{x}} = \frac{\cos\theta}{n}\left[-\mu_f \sum_{i=1}^{n} H(\dot{x}_i) + \mu_b \sum_{i=1}^{n} H(-\dot{x}_i)\right] - \sin\theta, \tag{32}$$

where $H(x) = \frac{1}{2}(1+\mathrm{sgn}x)$ is the Heaviside step function, θ is the inclination angle, and Fr is the Froude number defined as

$$Fr = \frac{\text{inertia}}{\text{gravity}} = \frac{L}{\tau^2 g} \tag{33}$$

where L is body length, τ the period of the extension-contraction, and g the gravitational acceleration. According to our experiments, the Froude number is very small ($Fr \leq 2\times10^{-4}$) indicating inertial force is extremely small compared to gravitational force. In comparison, Froude numbers for other snake gaits are one to two orders of magnitude larger: $Fr \approx 0.002 - 0.016$ for concertina motion [52] and $Fr \approx 0.02$ [17] for slithering. Clearly, rectilinear locomotion has lower inertial forces than the other snake gaits.

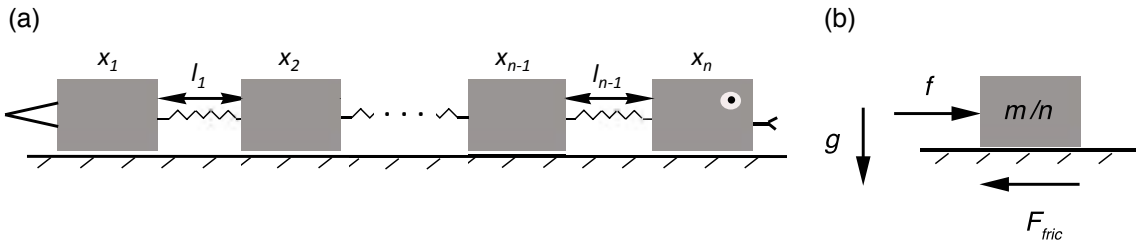

Figure 27: Mathematical model for rectilinear locomotion. (a) Schematic of n-link crawler and (b) forces applied to each block.

The low Froude number for rectilinear locomotion is consistent with the high repeatability of our experiments. If a snake has negligible inertia, snakes need very little lead time to reach steady speed. Moreover, each period of motion is dynamically similar to the first period starting from rest. We see evidence of these attributes in our experiments. Body speed is constant from beginning to end of the trial. Moreover, we observe a nearly instantaneous ramp up to steady speed at the beginning of the trackway. A similarly instantaneous deceleration is observed at the end of the trackway.

6.4 Experimental results

In this section, we present measurements of snake body-lifting, frictional properties, and kinematics, which together will be employed in our model to predict snake speed. Kinematics are presented in terms of traveling waves along the ventral surface. We lastly present scaling of kinematics among the three snake species we used in this study.

6.4.1 Snakes lift ventral surfaces to move forward

Fig.28 shows a video sequence of a boa crawling forward by lifting its ventral surface (Appendix D.7). We visualize this body lifting by shining a purple light from one side of the snake. In the first frame, the majority of the body is pressed against the ground, which prevents the side lighting from reaching the camera. At t = 0 s, the front of the body is lifted. At t = 2.5 s, this wave progresses backwards 15 cm at a speed of 6 cm/s, and is marked by a newly lifted segment of the snake. The continuous motion of this lifted region is shown in the Appendix D.7. We observe the wave of lifting propagates at the same speed as the wave of contraction, in correspondence with the assumptions of our model. We estimate lift height to be 1mm by measuring the thickness of the light sheet visible beneath the ventral surface.

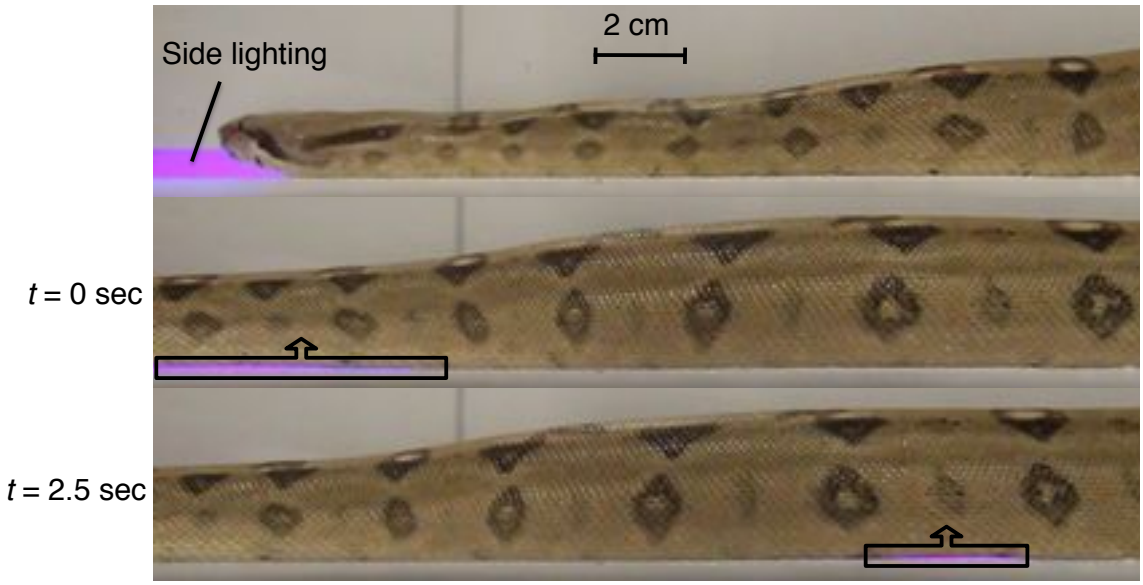

Figure 28: A boa constrictor lifting parts of its body during rectilinear locomotion. We shine a purple light from the side which passes underneath the snake to reveal lifted parts. For clarity, lifted regions are denoted by a black outline and an arrow indicating direction of lifting. The body is lifted approximately 1 mm and the corresponding wave speed is 6 cm/s.

Why do snakes lift 1 mm in height? We can rationalize this length scale using a simple scaling argument. The primary reason for lifting is to save energy. Thus, we hypothesize the energy expended to lift must be less than the frictional dissipation of sliding forward without lifting. The energy spent on lifting is $m_l g \Delta h$ where m_l is the mass of the snake's lifted section, g is the gravitational acceleration and Δh is the lift height. If the snake did not lift, it would dissipate a frictional energy $\mu_f m_l g \Delta x$, where μ_f is the forward friction coefficient, and Δx is body displacement in the direction of motion. For a boa constrictor with $\mu_f = 0.3$ and a forward displacement corresponding to the wave amplitude, Δx=0.27 cm, we find Δh should be less than 0.8 mm to keep the lifting cost less than friction dissipation. This value is comparable to that measured, in confirmation of our hypothesis. Using similar methods, we predict the Gaboon viper must lift to a comparable height of 1.9 mm. We find the Dumeril's boa has the smallest required lift height, a value of only 0.3 mm, because it has has the lowest friction coefficient of the three snakes studied. These estimates of ventral surface lifting will be incorporated into our prediction of snake energy expenditure in § 6.5.4.

6.4.2 Friction coefficients

Table 5 shows the sliding friction coefficients of conscious snakes, measured on an inclined plane. The Gaboon viper ($\mu_b = 0.32$) and red-tailed boas ($\mu_b = 0.42 \pm 0.05$) have the highest friction coefficients, nearly 5-7 times that of Dumeril's boas ($\mu_b = 0.06 \pm 0.01$). This difference is likely due to the difference in their habitat: Gaboon vipers and red-tailed boas live arboreally in rain forests and woodlands and so need high friction to climb trees. Dumeril's boas are terrestrial snakes, whose low friction coefficients make them poor climbers [119].

We observe in our experiments that snakes lift their bodies to move forward, an analogous behavior to legged animals which lift the leading foot rather than drag it on the ground. This indicates the forward friction coefficients reported in Table 5 are not dynamically relevant during locomotion. Thus, we prescribe the effective forward friction coefficient μ_f be zero in our modeling:

$$\mu_f = 0. \tag{34}$$

6.4.3 Tracking of body markers

To characterize the traveling wave, we track the position of 20 - 26 naturally-occurring body markers, whose spacings are roughly equal on a given snake. Appendix D.8 illustrates the tracked markers on a Dumeril's boa. As discussed in Appendix D.9 we consider only the ventral surface anterior to the tail. **Fig.29**a,c show the muscular traveling waves across the snake body. As shown in **Fig.29**c the ventral surface has the largest wave amplitude compared to middle and dorsal levels. Hereon, we report only on waves at the ventral surface, which is in contact with the substrate. Each point on the snake undergoes a periodic motion (period $\tau = 2$ - 5 seconds). The combination of a long trackway (3 -10 body lengths) and slow speed of the snakes (1 - 6 cm/s) permits us ample data on the traveling wave. We discard the first and last period of motion along the trackway and analyze the remaining 9 periods of motion for red-tailed boas, 7 periods of motion for Dumeril's boas, and 15 periods for the Gaboon viper.

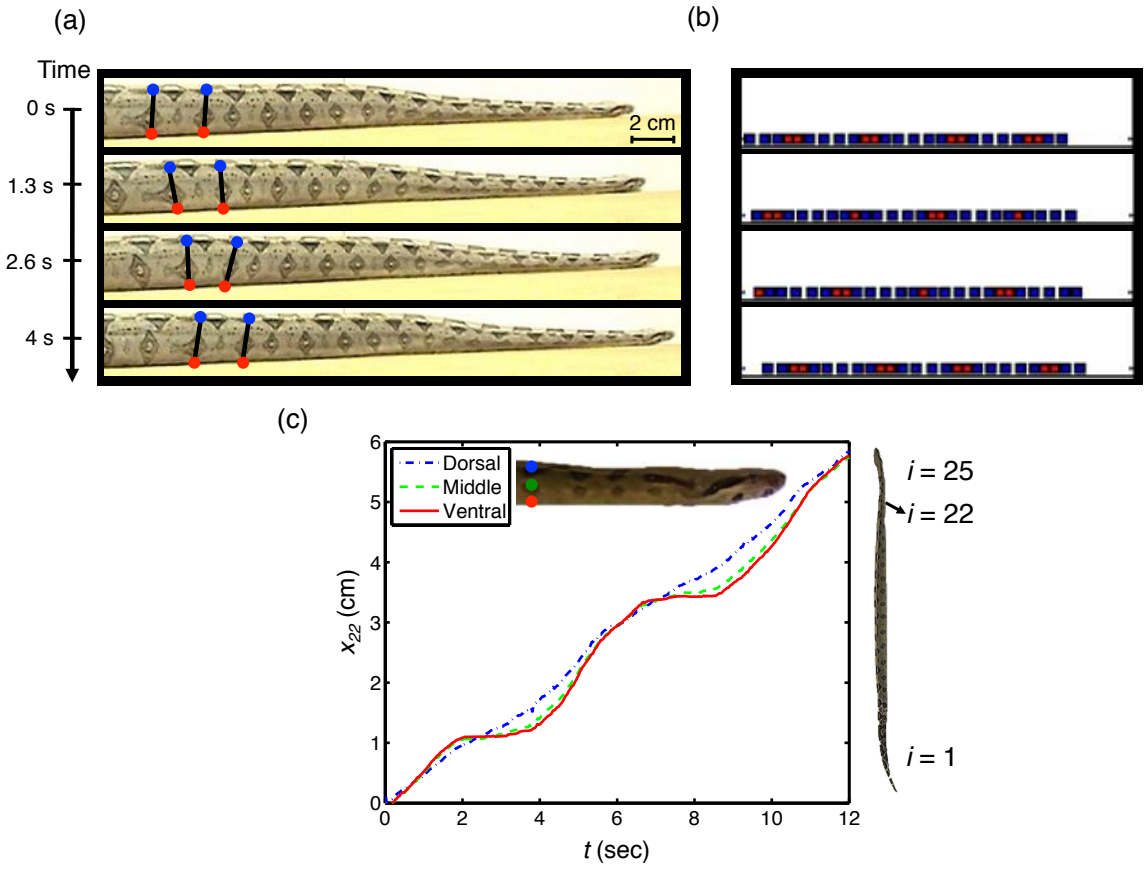

Figure 29: Unidirectional contraction-extension wave during rectilinear locomotion. (a) Image sequence of a boa constrictor performing rectilinear locomotion. The black lines follow the naturally occurring patterns on the snake skin and their spacing demonstrates the muscular strain at varying heights along the body. (b) One period of our n-link crawler model. The red blocks correspond to anchorage points. (c) Time course of the distance travelled by the 22nd spot on the snake, as shown in the inset. The colored lines indicate muscular traveling waves at three different elevations across the snake body: ventral, middle, and dorsal.

Consider the locomotion of the red-tailed boa; analysis of other snakes proceeds similarly. **Fig.30**a shows the time course of position for $n = 25$ naturally-occurring markers. The markers lie low on the snake's flanks but are visible just above the ground, as shown in **Fig.28**. In **Fig.30**a-b, we plot position in the ground reference frame x in order to show the distance travelled. The green curve on this plot corresponds to the position of the snake's head. Purple and red colors represent the snake's middle and tail, respectively.

The black arrows in **Fig.30**a indicate the direction of the traveling wave; the magnitude

of the slope of these arrows corresponds to the sum of magnitudes of the snake speed V and wave speed V_w. **Fig.30**b shows a magnified view of three points near the snake's head. These points perform a forward-backward oscillation combined with a constant speed in the forward direction.

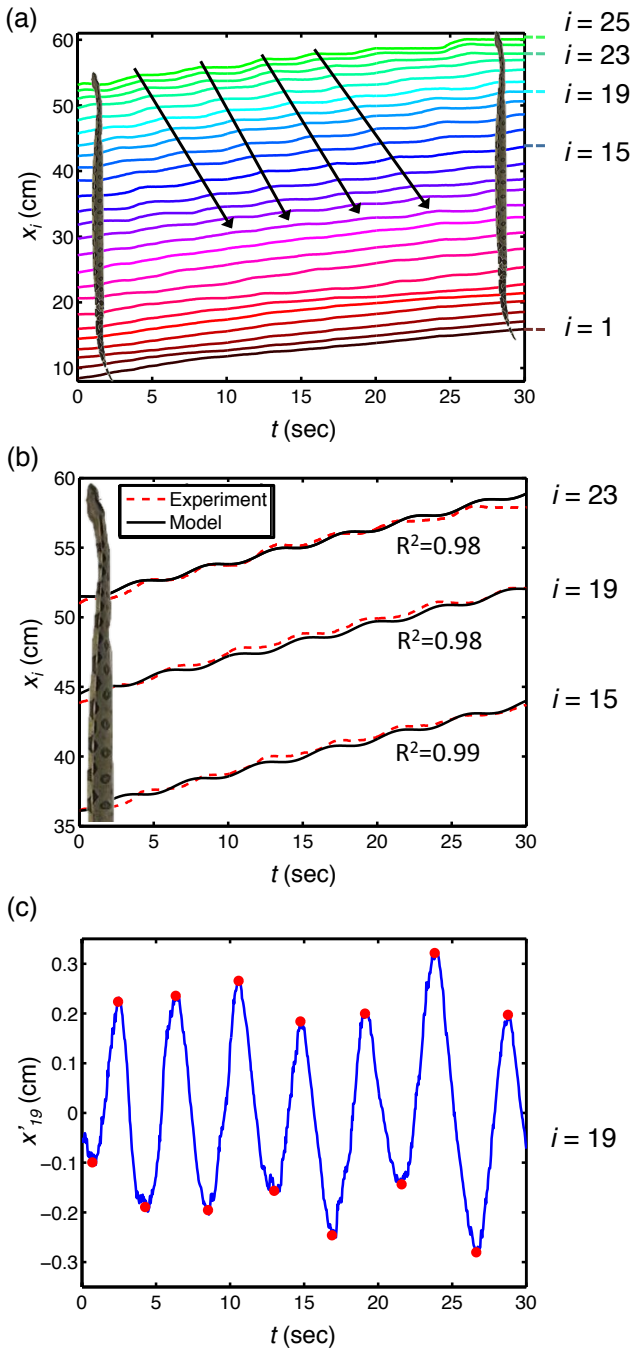

Figure 30: Body kinematics. (a) Time course of positions of 25 dots on the snake's body. The slope of the arrows has magnitude equal to absolute snake speed plus wave speed. (b) Time course of points 15, 19, and 23, as labeled in (a). (c) Peak detection of the traveling wave in the snake coordinate system. The noise in this plot has amplitude of around 0.2 mm, and is due to image processing noise.

The blue curve next to $i = 19$ in **Fig.30**a shows the position of the 19th marker from the snake's tail. **Fig.30**c shows this position x' in the moving frame of the snake. We curve fit the position data x' to the traveling wave equation,

$$x'(s,t) = A\sin(\omega t + ks) + s, \tag{35}$$

To determine the parameters in Eq. (35), we use the curve-fitting algorithm discussed in Appendices D.3 and D.4. This algorithm is applied to each marker along the snake for 7-15 periods, yielding values for the wave parameters. **Fig.31** the relation between these wave parameters and the snake's body length. Averages and standard deviations are taken across all n body markers on a snake performing rectilinear locomotion for several periods (where n for each individual is given in Table 5). We report means and standard deviations of different experimental parameters for each individual snake in **Fig.31**-**Fig.33**. Wave parameters were quite uniform: standard deviations of less than 20 percent were found for all, with the exception of a single red-tailed boa specimen which had a standard deviation of 40 percent.

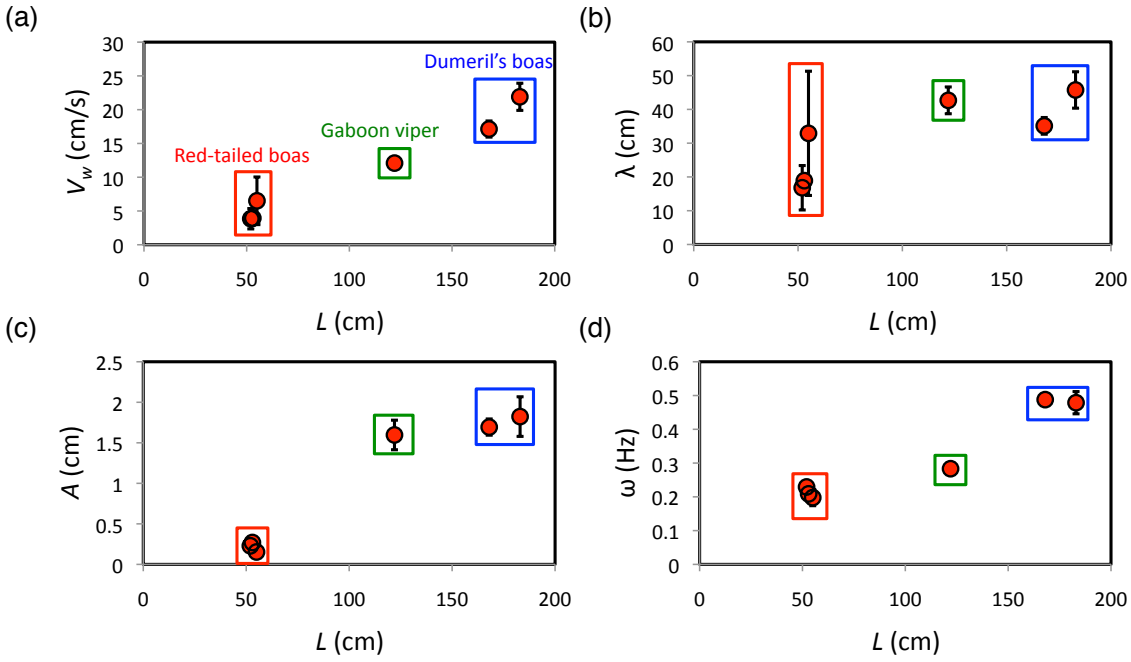

Figure 31: Scaling of wave kinematics. (a) Wave speed V_w, (b) wavelength λ, (c) wave amplitude A, and (d) wave frequency ω of snakes in rectilinear locomotion.

We used JMP software to determine statistical significance of measured wave parameters. The results of our statistical analysis are summarized in Table 6. We determine the

effect of body length L on several parameters including snake mass m, speed V, wave speed V_w, wave amplitude A, wave frequency f, and wavelength λ. Body length has a statistically significant effect on all parameters, with a significance level of $\alpha = 0.01$, with the exception of wavelength λ.

Table 6: The effect of snake body length L, on mass m, body speed V, wave speed V_w, wave amplitude A, wave frequency f, wavelength λ, percentage of body at rest, and Partial Cost of Transport PCT. Body length has a statistically significant effect, up to a significance level of $\alpha = 0.01$, on all parameters except λ, percentage of body at rest, and PCT. F is the F-statistic and p is the p-value.

		L (cm)				
		Slope	**Intercept**	**R^2**	**F**	**P**
Mass	m (kg)	0.0267	0	0.73	29.15	0.0029*
Body Speed	V (cm/s)	0.0275	0	0.79	44.35	0.0012*
Wave Speed	V_w (cm/s)	0.107	0	0.95	367.19	< 0.0001*
Wave Amplitude	A (cm)	0.01	0	0.86	93.35	0.0002*
Wave Frequency	f (Hz)	0.0028	0	0.81	191.02	< 0.0001*
Wavelength	λ (cm)	0.158	15.4	0.64	6.99	0.0573
Percentage of Body at Rest	% of body at rest	-0.0002	0.27	0.024	0.098	0.77
Partial Cost of Transport	PCT (j/kg m)	0.003	1.32	0.005	0.018	0.9

6.4.4 Scaling of kinematics

Waveform parameters are found to depend upon body size, as shown in **Fig.31**a-d. In previous studies, such trends are typically described using power laws. However, the small range in body length (factor of four) prevents us from properly extrapolating power laws. We instead report in Table 6 the slopes of linear trend lines for wave speed, amplitude, and frequency as a function of body length. As a consequence of these trends, body speed also increases linearly with body length as shown in **Fig.32** (R^2 =0.79). Curve-fitting is quite accurate across these variables, despite our physical constraint that the lines have zero-intercept (R^2 =0.81 - 0.95). We comment on the physical significance of these trends in turn.

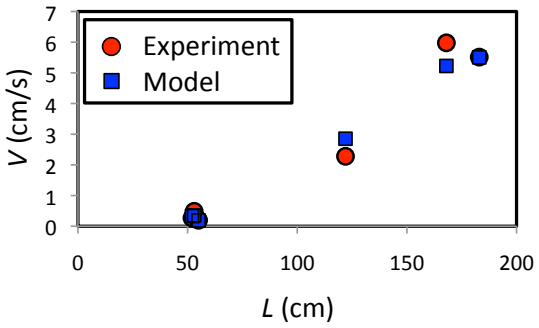

Figure 32: Snakes body speed V compared to model predictions.

Traveling waves have exceedingly small amplitude compared to body length: their ratio is 0.004 - 0.013. Such small amplitudes is atypical compared to other snake gaits. For instance, the amplitude in concertina and slithering is 0.1-0.14 body length [17, 52]. As we will show in our modeling in § 6.5.2, the low amplitude in rectilinear locomotion is the primary reason the gait is so slow.

Rectilinear locomotion is a slow mode of locomotion: speeds are only 0.2 - 6 cm/s, or 0.02-0.07 body lengths per second, for the 50-180 cm snakes studied. It typically takes 14 to 50 seconds to travel a single body length. The speeds of the boas in our study are comparable to those found by Lissman. He measured a speed of 0.37 cm/s on glass for two *Boa occidentalis* (length 58.5 ± 2.2 cm) [31]. Other gaits performed by related species are much faster. For example, a 90 cm Rosy Boa (*Lichanura trivirgata*) can slither at 10 cm/s on horizontal ground partially covered with small plants [120]. Indeed, rectilinear locomotion is not employed for its high speed.

Traveling waves are fast, ranging from 5 cm/s in the red-tailed boas to 25 cm/s in the Dumeril's boa. The high speed of the traveling wave is clearly visible in Appendices D.5-D.8: waves tend to zip down the body while the snake lumbers forward slowly. Across the snakes studied, wave speed is three times body speed ($R^2 = 0.82$).

Wavelength indicates how many waves are visible at a given moment. The ratio of wavelength to body length is 0.35 ± 0.14. Thus, at each instant, 2-3 waves are present along the body. This is consistent with previous reports by Lissman of two simultaneous traveling waves in *Boa occidentalis* [31].

6.5 Numerical results

We now present predictions from our numerical model. We investigate the effect of changes in kinematics and friction coefficients on snake body speed. We report results only for the

female Dumeril's boa, the fastest snake in our study, but these methods may be applied to other snakes in our study. The inputs to the model include snake friction coefficients, given in Table 5 and Eq. (34) and traveling wave kinematics, given in **Fig.31**. We change each of these inputs systematically in the following parameter study. We begin in § 6.5.1 by using the model to predict the stationary points of the snake on the ground. We then proceed in § 6.5.2 to predict how changes in one kinematic variable affect snake speed. In § 6.5.3, we predict how body lifting would improve body speed. Lastly, in § 6.5.4 we discuss the energetic cost of rectilinear locomotion.

We use numerical simulation to integrate the model presented in § 6.3. The inputs to the model are described in Appendix D.10. The snake's prescribed traveling wave, Eq. (35), in conjunction with the governing differential equation Eq. (32) provide a system which we integrate over several periods to determine steady body speed. We use MATLAB to find the numerical solution to this system. We apply the Dormand-Prince pair method, a member of the Runge-Kutta family of ordinary differential equation solvers, to find the solution of Eq. (32) numerically [77]. Using a dimensionless time step $\Delta t = 10^{-4}$, we solve Eq. (32) iteratively to determine the position of the snake's center of mass $\bar{x}(t)$.

6.5.1 Model predictions of stationary points and body speed

Fig.29a-b and Appendix D.8 compare one period of rectilinear locomotion of our n-linked crawler model to that of a snake. Red blocks correspond to stationary points on the snake's ventral surface, where we define stationary points as those with velocities less than 15% of body speed. These stationary points are important to track because only these points generate thrust.

Fig.33 shows the relation between body length and percentage of the body that is instantaneously stationary, as found using our image analysis. We found 18 - 35% of the snake body is instantaneously stationary. The uniform distribution of such "push points" along the body enables the snake to generate thrust even if the body is on heterogeneous slippery terrain. For example, if the middle of the snake is crossing a puddle, both the front and back end can still generate thrust to push it across.

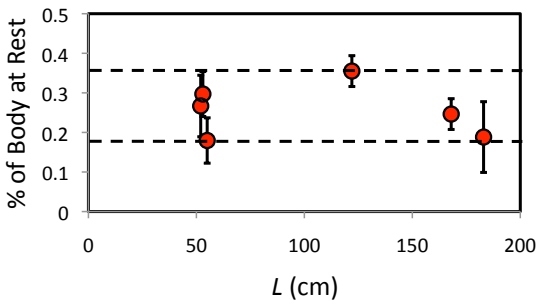

Figure 33: Fraction of the snake body that is instantaneously stationary.

Fig.32 shows the relation between body length and speed. Experiments are given by the red symbols and the model prediction by the blue. The model predictions based on friction coefficient and body kinematics are highly accurate. Accuracy ranges from 97% accuracy for the Dumeril's boa to 73% accuracy for the red-tailed boa.

6.5.2 Optimality in rectilinear locomotion

In rectilinear locomotion, snakes generate traveling waves prescribed by three kinematic variables, period τ, amplitude A, and wavelength λ. We hypothesize rectilinear locomotion is optimal with respect to these variables. Consequently, we expect changes in these variables to result in lower body speed. In this section, we test this hypothesis using our model.

Fig.34a-c show changes in body speed due to variation of one kinematic variable, while keeping the other two variables and the friction coefficients fixed at their observed values for the Dumeril's boa. We find wave period and amplitude most influence body speed, whereas wavelength has little effect. We discuss these variables each in turn.

As shown in **Fig.34**a, snake speed peaks at period $\tau = 1$ s. The period of snake locomotion from our experiments ($\tau = 2.1$ s) is close to the optimal period of wave propagation ($\tau = 1$ s) as shown in **Fig.34**a, suggesting that snakes indeed choose the optimal period for maximizing speed. Deviations from the optimal period of 1 s result in slower speeds. Larger periods corresponding to slower wave propagation, or fewer steps per second, result in slower body speed. Less intuitively, smaller periods also reduce speed, a phenomenon we may rationalize using Froude number.

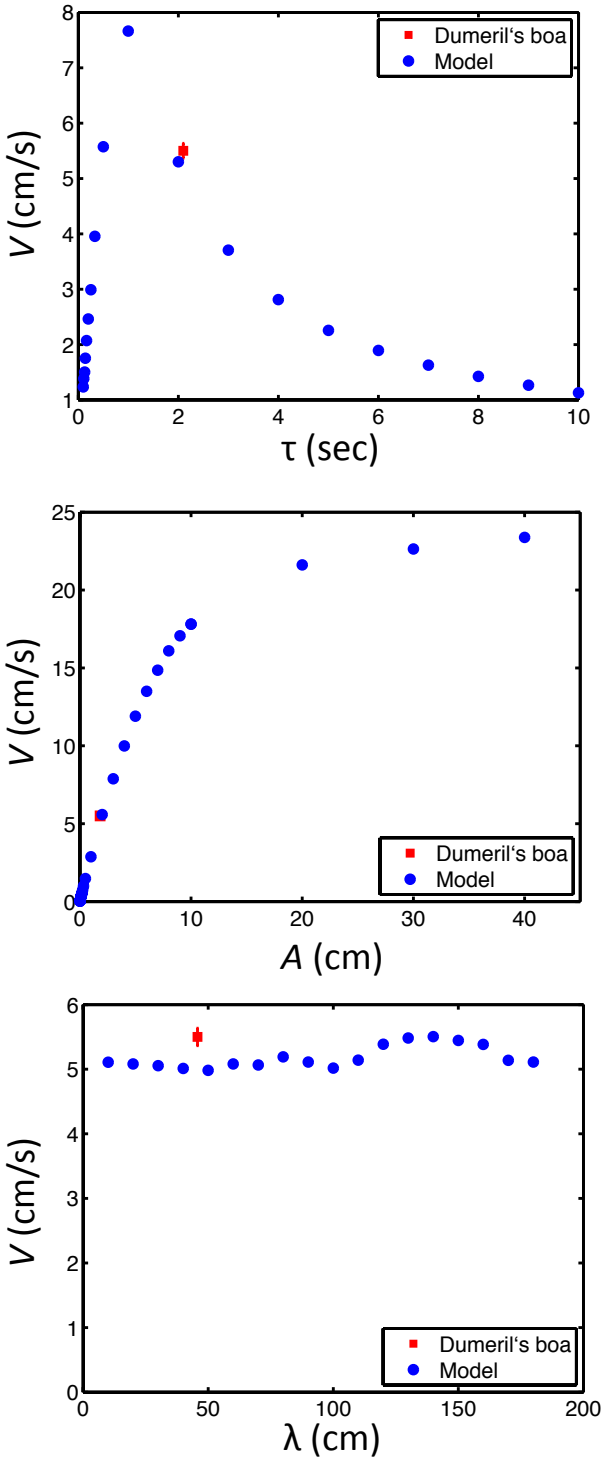

Figure 34: The relation between predicted body speed and changes in body kinematics. Variation in body speed as a function of (a) the period of wave propagation τ, (b) wave amplitude A, and (c) wavelength λ as predicted by our mathematical model. Red data point shows experimental measurements for Dumeril's boa.

To compare inertia to friction in rectilinear locomotion, we redefine the Froude number as

$$Fr^* = A/(\mu_b \tau^2 g). \tag{36}$$

In this formulation, we replace body length L in Eq. (33) with amplitude A, which, for rectilinear locomotion, is a more accurate measure of local speed relative to ground. The friction coefficient μ_b is used to account for friction force. If period of motion is smaller than 0.18 s, Fr^* will be larger than unity and thus the inertial force will be greater than backward friction force. This inertia causes the snake to slip backwards during rectilinear locomotion and slow down accordingly. An optimal wave period can be rationalized thusly: snakes should keep their wave periods sufficiently high to remain in the low-Froude number regime, but not so high that they begin to decrease their speed.

Fig.34b shows the snake's choice of wave amplitude is sub-optimal. In fact, increasing amplitude will increase body speed in the same way that taking longer steps increases the speed of walking. The maximum amplitude that can be taken before slipping occurs can also be rationalized using Froude number: a wave amplitude larger than 2.6 m will make the inertial force greater than the friction force and the snake will begin to slip. As a result, we expect a reduction in speed for amplitudes larger than 2.6 m. We do not observe such large amplitudes in nature because of the limiting strain in snake muscle.

Fig.34c shows wavelength does not affect body speed, at least on the homogenous substrates we have studied. Wavelength prescribes the number of waves along the body at a given instant. In our simulation, we increase the number of waves from 1 to 200. We do not observe an optimum because the number of waves does not affect Froude number. As long as Froude number is small, friction force is larger than inertial force, and the body continues to maintain its grip with the ground. Consequently peak body speed is set by the wave amplitude and period; additional waves do not move the body faster.

The trends in **Fig.34** are qualitatively accurate for other snakes. We conducted the same optimality analysis for other species of snakes used in our experiments and we observed similar trends for all of them. Specifically, both red-tailed boas and Gaboon viper have wave periods that are larger than the optimum values such that snakes are in the non-slipping regime. Moreover, their wave amplitudes are sub-optimal and wavelength does not impact body speed.

6.5.3 Benefits of lifting on surfaces of various roughness

Fig.35 shows the predicted relation between body speed and backwards friction coefficient. We present two trends, the body speed with body lifting (blue open points) and without

lifting (red closed points). For the latter, we use our measured forward friction coefficients, which is 0.017 ± 0.002 for the Dumeril's boa. The friction coefficient and body speed measured for the Dumeril's boa is denoted by the black square. For this friction coefficient, lifting increases body speed by 31%, indicating the importance of lifting behavior, at least on the surfaces tested in our experiments. On other surfaces, lifting remains beneficial for forward movement. We investigate numerically the effects of lifting on speed for a range of values in backward friction coefficient.

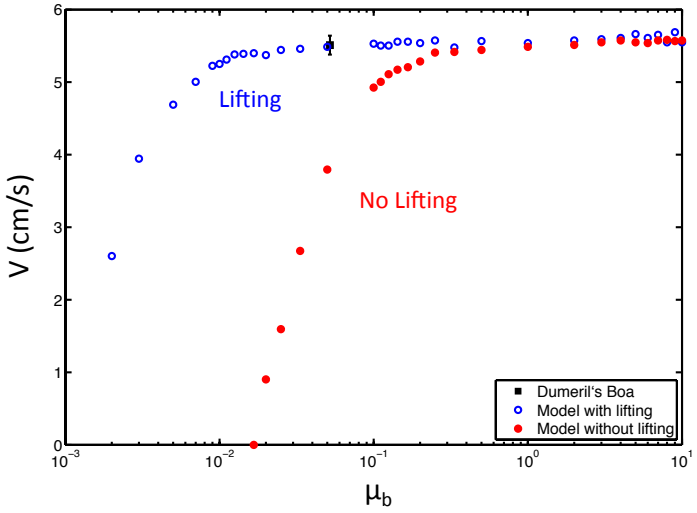

Figure 35: The relation between predicted body speed V, and backwards friction coefficient μ_b. Speed of a snake lifting its body is compared to one without body lifting. The black data point shows experimental measurements for Dumeril's boa.

At low values of backwards friction coefficient, locomotion is poor. If friction is zero ($\mu_b = 0$), the lifted snake remains stationary during rectilinear locomotion. Such inability to move has also been seen in previous work on other gaits. Slithering on a featureless surface yields no net motion [17]. Correspondingly, the non-lifted snake remains stationary if the backwards friction coefficient is equal to the the measured value of the forward friction coefficient, 0.017.

At low friction coefficients, lifted and non-lifted snakes differ in speed as shown on the left hand side of **Fig.35**. In this regime, the combined effects of Froude number and friction anisotropy each affect locomotion. For non-lifted snakes, as friction coefficient μ_b decreases, Froude number increases and frictional anisotropy decreases. Both these effects cause slipping and so decrease body speed. In contrast, the lifted snake has infinite friction anisotropy for any non-zero backwards friction coefficient. Thus, it can undergo larger

Froude numbers and thus larger inertial forces without a decrease in body speed. Thus, lifted snakes move more robustly than non-lifted snakes.

At intermediate friction coefficients, snakes increase in speed with increasing friction coefficient. Speed asymptotes at 5.5 cm/s. This asymptotic behavior begins at a friction coefficient of 0.01 for lifted snakes and 0.1 for non-lifting snakes. Thus, lifted snakes have a larger range of surfaces they can climb upon while still maintaining their high speed.

At the highest friction coefficients ($\mu_b \geq 0.5$), lifting no longer improves body speed. In this regime, Froude number Fr^* is smaller than 0.0008, and so the inertial force is infinitesimal, minimizing backwards body sliding during locomotion. Given that both simulations are prescribed by the same body kinematics, they converge to the same speed of 5.5 cm/s. Thus, on the roughest surfaces, which provide high friction coefficients, lifting does not necessarily increase body speed.

6.5.4 Energetics

Previously we investigated how kinematics and friction coefficients affect body speed. A lumbering gait like rectilinear locomotion should have a low rate of working, or NCT. We hypothesize rectilinear locomotion has a smaller NCT than other gaits since it is the slowest and less energy is expended on inertia and lateral motion of body. We define a physical rate of work, or the Partial Cost of Transport PCT, which is a fraction of the net cost of transport, NCT, previously measured in snake metabolic experiments. We here use our model to estimate the scaling of PCT with body size.

The PCT of a snake performing rectilinear locomotion is the combination of work due to gravity W_{gravity}, dissipation associated with body lifting D_{lifting}, and inertia D_{inertia}. These terms are divided by snake mass m and the distance travelled in one period ΔL. Accordingly, this summation may be written

$$PCT = \frac{W_{\text{gravity}} + D_{\text{lifting}} + D_{\text{inertia}}}{m\Delta L}. \tag{37}$$

The gravitational work performed by a segment of mass m_i is $m_i g z_i$ where z_i is the vertical displacement. Since $\sum_{i=1}^{n} m_i z_i = m z_c$ where $z_c = \sin\theta \Delta L$ is the vertical displacement of center of mass, the work of gravity may be simplified as $mg\sin\theta\Delta L$, where m is the mass of the snake.

A snake lifts its segments to move them forward. We assume the energy used to lift a segment is not regained by the snake as useful work. Since all segments of the snake are lifted once during a period, from the view of energetics, we can consider the entire body mg lifting simultaneously. The energy dissipation due to a snake lifting its body is $mg\cos\theta\Delta h$ where Δh is the highest elevation of a segment.

The inertial losses associated with changing the snake's speed is given by D_{inertia}. Considering the change in speed of each segment, D_{inertia} may be written as $\sum_{i=1}^{n} m_i|\ddot{x}_i\Delta x_i|$ where m_i is the mass of ith segment, $\ddot{x}$ is the second time derivative of $x(t,s)$ presented in Eq. (35), and Δx_i is the displacement of ith segment. As a result, Eq. (37) may be written as

$$\text{PCT} = g\sin\theta + \frac{g\cos\theta\Delta h}{\Delta L} + \frac{\sum_{i=1}^{n} m_i|\ddot{x}_i\Delta x_i|}{m\Delta L} \tag{38}$$

Fig.36 illustrates PCT for three red-tailed boas, a Gaboon viper, and two Dumeril's boas. The PCT for these snakes ranges between 0.22-7.5 J/kg m. We do not account for the effect of snake metabolism in our calculation. Notwithstanding, our PCT estimates are up to an order of magnitude less than the NCT measures found for other snake gaits, consistent with the notion that rectilinear is indeed the most efficient gait.

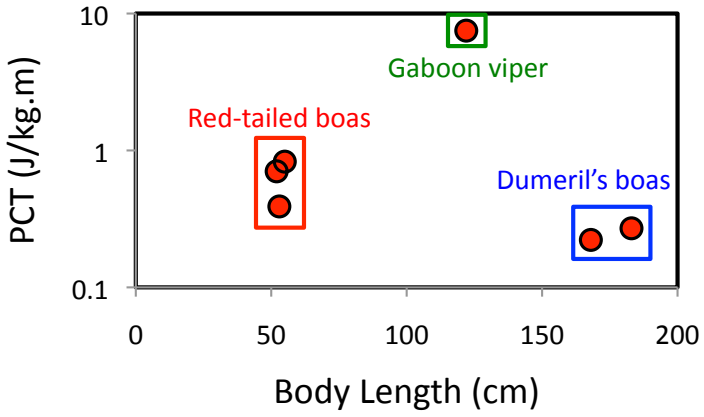

Figure 36: Calculated rate of working, or partial cost of transport (PCT) for three red-tailed boas, two Dumeril's boas, and a Gaboon viper.

By examining the relative magnitudes of the energies expended in the PCT, we can gain insight into the dominant energetics. Work done to lift the snakes, D_{lifting}, is dominant for red-tailed boas ($92 \pm 5\%$ of PCT). Conversely, work done against body inertia D_{inertia} is dominant for both Gaboon viper (97% of PCT) and Dumeril's boas ($90 \pm 1\%$ of PCT). Why does the red-tailed boa spend more energy on lifting than the other two snakes? As shown in Eq. (38), the lifting energy scales as the dimensionless $\Delta h/\Delta L$. The red-tailed boa lifts the highest of the snakes. Consequently, it has values of $\Delta h/\Delta L$ which are 2 - 15 times that for the other snakes, and so a correspondingly high lifting energy.

6.6 Discussion

6.6.1 Unique wave frequency scaling

Our study of rectilinear locomotion yields new insight into the fundamental differences between legged and legless locomotion. In both types of locomotion, we can characterize a frequency of bodily contacts with the ground. Legged animals exhibit decreasing frequencies with increasing body size. For example, elephants have lower leg frequencies than much smaller animals such as mice. The reason for this trend is well known [78, 121]: larger animals are more massive, and given the same specific muscular power, move more slowly and so have lower frequencies. This trend also extends to certain gaits in limbless locomotion. In concertina and lateral undulation, larger snakes also have lower frequencies [72, 122, 123].

Surprisingly, we find the opposite trend in rectilinear locomotion: larger animals tend to have higher frequencies, increasing by more than a factor of two, from 0.2 Hz to 0.5 Hz, as snake length increases from 52 to 183 cm. This trend is clearly limiting for large snakes. Is this trend universal across other animals that use unidirectional motion? To answer this question, we compare rectilinear kinematics to those previously measured for other animals, including maggots [2], caterpillars [3–6], and earthworms [7, 8]. **Fig.37**a-c shows the results of this comparison.

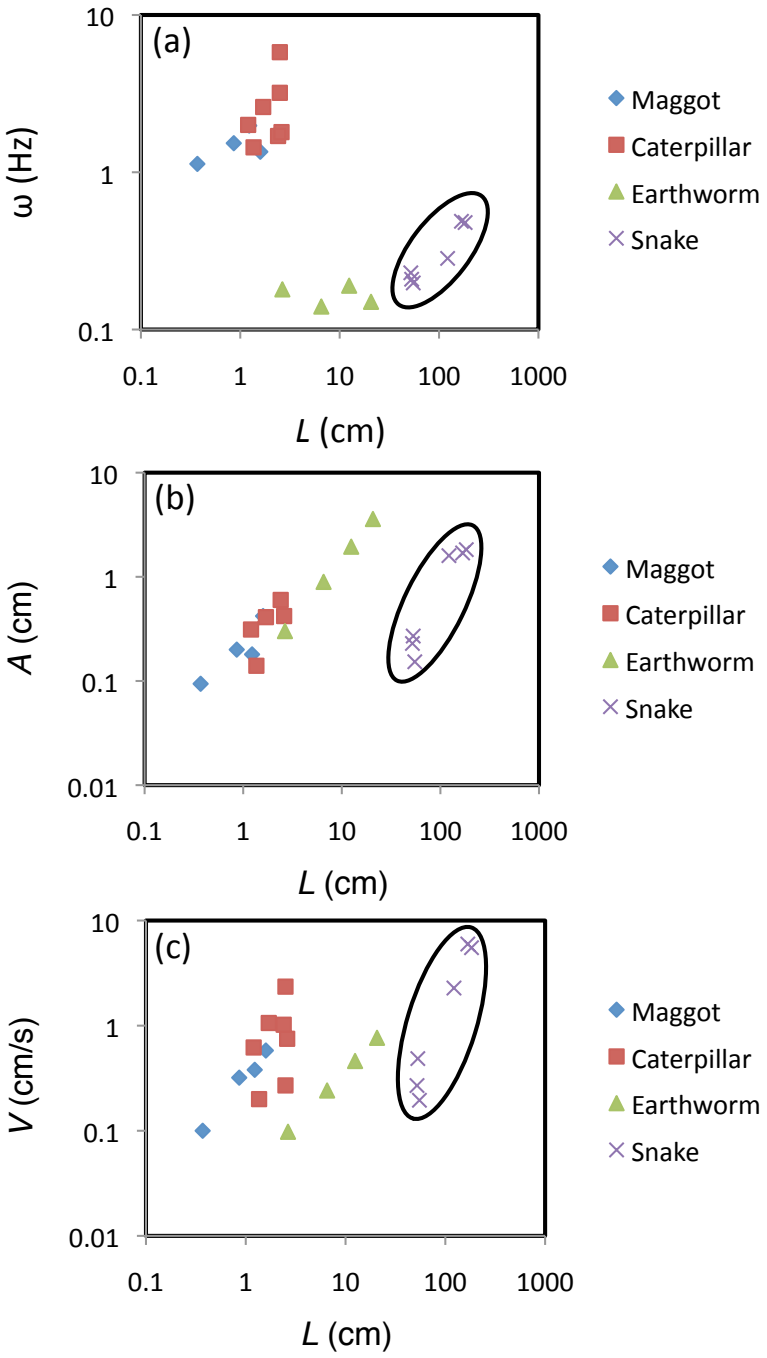

Figure 37: The relation between body length L and (a) wave frequency ω, (b) wave amplitude A, and (c) body speed V for several rectilinear movers, including maggots [2], caterpillars [3–6], earthworms [7, 8], and snakes.

Fig.37a shows the relation between frequency and body length. We find snakes are the only rectilinear movers to have increasing frequency with increasing body size ($P <$

0.0001). Caterpillar, maggots and earthworms maintain nearly constant frequency with size (P=0.35, 0.56, and 0.78, respectively). In particular, the earthworm maintains a relatively constant frequency over a factor of 10 increase in body length (only 17% decrease in frequency). This is very different from the trend for snakes. Nevertheless, both earthworms and snakes appear to fit well along the same power law scaling ($\omega = 0.12L^{0.143}$, $R^2 = 0.84$). The accuracy of this trend line suggesting that their motion is indeed similar, despite quite different methods for generating force (hydrostatic pressure versus muscles).

Earthworms and snakes also tend to fit in the same category if their frequency range is compared to other animals. In **Fig.37**a, there exist two discrete regimes in frequency. Large animals such as snakes and earthworms ($\omega = 0.14 - 0.5$ Hz) have ten times lower frequencies than small animals such as maggots and caterpillars ($\omega = 1.1 - 5$ Hz).

Fig.37b-c show trends for amplitude and speed among maggots, caterpillars, earthworms, and snakes. Larger animals, with the exception of caterpillars, have greater amplitudes and faster speeds. This trend is typical in legged locomotion as well [78]. In terms of amplitude, maggots, caterpillars and worms again fall on a single trend line ($A = 0.168L$, $R^2 = 0.98$): their amplitudes are 17% of their body length. In comparison, snakes performing rectilinear locomotion have much smaller amplitudes (1% of body length). As we saw earlier in § 6.5.2, snakes would benefit from increasing their amplitude in rectilinear locomotion. This inability likely arises from the contractile-extensile limits of their muscles, which can be bypassed by worms because of their reliance on hydrostatic pressure.

6.6.2 Improving rectilinear locomotion

Rectilinear locomotion is quite a slow gait, achieving only 0.2-6 cm/s for snakes of length 50-180 cm. It is best used for creeping up on prey and other activities requiring stealth. Are there any behaviors that can increase the speed or efficiency of the gait?

We measured the range of inclination angles that snakes can perform rectilinear locomotion. We observed the maximum angles snakes can climb on Styrofoam are all quite low: they are 15^o, 6^o, and 3^o, respectively, for red-tailed boas, Gaboon vipers, and Dumeril's boas. At higher inclination angles, snakes will attempt to climb using rectilinear motion, but inevitably slide down. Thus rectilinear locomotion alone cannot be used to climb sheer vertical surfaces. Tree-climbing snakes ascending trees by using different parts of their body performing concertina or rectilinear locomotion, exploiting interstices and other features of the tree opportunistically. Thus, rectilinear locomotion should be used in combination with other snake gaits to be effective.

6.7 Summary and future directions

In this study, we report on the rectilinear locomotion of snakes. We characterize the kinematics of a snake's traveling wave using measurements of wave speed, amplitude and frequency. We discover scaling trends in rectilinear locomotion which contrast strikingly to those of other snake gaits and animal locomotion in general. In particular, wave frequency increases with increasing body size for snakes performing rectilinear motion. Such a trend is anomalous for legged animals [78, 121] and other rectilinear movers such as maggots, earthworms and caterpillars.

We report a theoretical crawler model to investigate how snake behaviors, such as lifting and kinematics, influence performance in terms of body speed and efficiency. Inputs to our model are the kinematics of the traveling wave and the frictional properties of snakes. The model output is the speed of a snake's center of mass, which compares favorably with experiments (73 -97% accuracy). During our experiments we observe snakes lift parts of their bodies during rectilinear locomotion, and we hypothesize they do so to reduce frictional dissipation. Our model shows that localized body lifting increases the speed of a Dumeril's boa rectilinear locomotion by 31%. This result is similar to previous simulations on slithering locomotion, in which lifting increases body speed by 35% [17].

We identify which wave parameters are optimal in rectilinear propulsion. We show this result by using our model to calculate snake speed over a range of kinematic variables. The wave frequency chosen by a Dumeril's boa is close to optimum: higher frequencies cause slipping and lower frequencies decrease thrust and slow the snake. The snake's amplitude, however, is sub-optimal and is likely limited by anatomical constraints. Lastly, we find wavelength does not influence body speed on uniform surfaces. Instead, it may help with robustness of the gait's interactions with ground contacts. Having a smaller wavelength is similar to walking with a greater number of feet, which may help in tackling surfaces with frequent imperfections.

CHAPTER VII

SIDEWINDING: AN ANTI-SLIP CONTROL TEMPLATE

7.1 Introduction

Studying biological systems has resulted in developing robots with new capabilities including rapid running [124], slithering [41, 53], flying [125], and swimming [126]. In a few systems, an effective loop of biological and robotic hypothesis testing have proven effective [124, 127]. In this work, we consider limbless snake robots mainly because snake robots possess advantages over conventional wheeled and legged devices in that they can thread through tightly packed volumes. Choset's group at Carnegie Mellon University (CMU) has developed snake robots which can perform a suite of biologically inspired behaviors, including slithering, tree climbing, etc. [41, 92, 128, 129]. One gait that has proven useful in navigating on flat and bumpy terrains is sidewinding [50].

While there have been many biological studies of snakes, there have been few studies of snakes that have translated into new capabilities in robots [15, 16, 53, 130]. These studies would be of considerable value when studying locomotion over snake natural environment such as sand and loose soil. Sand-adapted snakes use such a gait, consisting of a rolling contact with the ground without slipping. Sidewinding motion of snakes has been studied for nearly a century [1, 19, 34–36]. However, there is not yet a clear understanding of sidewinding on sand.

Mosauer, Gray, and Cowles study sidewinding from a qualitative perspective [19, 34, 35]. Jayne reports on muscular activities of sidewinder rattlesnakes moving on a treadmill [1]. There have been a few measurements [36] that indicate this gait confers energetic advantages on such surfaces, mainly through lack of slipping at the points of contacts. Secor *et al.* use respirometry technique to measure the energetic cost of sidewinding. They put sidewinders on a treadmill and report on their burst speed, endurance, and the net cost of transport. They show that Net Cost of Transport (NCT) of sidewinders is 8 J/kg m compared to 23 J/kg m for slithering and 170 J/ kg m for concertina motion [16, 24, 36].

Sidewinding is an efficient and robust gait and is suitable for traversing a wide range of terrain. Implementation of such sidewinding gaits in snake-robots yields effective high-speed locomotion. Thus, several roboticists have revealed interest in studying sidewinding and have tried to develop this gait for hyper-redundant robots [50, 131]. Hatton and Choset use an elliptical helical wave to generate sidewinding for a snakebot. They study the role

of ellipse aspect ratio on climbing performance of the snakebot on hard ground [50]. This robot is successful on climbing on sand on slopes of up to 10 degrees. In our experiments, we find when this robot is challenged on sloping granular surfaces at inclinations of higher than 10 degrees, the robot causes material to yield along axial (along the body) and lateral (direction of motion) directions. This phenomena significantly decreases locomotor performance of this snake robot on loose material.

The study of locomotion on granular media, both for natural and artificial systems, is challenging for a variety of reasons. The first has to do with modeling. Unlike locomotion on solid ground, the deformation of the sand causes the region of contact unpredictable; prior works in snake robot locomotion often requires precise placement of ground contact. Moreover, the contact may induce large shear force, and as a result, the sand may fail to provide enough force to propel the system without slipping. In previous studies of snake locomotion, it was assumed that the ground is solid such that frictional forces were sufficiently large to ensure no slip.

We conduct the first set of quantitative sidewinding experiments on sand. We specifically focus on the impact of animal interaction with the granular substrate on its climbing performance. We discuss our methods in § 7.2. We proceed with our snake experiments in § 7.3. We then introduce our drag measurements in § 7.4. We finally present our snakebot experiments in § 7.5 and then summarize our findings and discuss possible future direction in § 7.6.

7.2 Methods

7.2.1 Animal care

We collected six sidewinder rattlesnakes, *Crotalus cerastes*, ($N = 6$, $m = 97.8 \pm 18.4$ g, $L = 48.0 \pm 6.4$ cm) and 180 kg of sand from Yuma Arizona (**Fig.38**a). All of these snakes are housed at Zoo Atlanta where the experiments are conducted. We use nail polish to paint 7-10 marks on each snake for tracking purposes (**Fig.38**a).

7.2.2 Experimental setup

We designed and built an air-fluidized bed of size 2 x 1 m^2 to control the sand compactness and inclination angle (**Fig.38**c). 3 AOS high-speed cameras were used to record sidewinding of both snakes and the robot. We recorded videos at 1024×1280 pixels and 250 frames per second (fps). We used a Matlab code developed by Hedrick [132] to analyze the videos.

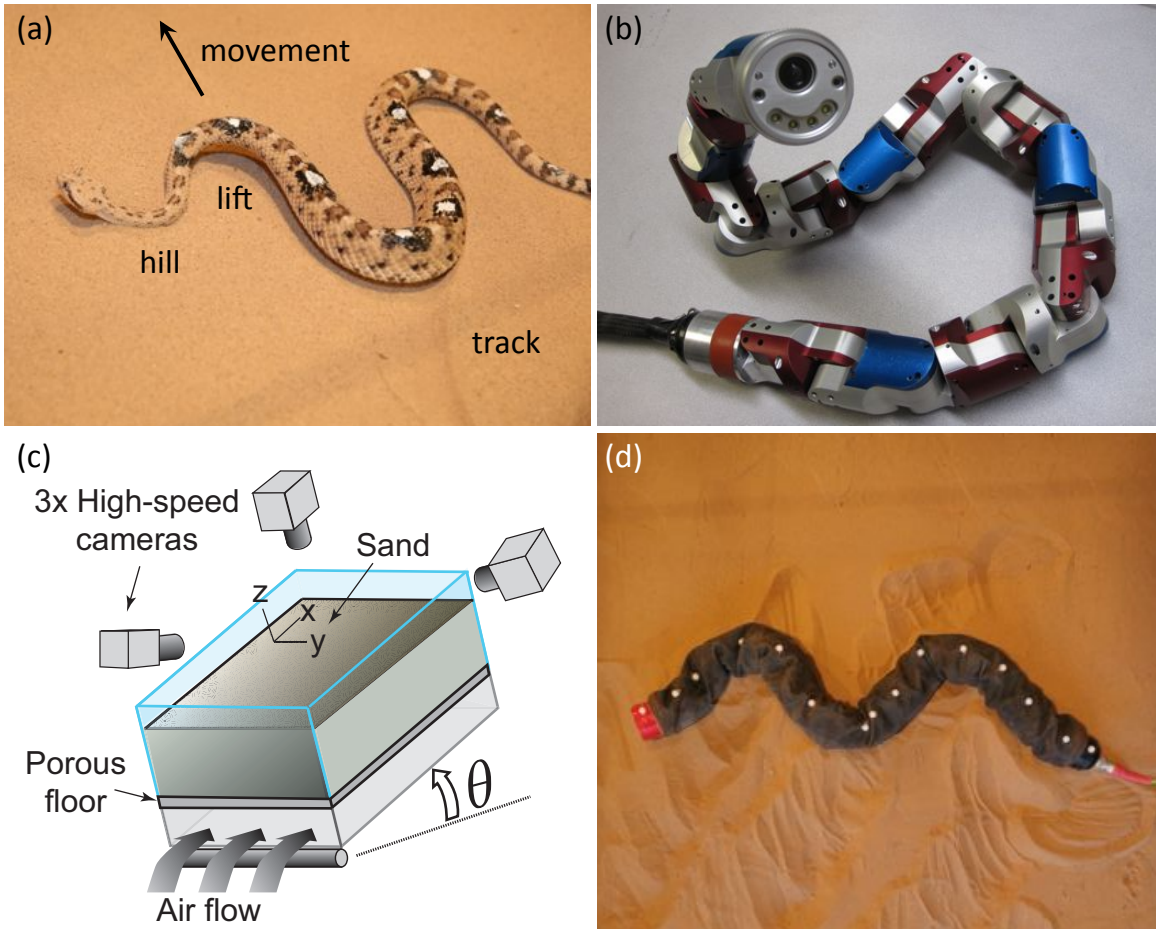

Figure 38: Sidewinder rattlesnakes and snakebot. (a) A sidewinder rattlesnake climbing a slope of 20 degrees on loose sand. (b) Snakebot developed at Carnegie Mellon University (Credit: Biorobotics lab, CMU). (c) Schematic of trackway (credit: Nick Gravish), and (d) snake robot in skin.

7.3 Snake experiments

A Sidewinder snake makes two static contacts with the substrate at each time. The position of these contact points move from snake head to its tail. Snake tracks look like straight lines in parallel. The length of each track line is the same as snake body length and the spacing of tracks is determined by the spacing of contact points on snake body. **Fig.38**a shows a sidewinder snake climbing loose sand at slope of 20 degrees.

Sidewinders can climb on sand without any axial (along the body) or lateral (direction of motion) slip. We challenge the snakes over sand and record their 3D kinematics. We find that sidewinders maintain static contact with sand across angles. Inset of **Fig.39**b shows the time course of x-displacement for a sidewinder snake climbing at inclination of 20 degrees.

We expanded this plot in the vertical direction for clarity. The highlighted region shows the horizontal segments of these plots corresponding to static contact with substrate. We observe that as angle is increased the animals replace the traditional sidewinding contacts with lengthened contacts such that no points along the body slips down the hill. **Fig.39**a shows a sidewinder rattlesnake at slopes of 0 and 20 degrees on loose sand. The contact regions highlighted by black lines become larger on higher inclination angles. As shown in **Fig.39**b the normalized contact length is almost doubled from 0 to 20 degrees. We hypothesize this control mechanism allows sidewinders to minimize slip on loose granular media. To test this hypothesis we need to conduct our own drag measurements in loose sand at different inclinations as detailed in § 7.4.

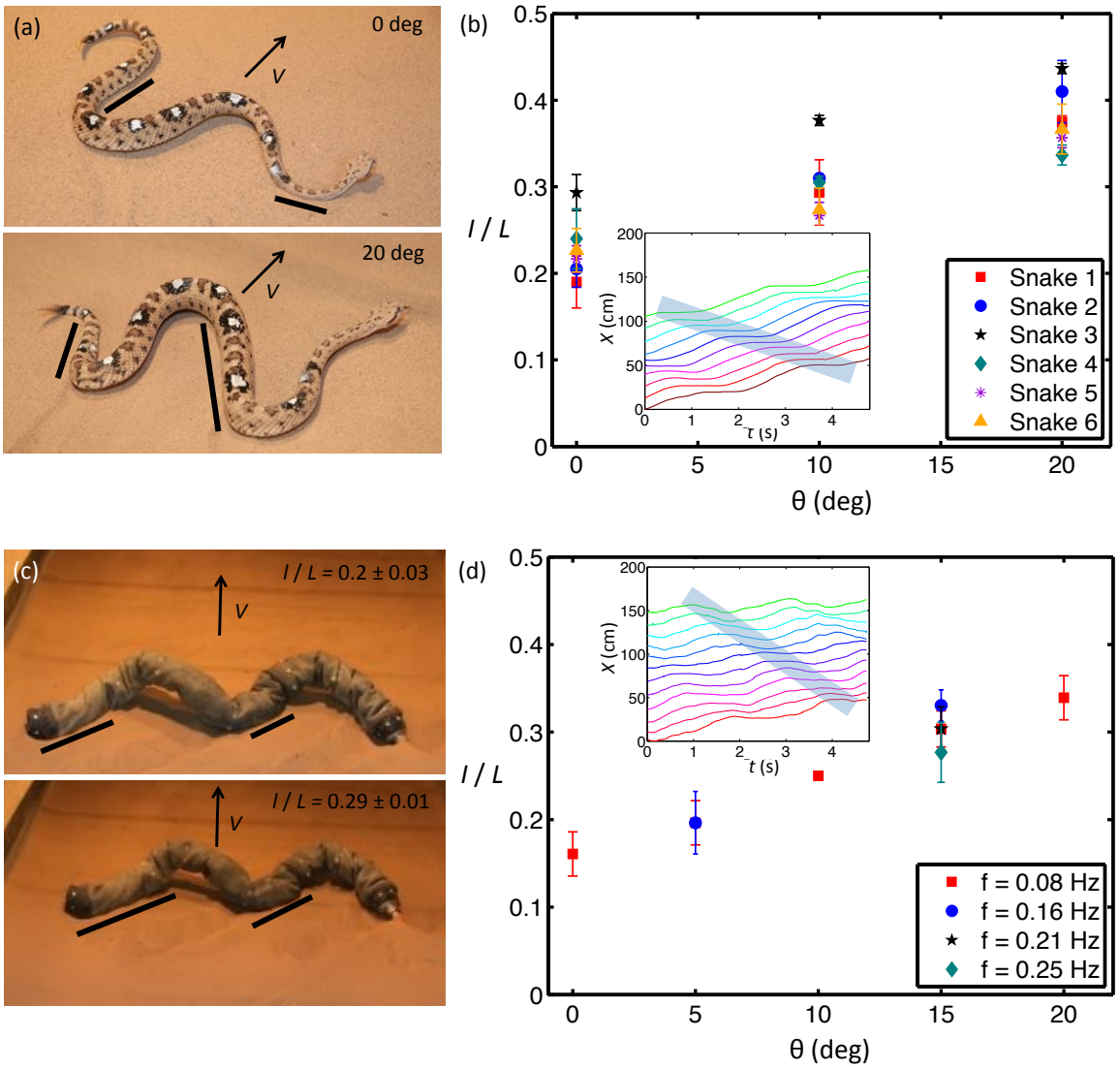

Figure 39: Contact length versus inclination angle for sidewinders and snake robot. (a) A sidewinder snake climbing slopes of 0 and 20 degrees. The black lines highlight parts of snake body that are in contact with sand. Contact length, l normalized by the body length, L as a function of inclination angle, θ for (b) six sidewinder rattlesnakes and (d) snake robot. The insets show x-displacement at inclination of 20 degrees expanded in the vertical direction for clarity. The highlighted regions illustrate the contacts snake and snake robot make with sand. Horizontal lines correspond to static contacts. (c) Snakebot climbing slope of 15 degrees at wave frequency of 0.08 Hz and contact lengths of 0.2 ± 0.03 (slipping and rolling) and 0.29 ± 0.01 (successful).

7.4 Sand reaction forces

In order to understand the interaction of sidewinder rattlesnakes with sand we need to measure drag forces sand could provide as a function of penetration depth and inclination angle. Challenged by lack of models of shear in granular media, we performed our own drag measurements. **Fig.40**b shows drag force, F as a function of horizontal displacement, D at different penetration depths, d. Force increases substantially for a small displacement until it reaches the yield force, F_y. After this point, there is a significant decrease in the slope of force-displacement curve. As shown in **Fig.40**b, the yield regime is not as distinct for loose sand since it behaves like a ductile material as opposed to compact sand that behaves like a brittle material. Thus, we fit a function to the force-displacement curve and call its slope at $x = 0$ the stiffness of material. The function we fit to this curve is $F = a * (1 - exp(x/b)) + c * x$. This accounts for an exponential saturation at the onset of drag, plus a linearly increasing term which accounts for the pile buildup during the drag. From this we can get a scale free estimate of ground stiffness by plotting the slope of the fit curve at $x = 0$, $k = a/b + c$ as shown in **Fig.40**c.

Fig.40c illustrates sand stiffness, k is decreased by half due to an increase in inclination angle, θ from 0 to 20 degrees. The drag force, F is linearly proportional to the contact length, l and stiffness, k as following [133, 134]:

$$F = k(\theta, d) l \delta \tag{39}$$

where δ is a small displacement (smaller than yield displacement). According to Eq. (39) from 0 to 20 degrees inclination, a snake needs to double its contact length to compensate for the decrease of sand stiffness. This control template is one of the main behaviors sidewinders demonstrate for successful climbing on high inclinations.

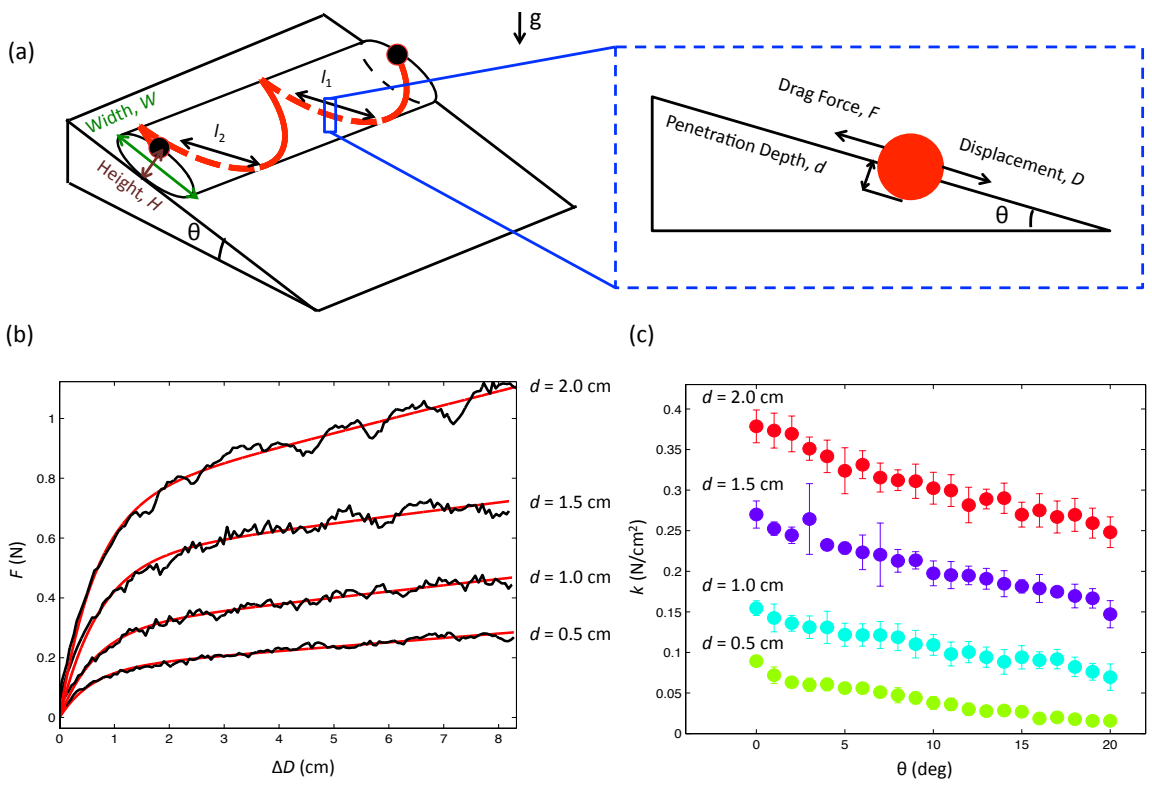

Figure 40: Granular drag. (a) Fundamental interaction. The zoom box shows side view of snake body where it makes contact with the substrate. (b) Drag force, F versus horizontal displacement, D and (c) sand stiffness, k versus inclination angle, θ for different penetration depths, d (credit: Nick Gravish).

7.5 Snakebot experiments

Our biological measurements suggests a strategy for improvement of the snake robot. Since the robot does not make the proper contact length, it is not successful in climbing inclinations larger than 10 degrees. Increasing the portion of the body in contact with the surface can increase both stability of the robot and yield forces of the granular substrate. This is accomplished by adjusting the elliptical helix aspect ratio. As shown in **Fig.39**d, the minimum contact length for successful climbing on loose sand (for neither rolling nor slipping to occur) is almost doubled from 0 degrees to 20 degrees. This is consistent with the similar measurement we did for sidewinders.

Fig.39d illustrates the normalized contact length for different wave frequencies that snakebot can follow with minimum position error. In this range, wave frequency does not have an impact on minimum contact length for successful climbing. We observed this contact length reduces for a wave frequency of 0.31 Hz, which is due to high inertial

forces. However, the experiments at frequencies higher than 0.25 Hz are not very repeatable as a result of significant position errors. The inset in **Fig.39**d shows the time course of x-displacement for the snakebot climbing inclination of 20 degrees. This plot is also expanded vertically for clarity. The highlighted region corresponds to the contacts with sand.

7.6 Summary and future directions

Snake robots could be used for effective and fast search and rescue or exploratory operations to save people in disaster situations. However, they have limited mobility on complex terrain involved in such scenarios. Sidewinding is a robust and efficient mode of motion that is suitable for traversing a wide range of slippery and loose terrain. Although, the first paper on sidewinding was published around a century ago there has never been a quantitative study of this gait on snakes natural environments. We look to nature to see how sidewinder rattlesnakes, champion of sidewinding on sandy terrain, traverse loose sand. We find they never slip even when subjected to extreme hills. We notice they increase contact length with sand on higher inclinations. We hypothesize this control template is the key to their successful climbing.

Very little is known about yielding of granular media on slopes. Thus, to understand how the snake prevents slipping we perform the first drag measurements in loose sand at different inclinations and penetration depths. We find that increasing the contact area with sand on higher inclinations would balance the decrease in sand stiffness and minimize slipping. We try this control template on the first sidewinding snake robot developed at CMU and we observe it helps the robot to successfully climb slopes of up to 20 degrees on loose sand. We now understand more about sidewinding locomotion of snakes on their natural environment, behavior of granular media at different inclinations, and how to make better effective search and rescue robots for traversing complex terrain.

CHAPTER VIII

CONCLUDING REMARKS

In this thesis, the mechanics and energetics of snake locomotion is studied through a series of experimental and theoretical techniques. The focus of this study is on physics of interactions a snake makes with its deformable or granular environment. We take this approach to investigate concertina, rectilinear, and sidewinding gaits of snake locomotion.

Functional bio-inspired surfaces have been of great interest to researchers for many years and have a wide range of applications. We are specifically interested in designing such a surface for making effective interactions with the environment and reducing cost of locomotion. In chapter 2, we report on the remarkable proficiency of snakes in controlling their frictional properties to effectively traverse a variety of complex terrain. Several studies have shown the friction coefficients of a snake sliding towards its tail is larger than that of sliding towards its head. Passive mechanisms such as geometry and surface texture of scales are considered as the key players leading to this friction anisotropy. However, the active mechanisms involved in friction adjustments of snakes have never been explored. We report on a snake ability to control the angle between its ventral scales and the substrate by lifting parts of its body. In addition to conducting experiments using a corn snake, we develop a model to study the interaction of two elastic beams. We verify our model using experimental data and use it to explore the effect of torsional stiffness, bending stiffness, and angle of attack of an individual scale on frictional properties of a snake. These are the parameters that could actively be controlled by snakes. We find that bending and torsional stiffnesses do not have a significant contribution to the frictional forces. However, angle of attack, θ is an important player and increasing θ from 30 to 60 degrees decreases peak horizontal force by 37%.

Narrow crevices are challenging terrain for most organisms and biomimetic robots. Snakes move through crevices using sequential folding and unfolding of their bodies in the manner of an accordion or "concertina." In chapter 3, we elucidate this effective means of moving through channels. We measure the frictional properties of corn snakes, their body kinematics and the transverse forces they apply to channels of varying width and inclination. To climb channels inclined at 60°, we find snakes use a combination of ingenious friction-enhancing techniques including digging their ventral scales to double their frictional coefficient and pushing channel walls transversely with up to nine times body

weight. Theoretical modeling of a one-dimensional n-linked crawler is used to calculate the transverse force factor of safety: we find snakes push up to four times more than required to prevent sliding backwards, presumably trading metabolic energy for an assurance of wall stability.

Snakes adaptations for movement across complex dry terrain serve naturally as inspirations for search-and-rescue robotics. In chapter 4, we present experiments on inclined surfaces to show a snakes scales are critical anatomical features that enable climbing. We find corn snakes actively change their scale angle of attack by contracting their ventral muscles and lifting their bodies. We use this novel paradigm to design Scalybot, a two-link limbless robot with individually controlled sets of belly scales. The robot ascends styrofoam plates inclined up to 45°, demonstrating a climbing ability comparable to that of a corn snake in the same conditions. The robot uses individual servos to provide a spatial and temporal dependence of its belly friction, effectively anchoring the stationary part of its body while reducing frictional drag of its sliding section. The ability to actively modulate friction increases both the robots efficiency over horizontal surfaces and the limiting angles of inclination it can ascend.

Metabolic cost measurements can be used to compare the efficacy of various locomotor strategies, a particular useful technique for studying snakes which have several modes of locomotion. Traditionally, respirometry techniques have been used although they cannot measure anaerobic metabolism of snakes. In chapter 5, we present a methodology to measure total metabolic cost of concertina locomotion using Magnetic Resonance Spectroscopy (MRS). We measure metabolic power and calculate mechanical power and efficiency at slopes of various inclination. Our measurement of mean metabolic power of concertina locomotion on horizontal surfaces is 16% higher than previously reported values using respirometry, indicating the importance of anaerobic metabolism. Efficiency of concertina locomotion remains constant at 8-11% across inclinations, a trend which is similar to that for human walking. This low efficiency is the main reason this gait is used only to climb narrow channels or traverse slippery substrates. The methodology proposed in this study may be employed for energetic studies of animals moving at any terrestrial locomotory mode.

In rectilinear locomotion, snakes propel themselves using uni-directional traveling waves of muscular contraction, in a style similar to earthworms. In chapter 6, we study rectilinear locomotion of three species of snakes, including red-tailed boa constrictors, Dumeril's boas, and Gaboon vipers. The kinematics of a snake's extension-contraction traveling wave

are characterized by wave frequency, amplitude, and speed. We find wave frequency increases with increasing body size, an opposite trend than that for legged animals. We predict body speed with 73 - 97% accuracy using a mathematical model of a one-dimensional n-linked crawler that uses friction as the dominant propulsive force. We apply our model to show snakes have optimal wave frequencies: higher values increase Froude number causing the snake to slip; smaller values decrease thrust and so body speed. Other choices of kinematic variables, such as wave amplitude, are sub-optimal and appear to be limited by anatomical constraints. Our model also shows that local body lifting increases a snake's speed by 31%, demonstrating that rectilinear locomotion benefits from vertical motion similar to walking.

Current search and rescue robots have difficulties traversing sandy and rocky surfaces. However, there are several animal species successful moving on such terrain. In chapter 7, we analyze one of the most successful animals on such environment, sidewinder rattlesnakes. They can climb on sand at inclination angles very close to angle of repose. In this chapter, we talk about a snake robot developed at Carnegie Mellon University that is capable of performing all of the snake gaits including sidewinding. However, it cannot climb on sand. We perform the first study of sidewinding snakes on their natural environments to understand the physics behind their successful locomotion on sand. We hypothesize sidewinding is a gait which saves energy and proves kinematic efficiency by minimizing granular deformation and slip. We find that at inclinations of up to 20 degrees, snakes climb without any axial or transverse slip. We observe their contact length at 20 degrees is almost twice as that at 0 degrees. Drag measurements reveal that downhill yield forces decrease by half over the same range of inclinations. Thus, snakes increase the length of body in contact with the ground to compensate for that. We use these insights to improve the performance of the first sidewinding robot on granular media. We find this control template is effective for the CMU snake robot and could potentially benefit other search and rescue robots.

Over the past two years, 700 natural disasters were registered worldwide affecting more than 450 million people. Robotic search and rescue is crucial for fast and effective rescue operation. These scenarios involve moving on complex terrain on which current search and rescue robots have difficulties locomoting. However, snakes are the champions of maneuvering on such terrain. In this work, we investigate the role of snakes' functional surfaces in making effective interactions with their complex environment. Snakes can remarkably control frictional and drag forces on a variety of substrates using different mechanisms. On a compliant non-granular surface, snakes can adjust their scales angles of attack to increase

their backwards friction coefficient. They can also push sides of a channel to provide additional frictional force, or lift parts of their body to create infinite friction anisotropy. Facing with a granular substrate, they use a different control template to attain enough drag force. Controlling their contact lengths with the substrate, snakes can successfully climb loose sand at inclinations close to angle of repose. The findings of this research have resulted in building two snake-like robots in our lab and developing sidewinding gait for CMU snake robot. We believe our discoveries could help roboticists develop all-terrain search and rescue and exploratory robots.

APPENDIX A

SNAKESKIN TRIBOLOGY

A.1 Experimental techniques

A.1.1 Measuring geometry of snakes' ventral scales

Parameters such as scale width and length are measured conventionally, with a fine micrometer. The thickness and radius of curvature of the scale tip are both obtained from a number of SEM images. Using computer software to best fit a circle to the cross-section of a scale tip SEM image, we find the scale tip radius of curvature.

A.1.2 Measuring elastic modulus of transparent films

We use ASTM D 882 - Tensile Testing of Thin Plastic Sheeting standard for measuring elastic modulus of a transparent film. The equipment used for this test is a DDL Instron tensile test machine as shown in Appendix **Fig.A.1**a. The force-displacement curve for a transparent film is shown in Appendix **Fig.A.1**b.

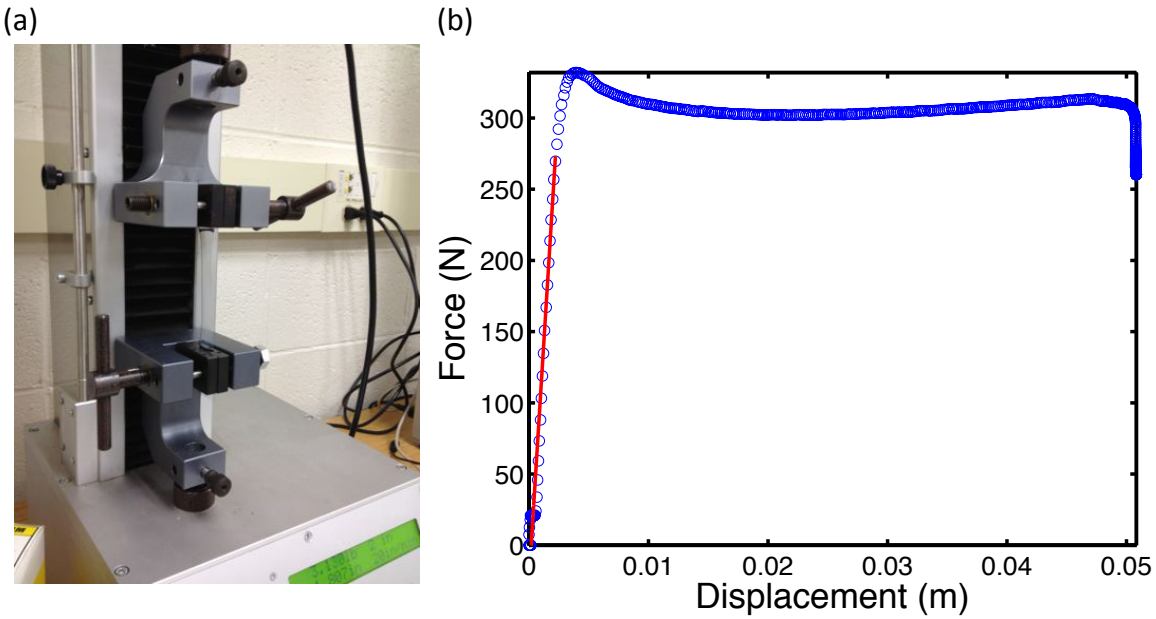

Supplementary Figure A.1: (a) Tensile test machine. (b) Force-displacement curve for a transparent film used in our experiments.

A.1.3 Calibration of transparent films

In order to calibrate the transparent films we look at their interaction with glass. We attach a glass cantilever to the end of a weight micro scale (Appendix **Fig.A.2**a) and put the transparent array on a micrometer platform. Placing the tip of the glass cantilever close to the tip of the film and adjusting the platform dial, a force-displacement curve could be made for the transparent film (Appendix **Fig.A.3**). As shown in this figure, increasing the contact height, a would decrease the slope of force-displacement curve. Moreover, load increases linearly with increasing displacement until the limit of static friction is reached. Then the slope of force-displacement curve decreases as glass slides towards the tip of transparency. We use the data from this experiment to verify our numerical model. As illustrated in Appendix **Fig.A.3**, there is a good match between the experimental data and simulation results.

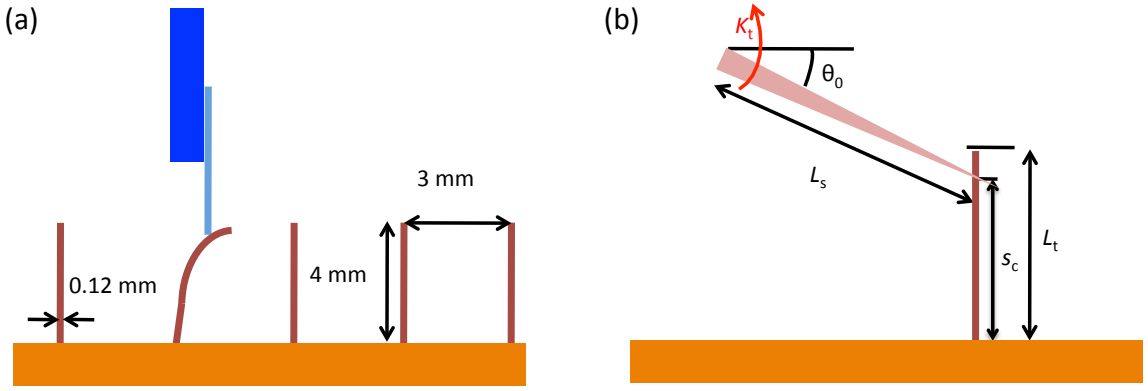

Supplementary Figure A.2: (a) Experimental setup for calibrating the transparent film and (b) schematic for interaction of snake scale with a transparent film.

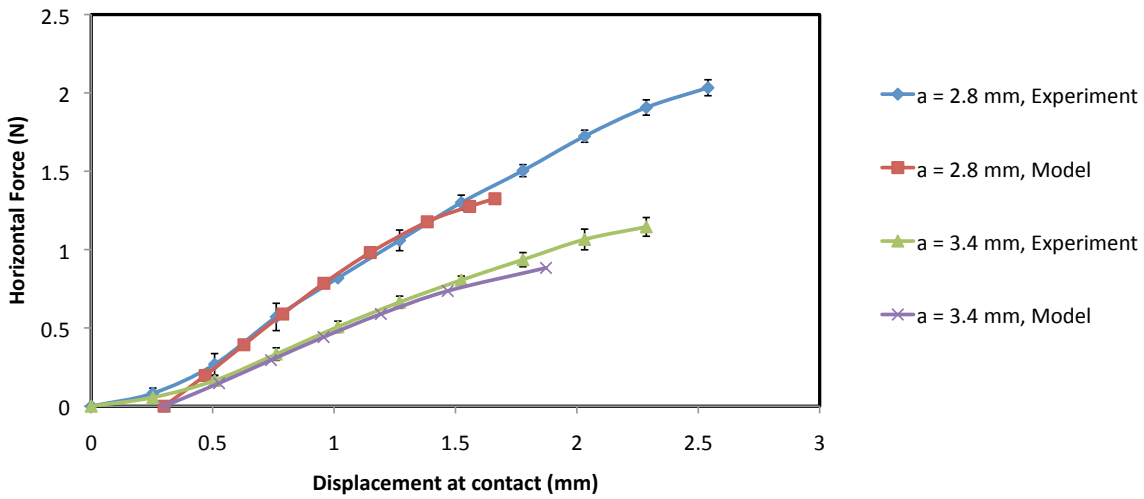

Supplementary Figure A.3: Interaction of glass and a transparent film at two different contact heights, a. The plot illustrates horizontal force as a function of horizontal displacement of transparent film where it makes a contact with glass.

A.1.4 Friction measurements

Friction is measured using an inclined plane experiment. Placing an object on the surface and tilting the plane increases the static friction force felt by the object. The incline at which the object begins to slide down the slope reflects the static friction coefficient of that object on the substrate. The details of this experiment are discussed by Marvi et al [52]. We use this technique to measure the friction coefficient of glass, transparent film, and snake ventral scales sliding on a transparent film. We also measure the friction coefficient of a snake on Styrofoam using this technique. This experiment is conducted while the snake is conscious and unconscious. We use Styrofoam for this experiment because its roughness is greater than the corn snake scale thickness of 45 μm and as shown in **Fig.1**a scales can have a good grip on the surface [52].

A.2 Input Parameters

The input parameters to the model are tabulated in Appendix Table A.1.

Parameter	Scale	Transparency
L	6 mm	4 mm
θ_0	n/a	90 deg
θ_{0i}	10-60 deg	n/a
k_t	5, 10, 15 N-mm/rad	n/a
b	12 mm	24.2 mm
h_0	0.45 mm	0.12
h_e	0.045 mm	0.12
E	200, 400, 1000 MPa	2280 MPa
Nodal points	21	21

Description	Value
Friction coefficient (max ratio of shear force to normal force) at contact point between scale and transparency	0.13
Step size for scale base translation	0.05 mm
Initial vertical overlap between scale and transparency	0.5 mm

Supplementary Table A.1: Input parameters.

A.3 Outline of computational algorithm

1. Define initial angle of scale.
2. Set relative base horizontal positions of scale and transparency so that tip of scale just touches left face of transparency.
3. Set relative base vertical positions of scale and transparency to achieve desired vertical overlap.
4. Define current contact point on scale as tip of scale.

5. Define current contact point on transparency as intersection point of scale and transparency.

6. Translate base of scale to the right one translation step.

7. Through a 2D Secant-Method search, find the horizontal force, F, and vertical force, W, that correspond to the current contact point on scale coinciding (within a specified tolerance) with current contact point on transparency.

8. Based on computed F and W and the slope of the transparency at the contact point, calculate the normal, N, and tangential, T, forces exerted on scale.

9. Compute the ratio: $|T|/N$. If this ratio exceeds the assumed coefficient of friction, execute slip:

   a. If $T > 0$, scale tip is being restrained by friction from sliding upward, so set new contact point slightly higher on the transparency.

   b. If $T < 0$, scale tip is being restrained by friction from sliding downward, so set new contact point slightly lower on the transparency.

10. Check for interpenetration (which would be unphysical): See if any points on scale are directly to the right of points on transparency (beyond a specified tolerance). If so, adjust contact points on scale and on transparency in direction of location where max interpenetration is found.

11. After contact point adjustment return to Step 7.

12. When friction and interpenetration conditions are met, execute next scale base translation step and return to Step 7.

Note: The last point of scale-transparency contact is defined as the last equilibrium configuration for which friction and interpenetration conditions can be satisfied. It is generally found that the contact point on the transparency continues to adjust all the way to the tip of the transparency, but the friction ratio remains too high. Thus, it appears that the instability point associated with the scale slipping past the transparency has been reached.

APPENDIX B

CONCERTINA LOCOMOTION

B.1 Video 1

The role of active control of snake's scales in increasing its backward friction coefficient while climbing a steep slope.
www.youtube.com/watch?v=kw8vRuncg2c

B.2 Video 2

A corn snake climbing a tree using concertina locomotion. Snakes seek crevices to ascend trees.
www.youtube.com/watch?v=PZEk6xO7Mz8

B.3 Video 3

A corn snake performing concertina locomotion through 5 channels of different widths (from top to bottom: 2 cm, 3 cm, 4 cm, 5 cm, and 6 cm). The effect of width on concertina locomotion is emphasized in this video. The gait changes from concertina to lateral undulation at width of 5 cm.
www.youtube.com/watch?v=gbCXeD_2580

B.4 Video 4

The top and side views of a corn snake moving in concertina mode. The snake lifts parts of its body during concertina locomotion; however, we neglect this effect in our model.
www.youtube.com/watch?v=42wzVEGtY18

APPENDIX C

SCALYBOT

C.1 Video 1

Concertina locomotion of a corn snake.
youtube.com/watch?v=lTMfD_uOlXA

C.2 Video 2

A corn snake climbing an inclination of 45 degrees on Styrofoam. Snake uses its ventral scales as an emergency braking system to avoid sliding down the hill.
youtube.com/watch?v=HZyWNn4ou2A

C.3 Video 3

Scalybot uses an open-loop control system to adjust its scales angles of attack and climb an inclination of 45 degrees on Styrofoam.
youtube.com/watch?v=--LkMsDfzls

APPENDIX D

RECTILINEAR LOCOMOTION

D.1 Snake species originally used for rectilinear experiments

The snake species we originally used for our rectilinear experiments include Rhino vipers, Madagascan giant hognose, Green anaconda, Pine snake, Red-tailed green ratsnake, North American ratsnake, Scarlet kingsnake, Reticulated python, Carpet python, Blood python, Burrowing python, Egg-eating snake, Greet-tree python, Emerald tree boa, Amazon tree boa, Rosy boa, Woma, and Boelens python. They will not be reported on further in this study.

D.2 Sidewall effect

We observe snakes tend to do rectilinear locomotion when they are close to a sidewall. We investigate whether the wall can aid to propel the snake using an array of micro-scales [52] to measure the force a boa constrictor applies to the side wall. We observed the force a boa constrictor applies to the sidewall is around 10% of its body weight. We found the sliding friction coefficient is 0.4 for a boa's flank and a plexiglass sidewall. We incorporated the friction force between the snake flank and the sidewall into our model and found a negligible 1% reduction in the speed prediction. We thus safely neglect this effect in our model, and assume sidewalls do not affect body speed. This is likely due to the snake's applying little force to the wall compared to the ground.

D.3 Wave processing algorithms

The snake's traveling wave is characterized by three parameters that are determined through the the algorithms below. These parameters include the wave frequency ω, the wave amplitude A, and the wave number k. Below, we describe our MATLAB algorithms to determine these parameters.

To determine the amplitude and frequency of the wave, we apply a peak detection algorithm. **Fig.30**c shows the resulting peak detection of position data x'. The algorithm begins by using first and second derivatives of position x' to find local minima and maxima. In general, a trough is reached when the first derivative of position x' is zero and the second derivative is positive; similarly for a peak. Due to presence of noise in the data we take extra

steps to make sure peaks and troughs are captured correctly. The details of the algorithm we used for this purpose are explained in Appendix D.4. Elapsed time between two peaks is equal to the wave period τ ; the wave frequency is $\omega = 2\pi/\tau$. The difference in positions of peaks and troughs is equal to twice the wave amplitude A.

Having solved for amplitude and frequency, we then determine the traveling wave speed V_w. This variables cannot be measured by following a single marker alone. Instead we must compare information between adjacent markers to determine how quickly the wave travels down the snake. To this end, we have written a special wave-speed measuring algorithm. The algorithm first determines the maximal contracted and extended positions of each ventral surface marker on the snake. Starting with the head, peaks in motion for one ventral surface marker are matched to those occurring down the ventral surface at later points in time. The process continues until each peak is matched to the next one occurring most closely in both space in time. This process is equivalent to drawing diagonal lines linking adjacent peaks on the position-time diagram shown in **Fig.30**a. These diagonal lines mark the traveling wave path. Wave speed V_w is calculated by subtracting body speed from the slope of black arrows shown in **Fig.30**a. Wavelength λ is given by the product $\lambda = V_w\tau$. Wavenumber is $k = 2\pi/\lambda$.

D.4 Peak detection algorithm

Different steps of the algorithm we used to detect the peaks and troughs of each tracked spot are as following:

1. Find the difference between the highest and lowest x' and find the highest slope in the entire time frame.

2. Run linear and quadratic maps along the data using 5% of the data set.

3. If the slope of the linear fit is sufficiently close to zero (less than 2% of the highest slope found in step 1) record the center of the map's x and y coordinates and sign of the second order term in quadratic map (corresponding to the sign of second derivative). An extreme with positive/negative second order derivative would be a trough/peak.

4. Create a running tally of all the peaks/troughs.
   A: New troughs are not accepted unless the previous marker is a peak, and vice versa.
   B: New peak/trough is not accepted unless its distance from the previous trough/peak is at least 15% of the max deviation found in step 1.

5. Wave amplitude for each tracked spot will be half the average difference in x' of each peak/trough from its previous trough/peak.

6. Wave period for each tracked spot will be twice the average difference in time t of each peak/trough from its previous trough/peak.

   In order to make sure about the accuracy of this algorithm in properly detecting all of the peaks and troughs, we plotted x' versus time for all of the tracked spots with a marker on the detected peaks/troughs as shown in **Fig.30**c.

D.5 Video 1

A red-tailed boa constrictor performing rectilinear locomotion. Time is sped up 3 times.
`www.youtube.com/watch?v=40g9ldVHEHs`

D.6 Video 2

A Dumeril's boa performing rectilinear locomotion relative to the snake coordinate frame.
`www.youtu.be/2CbGwO0u59Q`

D.7 Video 3

A red-tailed boa constrictor lifting parts of its body during rectilinear locomotion. There is a purple light shining from the side to illustrate lifted parts.
`www.youtube.com/watch?v=Gyx-h7uyN1Y`

D.8 Video 4

Spots tracked on the snake's flanks compared to our model predictions for a female Dumeril's boa of length 183 cm. The red blocks correspond to stationary parts of the body.
`www.youtube.com/watch?v=d_qe2UhBSiU`

D.9 Kinematics of non-ventral surface and tail

Although propulsive forces applied by the snake occur on its ventral surface, the muscles extend from the ventral to the dorsal surface. In this section, we present qualitative observations of this muscular movement in order to give insight into how forces are generated. **Fig.29**a illustrates the passage of the contraction traveling wave. We draw black lines to denote the inclination of the naturally-occurring diamond patterns on the snake's skin. The

spacing of these lines indicate the level of strain on the snake's skin. Blue and red endpoints denote the lines' intersection with the dorsal and ventral surface, respectively.

Initially, the lines are parallel indicating the dorsal and ventral surface each have zero strain. Throughout the image sequence, the blue dorsal points have fixed spacing and travel forward at constant speed. Red ventral points exhibit sinusoidal traveling waves of contraction, varying from maximum spacing at 1.3 s to minimum spacing at 2.6 s. At 4 s, the cycle ends with the lines oriented parallel again. Points downstream then undergo a similar cycle, as the traveling wave makes its way down the snake.

We analyze videos of the snake's motion to quantify the traveling wave of contraction. **Fig.29**c shows the displacement as a function of time of a single cross-section of the boa's body ($i = 22$). The purple, green and red curves show the distance traveled of points on three elevations, dorsal, middle and ventral. We observe the skin exhibits increasing strain with increasing distance from the snake's backbone. In particular, the ventral surface, shown in red, has the largest wave amplitude. There is little contraction at the dorsal level due to the inextensible spine and so points on the snake's backbone move at nearly constant speed. Only the ventral surface of the snake generates frictional propulsive force so we hereon report only ventral waveforms.

A snake's tail is often short, 0.1 ± 0.02 times their body length, and so lightweight as to be dynamically negligible. In our videos, we observed the tail muscles oscillate at a much lower amplitude, $10\% - 20\%$ relative to the amplitude in the snake's middle. This low amplitude is due to the snake's tail having relatively fewer muscles than the rest of the snake. As a result, the tail does not generate its own thrust but instead is dragged by the body during locomotion. We track the wave amplitude to determine the "beginning of the tail," where there is a sudden drop in wave amplitude. For modeling considerations we consider only the pre-tail wave amplitudes and assume they propagate from the head to the tail tip.

D.10 Input to model

Since our model is discrete, we must use a discrete approximation to the traveling wave as the prescribed kinematics. The input to our model is $dx'_i(t)/dt = A\omega\cos(\omega t + ki/nL)$ where i is the number of the segment. Solving Eq. (32) we can calculate the acceleration $\ddot{\bar{x}}$ and speed of model center of mass, V, at each iteration knowing the initial conditions of the model. As discussed in § 6.3, *ode45* function in MATLAB to find the numerical solution to this system. This function uses a Runge-Kutta ordinary differential equation solver to iteratively find the solution of Eq. (32).

According to Eq. (32), for our numerical simulation, we require the snake's body kinematics (the speed and direction of each point on the snake's body) in order to estimate its center-of-mass speed. For each snake in our study, we tracked naturally occurring markers on the ventral surface as the snake moved forward. These markers ranged between 20 and 26. These spots are not equally spaced on the snake body and the average spacing is also different in different species. We track these spots to get the wave kinematics along the body and once we characterize the traveling wave, we can estimate $x'(t)$ at any point along the body using Eq. (35). For our simulation we use the same number of masses as the number of spots tracked. However, we equally space these masses along the body.

D.11 Individual animal subjects

Species	L (cm)	m (kg)	μ_f	μ_b	n
Boa constrictor 1	53	0.057	0.25	0.43	23
Boa constrictor 2	52	0.054	0.31	0.38	25
Boa constrictor 3	55	0.074	0.36	0.46	25
Dumeril's boa 1	183	4.95	0.02	0.05	25
Dumeril's boa 2	168	6.45	0.02	0.07	26
Gaboon viper	120	2.26	0.12	0.32	20

Supplementary Table D.1: The lengths (L), masses (m), forward and backward sliding friction coefficients (μ_f and μ_b), and number of naturally-occurring spots (n) of snakes used in our experiments.

APPENDIX E

SCHOLARLY ACHIEVEMENTS

E.1 Publications

E.1.1 Book

1. **H. Marvi**, D. Hu, *Locomotion of Snakes*, Springer, Heidelberg, Germany (In Preparation, Scheduled to Appear in 2014).

E.1.2 Patent

1. **H. Marvi**, G. Meyers, D. Hu, J. Glisson, A. Hirabayashi, A. Pavone,"Scalybot," *U.S. Provisional Patent*, 61/561,574, November 2011.

E.1.3 Journal papers

1. **H. Marvi**, J. Cook, J. Leisen, D. Hu, "Evaluation of energetic cost of concertina locomotion via in vivo 31P NMR spectroscopy." (In Review)

2. **H. Marvi**, J. Bridges, D. Hu,"Snakes Mimic Earthworms: Propulsion Using Rectilinear Traveling Waves," *Journal of the Royal Society Interface*, 10(84), 2013.

3. **H. Marvi**, D. Hu,"Friction Enhancement in Concertina Locomotion of Snakes," *Journal of the Royal Society Interface*, 9(76), pp 3067-3080, 2012.

4. **H. Marvi**, J. Cook, J. Streator, D. Hu,"Tribology of Snakeskin," (In Preparation)

5. **H. Marvi**, N. Gravish, C. Gong, J. Mendelson, H. Choset, D. Goldman, D. Hu,"An anti-slip control template for limbless locomotion on loose terrain," (In Preparation)

E.1.4 Refereed Conference Proceedings

1. **H. Marvi**, G. Meyers, G. Russell, D. Hu,"Scalybot: a Snake-inspired Robot with Active Frictional Anisotropy," *ASME Dynamic Systems and Control Conference*, Arlington, VA, November 2011. (Invited Paper, Best ASME Student Paper of the Year in Mechatronics)

E.2 Academic presentations

E.2.1 Conference oral presentations

1. **H. Marvi**,"Friction Control in Snakes and Snake Robots," *Milliken Graduate Research Symposium*, Spartanburg, SC, March 2013. (Invited Presentation)

2. **H. Marvi**, R. Chrystal, J. Shieh, J. Mendelson, R. Hatton, H. Choset, D. Goldman, D. Hu,"Sidewinding Snakes on Sand," *Society for Integrative and Comparative Biology (SICB) Annual Meeting*, San Francisco, CA, January 2013.

3. **H. Marvi**, J. Streator, D. Hu,"Snakeskin Tribology," *Materials Research Society (MRS) Fall Meeting*, Boston, MA, November 2012.

4. **H. Marvi**, D. Dimenichi, R. Chrystal, J. Mendelson, D. Goldman, D. Hu,"Sidewinding Snakes on Sand," *65th Annual Meeting of APS Division of Fluid Dynamics*, San Diego, CA, November 2012.

5. **H. Marvi**, D. Hu,"The Role of Functional Surfaces in the Locomotion of Snakes," *Physics of Living Systems Student Research Network (PoLS SRN) meeting*, New Haven, CT, July 2012.

6. **H. Marvi**, J. Streator, D. Hu,"Snakeskin Tribology: How Snakes Generate Large Frictional Anisotropy," *American Physical Society (APS) March Meeting*, Boston, MA, February 2012.

7. **H. Marvi**, J. Cook, and D. Hu,"Rectilinear Locomotion of Snakes and the Design of Scalybot 2," *Society for Integrative and Comparative Biology (SICB) Annual Meeting*, Charleston, SC, January 2012.

8. **H. Marvi**, D. Hu,"Concertina Locomotion of Snakes," *63rd Annual Meeting of APS Division of Fluid Dynamics*, Long Beach, CA, November 2010.

E.2.2 Poster sessions

1. J. Cook, **H. Marvi**, J. Leisen, D. Hu,"Measuring Energetic Cost of Snake Locomotion Using NMR Spectroscopy," *Air Products Undergraduate Research Fair at Georgia Tech*, Atlanta, GA, April 2013. (Third Place)

2. J. Shieh, G. Tamayo, Q. Tran, **H. Marvi**, J. Mendelson, H. Choset, D. Goldman, D. Hu,"The Mechanics of Sidewinding on Sand," *8th Annual Undergraduate Research*

Symposium at Georgia Tech, Atlanta, GA, April 2013. (Second Place in College of Engineering)

3. J. Cook, **H. Marvi**, J. Leisen, D. Hu,"Measuring Energetic Cost of Snake Locomotion Using NMR Spectroscopy," *8th Annual Undergraduate Research Symposium at Georgia Tech*, Atlanta, GA, April 2013.

4. **H. Marvi**, G. Meyers, J. Cook, E. Chang, D. Hu,"Scalybot: A Snake-inspired Robot," *Physics of Living Systems Student Research Network (PoLS SRN) meeting*, New Haven, CT, July 2012.

5. **H. Marvi**, G. Meyers, J. Cook, E. Chang, D. Hu,"Scalybot: A Snake-inspired Robot," *Georgia Tech Research and Innovation Conference*, Atlanta, GA, February 2012. (Best Poster)

Bibliography

[1] B. Jayne, "Muscular mechanisms of snake locomotion: an electromyographic study of the sidewinding and concertina modes of Crotalus cerastes, Nerodia fasciata and Elaphe obsoleta," *J. exp. Biol*, vol. 140, no. 1, pp. 1–33, 1988.

[2] D. Berrigan and D. Pepin, "How maggots move: allometry and kinematics of crawling in larval diptera," *Journal of insect physiology*, vol. 41, no. 4, pp. 329–337, 1995.

[3] J. Brackenbury, "Fast locomotion in caterpillars," *Journal of insect physiology*, vol. 45, no. 6, pp. 525–533, 1999.

[4] J. Brackenbury, "Locomotory modes in the larva and pupa of chironomus plumosus (diptera, chironomidae)," *Journal of Insect Physiology*, vol. 46, no. 12, pp. 1517–1527, 2000.

[5] B. Joos, "Adaptations for locomotion at low body temperatures in eastern tent caterpillars, malacosoma americanum," *Physiological zoology*, pp. 1148–1161, 1992.

[6] T. Casey, "Energetics of caterpillar locomotion: biomechanical constraints of a hydraulic skeleton," *Science*, vol. 252, no. 5002, pp. 112–114, 1991.

[7] K. Quillin, "Kinematic scaling of locomotion by hydrostatic animals: ontogeny of peristaltic crawling by the earthworm lumbricus terrestris," *Journal of experimental biology*, vol. 202, no. 6, pp. 661–674, 1999.

[8] K. Quillin, "Ontogenetic scaling of burrowing forces in the earthworm lumbricus terrestris," *Journal of Experimental Biology*, vol. 203, no. 18, pp. 2757–2770, 2000.

[9] N. Laframboise and B. Loko, "Natural disasters: Mitigating impact, managing risks," 2012.

[10] I. Erkmen, A. Erkmen, F. Matsuno, R. Chatterjee, and T. Kamegawa, "Snake robots to the rescue!," *Robotics & Automation Magazine, IEEE*, vol. 9, no. 3, pp. 17–25, 2002.

[11] H. Kitano, S. Tadokoro, I. Noda, H. Matsubara, T. Takahashi, A. Shinjou, and S. Shimada, "Robocup rescue: Search and rescue in large-scale disasters as a domain for autonomous agents research," in *Systems, Man, and Cybernetics, 1999. IEEE SMC'99 Conference Proceedings. 1999 IEEE International Conference on*, vol. 6, pp. 739–743, IEEE, 1999.

[12] I. Kassim, L. Phee, W. Ng, F. Gong, P. Dario, and C. Mosse, "Locomotion techniques for robotic colonoscopy," *Engineering in Medicine and Biology Magazine, IEEE*, vol. 25, no. 3, pp. 49–56, 2006.

[13] A. M. Andruska and K. S. Peterson, "Control of a snake-like robot in an elastically deformable channel," *Mechatronics, IEEE/ASME Transactions on*, vol. 13, no. 2, pp. 219–227, 2008.

[14] M. Yim, K. Roufas, D. Duff, Y. Zhang, C. Eldershaw, and S. Homans, "Modular reconfigurable robots in space applications," *Autonomous Robots*, vol. 14, no. 2, pp. 225–237, 2003.

[15] H. Marvi and D. Hu, "Friction enhancement in concertina locomotion of snakes," *Journal of the Royal Society Interface*, vol. 9, no. 76, pp. 3067–3080, 2012.

[16] H. Marvi, J. Bridges, and D. Hu, "Snakes mimic earthworms: propulsion using rectilinear traveling waves," *Journal of the Royal Society Interface*, vol. 10, no. 84, 2013.

[17] D. Hu, J. Nirody, T. Scott, and M. Shelley, "The mechanics of slithering locomotion," *Proceedings of the National Academy of Sciences*, vol. 106, no. 25, p. 10081, 2009.

[18] S. Secor, B. Jayne, and A. Bennett, "Locomotor Performance and Energetic Cost of Sidewinding by the Snake *Crotalus cerastes*," *Journal of Experimental Biology*, vol. 163, pp. 1–14, 1992.

[19] J. Gray, "The mechanism of locomotion in snakes," *Journal of Experimental Biology*, vol. 23, no. 2, pp. 101–120, 1946.

[20] B. C. JAYNE and J. D. DAVIS, "Kinematics and performance capacity for the concertina locomotion of a snake (coluber constrictor)," *Journal of Experimental Biology*, vol. 156, no. 1, pp. 539–556, 1991.

[21] G. Byrnes and B. C. Jayne, "Substrate diameter and compliance affect the gripping strategies and locomotor mode of climbing boa constrictors," *The Journal of experimental biology*, vol. 213, no. 24, pp. 4249–4256, 2010.

[22] H. W. Greene, *Snakes: The Evolution of Mystery in Nature*. Princeton: University of California Press, 1997. p 36.

[23] C. Gans, "Locomotion without limbs," *Natural History*, vol. 75, no. 2, 1966.

[24] M. Walton, B. C. Jayne, and A. F. Bennett, "The energetic cost of limbless locomotion," *Science*, vol. 249, pp. 524–527, 1990.

[25] F. Chernousko, "Modelling of snake-like locomotion," *Applied mathematics and computation*, vol. 164, no. 2, pp. 415–434, 2005.

[26] F. Jing and S. Alben, "Optimization of two-and three-link snakelike locomotion," *Physical Review E*, vol. 87, no. 2, p. 022711, 2013.

[27] E. Home, "Observations intended to show that the progressive motion of snakes is partly performed by means of the ribs," *Philosophical Transactions of the Royal Society of London*, vol. 102, pp. 163–168, 1812.

[28] C. Bogert, "Rectilinear locomotion in snakes," *Copeia*, vol. 1947, no. 4, pp. 253–254, 1947.

[29] E. Wiedemann, "On the biology of feeding the adder, *Vipera berus*," *Zool. Anz*, vol. 97, pp. 278–286, 1932.

[30] W. Mosauer, "On the locomotion of snakes," *Science*, vol. 76, pp. 583–585, 1932.

[31] H. W. Lissman, "Rectilinear locomotion in a snake (*boa occidentalis*)," *J Exp Biol*, vol. 26, pp. 368–379, 1950.

[32] J. Gray and H. Lissmann, "The kinetics of locomotion of the grass-snake," *Journal of Experimental Biology*, vol. 26, no. 4, pp. 354–367, 1950.

[33] B. R. Moon and C. Gans, "Kinematics, muscular activity and propulsion in gopher snakes," *Journal of Experimental Biology*, vol. 201, no. 19, pp. 2669–2684, 1998.

[34] W. Mosauer, "A note on the sidewinding locomotion of snakes," *The American Naturalist*, vol. 64, no. 691, pp. 179–183, 1930.

[35] R. B. Cowles, "Sidewinding locomotion in snakes," *Copeia*, pp. 211–214, 1956.

[36] S. M. Secor, B. C. Jayne, and A. F. Bennett, "Locomotor performance and energetic cost of sidewinding by the snake crotalus cerastes," *Journal of experimental biology*, vol. 163, no. 1, pp. 1–14, 1992.

[37] J. K. Hopkins, B. W. Spranklin, and S. K. Gupta, "A survey of snake-inspired robot designs," *Bioinspiration & biomimetics*, vol. 4, no. 2, p. 021001, 2009.

[38] M. Mori and S. Hirose, "Development of active cord mechanism acm-r3 with agile 3d mobility," in *Intelligent Robots and Systems, 2001. Proceedings. 2001 IEEE/RSJ International Conference on*, vol. 3, pp. 1552–1557, IEEE, 2001.

[39] C. Wright, A. Johnson, A. Peck, Z. McCord, A. Naaktgeboren, P. Gianfortoni, M. Gonzalez-Rivero, R. Hatton, and H. Choset, "Design of a modular snake robot," in *IEEE/RSJ International Conference on Intelligent Robots and Systems*, pp. 2609–2614, 2007.

[40] K. J. Dowling, *Limbless locomotion: learning to crawl with a snake robot*. PhD thesis, Carnegie Mellon U., Pittsburgh, PA, 1997.

[41] M. Tesch, K. Lipkin, I. Brown, R. Hatton, A. Peck, J. Rembisz, and H. Choset, "Parameterized and scripted gaits for modular snake robots," *Advanced Robotics*, vol. 23, no. 9, pp. 1131–1158, 2009.

[42] F. Barazandeh, B. Bahr, and A. Moradi, "How self-locking reduces actuators torque in climbing snake robots," in *Advanced intelligent mechatronics, 2007 IEEE/ASME international conference on*, pp. 1–6, IEEE, 2007.

[43] A. Ghanbari, M. M. S. Fakhrabadi, and A. Rostami, "Dynamics and ga-based optimization of rectilinear snake robot," in *Intelligent Robotics and Applications*, pp. 613–622, Springer, 2009.

[44] C. Liu and W. Liao, "A snake robot using shape memory alloys," in *Robotics and Biomimetics, 2004. ROBIO 2004. IEEE International Conference on*, pp. 601–605, IEEE, 2004.

[45] S. Hirose and H. Yamada, "Snake-like robots [tutorial]," *Robotics & Automation Magazine, IEEE*, vol. 16, no. 1, pp. 88–98, 2009.

[46] R. Khan, M. Watanabe, A. A. Shafie, *et al.*, "Kinematics model of snake robot considering snake scale," *American Journal of Applied Sciences*, vol. 7, no. 5, p. 669, 2010.

[47] M. Sato, M. Fukaya, and T. Iwasaki, "Serpentine locomotion with robotic snakes," *IEEE Control Systems Magazine*, vol. 22, no. 1, pp. 64–81, 2002.

[48] G. S. Chirikjian and J. W. Burdick, "A hyper-redundant manipulator," *Robotics & Automation Magazine, IEEE*, vol. 1, no. 4, pp. 22–29, 1994.

[49] J. Burdick, J. Radford, and G. Chirikjian, "A sidewinding locomotion gait for hyper-redundant robots," *Advanced Robotics*, vol. 9, no. 3, pp. 195–216, 1994.

[50] R. L. Hatton and H. Choset, "Sidewinding on slopes," in *Robotics and Automation (ICRA), 2010 IEEE International Conference on*, pp. 691–696, IEEE, 2010.

[51] H. Marvi, J. Cook, J. Streator, and D. Hu, "Snakeskin tribology: How snakes generate large frictional anisotropy." In Preparation, 2013.

[52] H. Marvi and D. Hu, "Friction enhancement in concertina locomotion of snakes." *Journal of the Royal Society Interface*, in press, 2012.

[53] H. Marvi, G. Meyers, G. Russell, and D. Hu, "Scalybot: a snake-inspired robot with active control of friction," in *Proceedings of ASME Dynamic Systems and Control Conference*, pp. 443–450, 2011.

[54] H. Marvi, J. Cook, J. Leisen, and D. Hu, "Evaluation of energetic cost of concertina locomotion via *in vivo* ^{31}p nmr spectroscopy." In Review, 2013.

[55] H. Marvi, N. Gravish, C. Gong, J. Mendelson, H. Choset, D. Goldman, and D. Hu, "An anti-slip control template for limbless locomotion on loose terrain." In Preparation, 2013.

[56] M. Scherge, S. Gorb, and S. Gorb, *Biological micro-and nanotribology: nature's solutions*. Springer Verlag, 2001.

[57] A. Filippov and S. N. Gorb, "Frictional-anisotropy-based systems in biology: structural diversity and numerical model," *Scientific reports*, vol. 3, 2013.

[58] E. Arzt, S. Gorb, and R. Spolenak, "From micro to nano contacts in biological attachment devices," *Proceedings of the National Academy of Sciences*, vol. 100, no. 19, pp. 10603–10606, 2003.

[59] S. Gorb, "Biological microtribology: anisotropy in frictional forces of orthopteran attachment pads reflects the ultrastructure of a highly deformable material," *Proceedings of the Royal Society of London. Series B: Biological Sciences*, vol. 267, no. 1449, pp. 1239–1244, 2000.

[60] M. Urbakh, J. Klafter, D. Gourdon, and J. Israelachvili, "The nonlinear nature of friction," *Nature*, vol. 430, no. 6999, pp. 525–528, 2004.

[61] Z. Dai, S. Gorb, and U. Schwarz, "Roughness-dependent friction force of the tarsal claw system in the beetle Pachnoda marginata (Coleoptera, Scarabaeidae).," *The Journal of experimental biology*, vol. 205, no. Pt 16, p. 2479, 2002.

[62] J. Hazel, M. Stone, M. Grace, and V. Tsukruk, "Nanoscale design of snake skin for reptation locomotions via friction anisotropy," *Journal of biomechanics*, vol. 32, no. 5, pp. 477–484, 1999.

[63] R. Berthé, G. Westhoff, H. Bleckmann, and S. Gorb, "Surface structure and frictional properties of the skin of the amazon tree boa corallus hortulanus (squamata, boidae)," *Journal of Comparative Physiology A: Neuroethology, Sensory, Neural, and Behavioral Physiology*, vol. 195, no. 3, pp. 311–318, 2009.

[64] M. J. Benz, A. E. Kovalev, and S. N. Gorb, "Anisotropic frictional properties in snakes," in *SPIE Smart Structures and Materials+ Nondestructive Evaluation and Health Monitoring*, pp. 83390X–83390X, International Society for Optics and Photonics, 2012.

[65] J. Gray and H. W. Lissman, "The kinetics of locomotion of the grass-snake," *J. Exp. Biol.*, vol. 26, pp. 354–367, 1950.

[66] C. Schmidt and S. Gorb, *Snake scale microstructure: phylogenetic significance and functional adaptations*. E. Schweizerbart'sche Verlagsbuchhandlung, 2012.

[67] H. Abdel-Aal, M. El Mansori, and S. Mezghani, "Multi-scale investigation of surface topography of ball python (python regius) shed skin in comparison to human skin," *Tribology letters*, vol. 37, no. 3, pp. 517–527, 2010.

[68] S. Timoshenko, S. P. Timoshenko, S. P. Timoshenko, and S. P. Timoshenko, *Strength of materials*, vol. 2. van Nostrand New York, 1956.

[69] S. Timoshenko, S. Woinowsky-Krieger, and S. Woinowsky, *Theory of plates and shells*, vol. 2. McGraw-hill New York, 1959.

[70] S. P. Timoshenko and J. M. Gere, *Theory of elastic stability*. Tata McGraw-Hill Education, 1961.

[71] J. Gray, "The mechanism of locomotion in snakes," *J. Exp. Biol.*, vol. 23, pp. 101–120, 1946.

[72] B. Jayne and J. Davis, "Kinematics and performance capacity for the concertina locomotion of a snake (Coluber constrictor)," *Journal of Experimental Biology*, vol. 156, no. 1, p. 539, 1991.

[73] J. Keller and M. Falkovitz, "Crawling of worms," *Journal of Theoretical Biology*, vol. 104, no. 3, pp. 417–442, 1983.

[74] S. Gray, *Animal locomotion*. Weidenfeld & Nicolson, 1968.

[75] K. Zimmermann, I. Zeidis, and C. Behn, *Mechanics of Terrestrial Locomotion: With a Focus on Non-pedal Motion Systems*. Springer Verlag, 2009.

[76] J. McDonald, *Handbook of biological statistics*. Sparky House Publishing, 2009.

[77] J. Dormand and P. Prince, "A family of embedded Runge-Kutta formulae," *Journal of Computational and Applied Mathematics*, vol. 6, no. 1, pp. 19–26, 1980.

[78] R. M. Alexander, *Principles of animal locomotion*. Princeton University Press, 2003.

[79] L. van Griethuijsen and B. Trimmer, "Kinematics of horizontal and vertical caterpillar crawling," *Journal of Experimental Biology*, vol. 212, no. 10, p. 1455, 2009.

[80] R. Johansson and G. Westling, "Roles of glabrous skin receptors and sensorimotor memory in automatic control of precision grip when lifting rougher or more slippery objects," *Experimental Brain Research*, vol. 56, no. 3, pp. 550–564, 1984.

[81] J. Burdick, J. Radford, and G. Chirikjian, "A sidewinding locomotion gait for hyper-redundant robots," in *Proceedings of IEEE Conference on Robotics and Automation*, pp. 101–106, 1993.

[82] M. Hoso, T. Asami, and M. Hori, "Right-handed snakes: convergent evolution of asymmetry for functional specialization," *Biology Letters*, vol. 3, no. 2, p. 169, 2007.

[83] E. Roth, "[] Handedness' in snakes? Lateralization of coiling behaviour in a cottonmouth, Agkistrodon piscivorus leucostoma, population," *Animal behaviour*, vol. 66, no. 2, pp. 337–341, 2003.

[84] O. Unver, A. Uneri, A. Aydemir, and M. Sitti, "Geckobot: a gecko inspired climbing robot using elastomer adhesives," in *International Conference on Robotics and Automation*, pp. 2329–2335, 2006.

[85] S. Trujillo, B. Heyneman, and M. Cutkosky, "Constrained convergent gait regulation for a climbing robot," in *International Conference on Robotics and Automation*, pp. 5243–5249, 2010.

[86] A. Asbeck, S. Kim, M. Cutkosky, W. Provancher, and M. Lanzetta, "Scaling hard vertical surfaces with compliant microspine arrays," *The International Journal of Robotics Research*, vol. 25, no. 12, p. 1165, 2006.

[87] M. Spenko, G. Haynes, J. Saunders, M. Cutkosky, A. Rizzi, R. Full, and D. Koditschek, "Biologically inspired climbing with a hexapedal robot," *Journal of Field Robotics*, vol. 25, no. 4-5, pp. 223–242, 2008.

[88] S. Hirose, P. Cave, and C. Goulden, *Biologically inspired robots: snake-like locomotors and manipulators*, vol. 64. Oxford University Press Oxford, UK, 1993.

[89] J. Hopkins, B. Spranklin, and S. Gupta, "A survey of snake-inspired robot designs," *Bioinspiration & Biomimetics*, vol. 4, p. 021001, 2009.

[90] R. Hoffstetter and J. Gasc, "Vertebrae and ribs of modern reptiles," *Biology of the Reptilia*, vol. 1, no. 5, pp. 201–310, 1969.

[91] G. Byrnes and B. Jayne, "Substrate diameter and compliance affect the gripping strategies and locomotor mode of climbing boa constrictors," *Journal of Experimental Biology*, vol. 213, no. 24, p. 4249, 2010.

[92] K. Lipkin, I. Brown, A. Peck, H. Choset, J. Rembisz, P. Gianfortoni, and A. Naaktgeboren, "Differentiable and piecewise differentiable gaits for snake robots," in *IEEE/RSJ International Conference on Intelligent Robots and Systems*, pp. 1864–1869, 2007.

[93] J. Vincent, O. Bogatyreva, N. Bogatyrev, A. Bowyer, and A. Pahl, "Biomimetics: its practice and theory," *Journal of the Royal Society Interface*, vol. 3, no. 9, p. 471, 2006.

[94] A. A. Biewener, *Animal locomotion*. OUP Oxford, 2003.

[95] C. R. Taylor, N. C. Heglund, T. A. McMAHON, and T. R. Looney, "Energetic cost of generating muscular force during running: a comparison of large and small animals," *The Journal of Experimental Biology*, vol. 86, no. 1, pp. 9–18, 1980.

[96] E. Ferrannini, "The theoretical bases of indirect calorimetry: a review," *Metabolism*, vol. 37, no. 3, pp. 287–301, 1988.

[97] R. Gratz and V. Hutchison, "Energetics for Activity in the Diamondback Water Snake, *Natrix rhombifera*," *Physiological Zoology*, vol. 50, no. 2, pp. 99–114, 1977.

[98] J. A. Ruben, "Aerobic and anaerobic metabolism during activity in snakes," *Journal of comparative physiology*, vol. 109, no. 2, pp. 147–157, 1976.

[99] Y. Winter, "Energetic cost of hovering flight in a nectar-feeding bat measured with fast-response respirometry," *Journal of Comparative Physiology B*, vol. 168, no. 6, pp. 434–444, 1998.

[100] E. Jequier, "Long-term measurement of energy expenditure in man: direct or indirect calorimetry," *Recent advances in obesity research*, vol. 3, pp. 130–135, 1981.

[101] G. E. Walsberg and T. C. Hoffman, "Direct calorimetry reveals large errors in respirometric estimates of energy expenditure," *Journal of Experimental Biology*, vol. 208, no. 6, pp. 1035–1043, 2005.

[102] K. Ugurbil, H. Rottenberg, P. Glynn, and R. Shulman, "Phosphorus-31 nuclear magnetic resonance studies of bioenergetics in wild type and atpase-escherichia coli cells," *Biochemistry*, vol. 21, no. 5, pp. 1068–1075, 1982.

[103] J. Zhang, H. Merkle, K. Hendrich, M. Garwood, A. From, K. Ugurbil, and R. J. Bache, "Bioenergetic abnormalities associated with severe left ventricular hypertrophy.," *Journal of Clinical Investigation*, vol. 92, no. 2, pp. 993–1003, 1993.

[104] S. Codd and J. D. Seymour, *Magnetic resonance microscopy*. Wiley-VCH, 2008.

[105] J. Clark, "Creatine and Phosphocreatine: A Review of Their Use in Exercise and Sport," *Journal of Athletic Training*, vol. 32, no. 1, pp. 45–51, 1997.

[106] D. Jackson, H. Shi, J. Singer, P. Hamm, and R. Lawler, "Effects of input pressure on in vitro turtle heart during anoxia and acidosis: a 31P-NMR study," *American Journal of Physiology-Regulatory, Integrative and Comparative Physiology*, vol. 268, no. 3, pp. R683–R689, 1995.

[107] D. Wemmer, N. Wade-Jardetzky, E. Robin, and O. Jardetzky, "Changes in the Phosphorus Metabolism of a Diving Turtle Observed by 31P-NMR," *Biochimica et Biophysica Acta*, vol. 720, pp. 281–287, 1982.

[108] B. Chance, S. Eleff, J. Leigh, D. Sokolow, and A. Sapega, "Mitochondrial regulation of phosphocreatine/inorganic phosphate ratios in exercising human muscle: a gated 31p nmr study," *Proceedings of the National Academy of Sciences*, vol. 78, no. 11, pp. 6714–6718, 1981.

[109] G. Karp, *Cell and Molecular Biology: Concepts and Experiments*. John Wiley & Sons, 2009.

[110] D. L. Nelson and M. M. Cox, *Lehninger principles of biochemistry*. Wh Freeman, 2010.

[111] A. E. Minetti, C. Moia, G. S. Roi, D. Susta, and G. Ferretti, "Energy cost of walking and running at extreme uphill and downhill slopes," *Journal of Applied Physiology*, vol. 93, no. 3, pp. 1039–1046, 2002.

[112] E. M. Haacke, R. W. Brown, M. R. Thompson, and R. Venkatesan, *Magnetic resonance imaging: physical principles and sequence design*, vol. 82. Wiley-Liss New York:, 1999.

[113] A. Webb and G. C. Kagadis, "Introduction to biomedical imaging," *Medical Physics*, vol. 30, p. 2267, 2003.

[114] C. R. Taylor, N. C. Heglund, and G. Maloiy, "Energetics and mechanics of terrestrial locomotion. i. metabolic energy consumption as a function of speed and body size in birds and mammals," *Journal of Experimental Biology*, vol. 97, no. 1, pp. 1–21, 1982.

[115] R. Webster, A. Okamura, and N. Cowan, "Toward active cannulas: Miniature snake-like surgical robots," in *IEEE/RSJ International Conference on Intelligent Robots and Systems*, pp. 2857–2863, 2006.

[116] S. M. Secor, B. C. Jayne, and A. C. Bennett, "Locomotor performance and energetic cost of sidewinding by the snake *Crotalus cerastes*," *J. Exp. Biol.*., vol. 163, pp. 1–14, 1992.

[117] E. Home, "Observations intended to show that the progressive motion of snakes is partly performed by means of the ribs," *Philosophical Transactions of the Royal Society of London*, vol. 102, pp. 163–168, 1812.

[118] K. Zimmermann and I. Zeidis, "Worm-like locomotion as a problem of nonlinear dynamics," *Journal of Theoretical and Applied Mechanics-Warsaw-*, vol. 45, no. 1, p. 179, 2007.

[119] J. Mehrtens, *Living snakes of the world in color*. Sterling, 1987.

[120] W. Mosauer, "How fast can snakes travel?," *Copeia*, pp. 6–9, 1935.

[121] K. Schmidt-Nielsen, *Scaling, why is animal size so important?* Cambridge Univ Pr, 1984.

[122] C. Gans and J. Gasc, "Tests on the locomotion of the elongate and limbless reptile Ophisaurus apodus (Sauna: Anguidae)," *Journal of Zoology*, vol. 220, no. 4, pp. 517–536, 1990.

[123] S. Renous, E. Hofling, and J. P. Gasc, "Analysis of the locomotion pattern of two microteiid lizards with reduced limbs, *Calyptommatus leiolepis* and *Nothobachia ablephara* (Gymnophthalmidae)," *Zool.*, vol. 99, pp. 21–38, 1995.

[124] U. Saranli, M. Buehler, and D. E. Koditschek, "Rhex: A simple and highly mobile hexapod robot," *The International Journal of Robotics Research*, vol. 20, no. 7, pp. 616–631, 2001.

[125] K. Y. Ma, P. Chirarattananon, S. B. Fuller, and R. J. Wood, "Controlled flight of a biologically inspired, insect-scale robot," *Science*, vol. 340, no. 6132, pp. 603–607, 2013.

[126] G. Dudek, M. Jenkin, C. Prahacs, A. Hogue, J. Sattar, P. Giguere, A. German, H. Liu, S. Saunderson, A. Ripsman, *et al.*, "A visually guided swimming robot," in *IEEE/RSJ International Conference on Intelligent Robots and Systems*, pp. 3604–3609, 2005.

[127] A. J. Ijspeert, A. Crespi, and J.-M. Cabelguen, "Simulation and robotics studies of salamander locomotion," *Neuroinformatics*, vol. 3, no. 3, pp. 171–195, 2005.

[128] A. Wolf, H. B. Brown, R. Casciola, A. Costa, M. Schwerin, E. Shamas, and H. Choset, "A mobile hyper redundant mechanism for search and rescue tasks," in *IEEE/RSJ International Conference on Intelligent Robots and Systems*, vol. 3, pp. 2889–2895, 2003.

[129] C. Wright, A. Johnson, A. Peck, Z. McCord, A. Naaktgeboren, P. Gianfortoni, M. Gonzalez-Rivero, R. Hatton, and H. Choset, "Design of a modular snake robot," in *Intelligent Robots and Systems, 2007. IROS 2007. IEEE/RSJ International Conference on*, pp. 2609–2614, IEEE, 2007.

[130] D. L. Hu, J. Nirody, T. Scott, and M. J. Shelley, "The mechanics of slithering locomotion," *Proceedings of the National Academy of Sciences*, vol. 106, no. 25, pp. 10081–10085, 2009.

[131] J. W. Burdick, J. Radford, and G. S. Chirikjian, "A 'sidewinding' locomotion gait for hyper-redundant robots," *IEEE Int. Conf. Robot. Autom.*, pp. 101–106, 1993.

[132] T. L. Hedrick, "Software techniques for two-and three-dimensional kinematic measurements of biological and biomimetic systems," *Bioinspiration & Biomimetics*, vol. 3, no. 3, p. 034001, 2008.

[133] N. Gravish, P. B. Umbanhowar, and D. I. Goldman, "Force and flow transition in plowed granular media," *Physical review letters*, vol. 105, no. 12, p. 128301, 2010.

[134] I. Albert, J. Sample, A. Morss, S. Rajagopalan, A.-L. Barabási, and P. Schiffer, "Granular drag on a discrete object: Shape effects on jamming," *Physical Review E*, vol. 64, no. 6, p. 061303, 2001.

VITA

Hamidreza Marvi was born in Neyshaboor, Iran. He received his B.Sc. from Iran University of Science and Technology in Mechanical Engineering and M.Sc. from the Sharif University of Technology in Mechanical/Biomedical Engineering in 2004 and 2007, respectively. He also received a Masters degree from Clemson University in Mechanical Engineering in 2009. Hamid then moved to Georgia Tech to pursue a Ph.D. in Mechanical Engineering. His current research interests are bio-inspired design, biomechanics of animal locomotion, biotribology, and robotics.